Structural and Functional Studies on the Interaction Network of E2 Ubiquitination Enzymes

Anding Huang

ISBN 978-90-393-5355-4

Doctoral thesis

Structural and Functional Studies on the Interaction Network of E2 Ubiquitination Enzymes

Anding Huang

NMR Spectroscopy Research Group, Bijvoet Center for Biomolecular Research,

Utrecht University, The Netherlands

June 2010

Het werk beschreven in dit proefschrift werd gefinancierd door de Nederlandse Organisatie voor Wetenschappelijk Onderzoek, gebied Chemische Wetenschappen (NWO-CW).

Copyright © 2010 Anding Huang
Cover painting artist Yanliu Lin

Printed in the Netherlands by Ridderprint Offsetdrukkerij B.V.

Structural and Functional Studies on the Interaction Network of E2 Ubiquitination Enzymes

Structurele en functionele studies van het interactie netwerk van E2 ubiquitinerings enzymen

(met een samenvatting in het Nederlands)

Proefschrift

ter verkrijging van de graad van doctor aan de Universiteit Utrecht op gezag van de rector magnificus, prof.dr. J.C. Stoof, ingevolge het besluit van het college voor promoties in het openbaar te verdedigen op maandag 28 juni 2010 des ochtends te 10.30 uur

door

Anding Huang

geboren op 18 April 1980 te Chong-Qing, China

Promotor: Prof. dr. R. Boelens

Co-promotor: Dr. R. N. de Jong

aan mijn ouders

Contents

Contents vii

Chapter 1
Introduction to the ubiquitination pathway 1

Chapter 2
Strategy for production of correctly folded E3 RING domains 21

Chapter 3
E2-c-Cbl recognition is necessary but not sufficient for ubiquitination activity 35

Chapter 4
Symmetry and asymmetry of the RING-RING dimer of Rad18 57

Chapter 5
The ability of human Rad6b to assemble ubiquitin chains is inhibited by Rad18 interaction 77

References 97

Summary 111

Samenvatting 115

Curriculum Vitae 119

Publications 121

Acknowledgement 123

Full Colour Figures 125
[1]

[1] Full colour figures are marked with an asterisk (*) throughout the text

Chapter 1

Introduction to the ubiquitination pathway

History of the ubiquitination pathway

Almost 30 years ago the basic concept of the ubiquitin proteolytic system was elucidated by Aaron Ciechanover, Avram Hershko and Irwin Rose, for which they were awarded the 2004 Nobel Prize in chemistry. Before this discovery, the consensus was that a cellular organelle, called the lysosome, degraded the extracellular and intercellular proteins [1]. However, in 1977 Etlinger and Goldberg found in crude reticulocyte extracts a soluble ATP-dependent proteolytic system different from the lysosome [2], which was shown to consist of several different proteins [3]. Later studies identified ubiquitin, which at that time had no known function, as a post-translational modification of the histone protein H2A [4]. Subsequently, a protein, named ATP-dependent proteolysis factor 1 (APF-1) that was previously linked to proteolytic degradation, was found to be the same protein as ubiquitin [5]. A few years later, it was discovered that a large ATP-dependent proteolytic protein complex, called the 26S proteasome, is responsible for the ubiquitin-dependent protein degradation [6, 7]. Initially the ubiquitination pathway was mainly implicated in the attachment of ubiquitin to specific target proteins, signaling them for degradation by the proteasome. These target proteins can be misfolded or regulatory cellular proteins and thus the ubiquitination pathway together with the proteasome plays an important regulatory function. More recently, it is known that the ubiquitination pathway is involved in a wide variety of other cellular functions, such as DNA transcription and repair, cell cycle and division, and apoptosis [8, 9, 10]. The importance of a correctly functioning ubiquitination pathway becomes clear from the numerous diseases that are, directly or indirectly, attributed to aberrations in the ubiquitin system [11, 12]. A few examples of diseases connected to the ubiquitination pathway are listed in Table 1.1.

Table 1.1: Examples of diseases in which the ubiquitination pathway is implicated.

Diseases	Defects/symptoms
Breast cancer	Mutation in BRCA1, an E3 enzyme
Multiple myeloma	Supression of apotosis induction of proliferation
Uterine cervical cancer	HPV-mediated accelerated degradation of p53 by the ubiquitination system
Angelman syndrome	Mutation in E6-AP, and E3 enzyme
Fanconi anemia	Mutation in the FANCD2 protein, a substrate of ubiquitination system

The ubiquitination cascade

The ubiquitination pathway consists of a cascade of enzymes that can specifically attach ubiquitin and polyubiquitin chains to certain target proteins to regulate their

cellular function [13]. Ubiquitin is a small 8.5 kDa protein consisting of 76 amino acids that is ubiquitously expressed in eukaryotes. Its structure consists of 5 β-strands, a short central α-helix and a small 3_{10} α-helix (Figure 1.1C). The C-terminal tail of ubiquitin is highly accessible, which allows the covalent attachment of ubiquitin via G76 to the lysine sidechain of target proteins via an isopeptide bond. Ubiquitin has 7 lysines at the surface and this enables formation of polyubiquitin chains. K63-linked ubiquitin chains often have signaling functions, and K48-linked ubiquitin chains are associated with protein degradation. In addition to ubiquitin, target proteins can also be tagged with ubiquitin–like (Ubl) proteins, such as NEDD8/RUB1, SUMO and ISG15 [14].

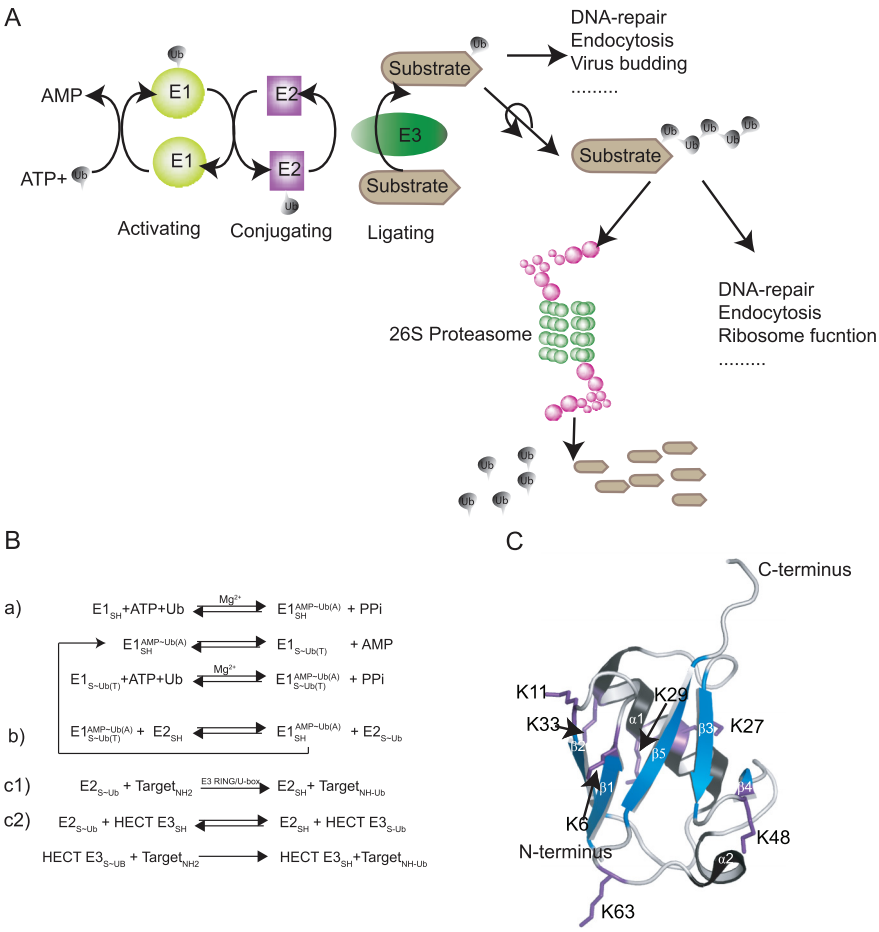

Figure 1.1: The ubiquitination pathway. **A.** Schematic representation of the pathway. **B.** Enzymatic mechanism of ubiquitin activation, conjugation and ligation cycle. **C.** A ribbon representation of ubiquitin (1D3Z). Its seven lysines are indicated.

The pathway consists of three enzymes: E1, the ubiquitin-activating enzyme, E2, a ubiquitin-conjugating enzyme and E3, a ubiquitin-ligase enzyme [15]. Together they shuttle ubiquitin to the target protein via a hierarchical enzymatic cascade (Figure 1.1A). In a few cases, additional factors such as the E4 ubiquitin elongating factor are needed for the reaction [16]. Only two human activation enzymes have been identified, UBE1/UBA1[17] and UBA6 [18], but there are approximately 36 E2 enzymes and several hundreds of E3 ligases. In this way, specific target proteins can be ubiquitinated in distinct ubiquitin pathways that can be formed by different combinations of E1, E2 and E3 enzymes.

The ubiquitination cascade starts with the activation of ubiquitin by the E1 enzyme. The best characterized activation mechanism is that of the yeast E1 UBA1 [19]. In the first step of ubiquitin activation, UBA1 binds both ATP $\bullet$ Mg^{2+} and ubiquitin, and forms an $E1^{AMP\tilde{}Ub(A)}$ complex with a phosphodiester bond between the hydroxyl group of the ubiquitin carboxyl terminus and the phosphate group of AMP. In the next step, the conserved catalytic Cys in the E1 enzyme reacts with the bound AMP$\sim$Ub (A) to form a thioester-bonded complex $E1_{S\tilde{}Ub(T)}$. Subsequently, this complex binds a second ATP $\bullet$ Mg^{2+} and ubiquitin, resulting in an E1 enzyme loaded with two ubiquitin molecules: one ubiquitin is covalently attached to the active Cys of E1 enzyme through a thioester bond and a second ubiquitin is associated non-covalently via AMP [20] (Figure 1.1B a). Next, the doubly loaded E1 associates with a cognate E2, and the thioester bonded ubiquitin is transferred from E1 to the active cysteine of the E2 enzyme forming an E2$\sim$Ub thioester complex (Figure 1.1B b). With the help of E3 enzymes, primarily RING type E3 ligases, ubiquitin is directly passed on from the E2 to a substrate by forming an isopeptide bond between the carboxyl group of the ubiquitin C-terminal residue Gly76 and the ε-amino group of a Lys residue of the target protein (Figure 1.1B c1). Alternatively, HECT domain (homologous to E6-AP C terminus) E3 ligases transfer ubiquitin from E2 to an internal cysteine through a further trans-thiolation step before transferring ubiquitin to the substrate (Figure 1.1B c2).

Ubiquitin contains seven lysine residues (Lys6, Lys11, Lys27, Lys29, Lys33, Lys48 and Lys63) (Figure 1.1C), so additional ubiquitin molecules can be ligated to one of the seven lysines of the previously attached ubiquitin molecule. As a consequence, substrate proteins can be modified by various ubiquitin signals: mono-ubiquitin and poly-ubiquitin chains which can be different in length and linkages between the ubiquitin moieties. The addition of a single ubiquitin (monoubiquitination) to a target protein is often found in regulating protein activity and location, and the formation of polyubiquitin chains has been implicated in targeting to 26S proteasome, immune signaling and DNA repair [21].

Downstream of ubiquitination, deubiquitinating enzymes (DUBs) can reverse

monoubiquitination or remodel polyubiquitin chains through cleaving ubiquitin-protein bonds [22]. Furthermore, the ubiquitin signals can also be interpreted by ubiquitin-binding domains (UBDs) proteins, which can preferentially bind to ubiquitin chains of specific length and linkage and further transmit these signals [23, 24].

E2 conjugating enzymes

The hierarchical E1-E2-E3 ubiquitination cascade is fiercely expanded at the E2 level where dozens of E2 enzymes can be charged by a few E1s and which is followed by an even more expanded E2-E3 interaction network. The E2 enzymes play a key role in the ubiquitin pathway, since the various possible complexes of E2 and E3 enzymes largely define the specificity of the pathway [25], and E2 enzymes are key mediators in ubiquitin chain assembly [26]. Our knowledge on E2 function is supported by a wealth of 3D structures of free enzymes and of complexes of E2 enzymes with conjugates, as I will summarize below. Despite this, our picture on the molecular mechanisms that underlie the specificity of E1-E2, E2-E3 and E2-target recognition, our understanding of the regulatory role of E2 enzymes and the characteristics of the active but unstable thioester intermediate E2∼Ub, is still incomplete.

In humans, 36 E2 proteins have been identified [27], which are listed in Table 1.2. For many of them structures are available in the Protein Data Bank. All E2 proteins contain a ∼150 residue catalytic core or ubiquitin conjugating domain (UBC) which is structurally conserved throughout many species. The UBC domain consists of four α-helices and a 3_{10} helix at one side of the protein and a four-stranded β-sheet at the other side (Figure 1.2A, C) [13]. Some E2s contain extensions at one or both ends of their core domain. Therefore the E2 enzymes can be classified into four types: UBC only (type I), UBC with a C-terminal extension (type II), UBC with a N-terminal extension (type III) and UBC with both extensions (type IV). These extensions play important functional roles in the ubiquitin pathway, since they have been shown to interact with the E3 ligases and are involved in noncovalent interactions with ubiquitin. For example, the N-terminal extension of UbcH10 interacts with the E3 ligase APC2 and regulates the E3 activity [28]. Another example is the C-terminal extension of Ube2K which binds noncovalently to ubiquitin and which facilitates the formation of polyubiquitin chains [29](Figure 1.2C) .

The catalytic core of human UBCs is highly conserved (Figure 1.2B). All catalytic active E2s contain both a catalytic Cys and a Trp residue positioned 7-20 amino acids C-terminal relative to the Cys. In addition, there are generally the conserved sequence Y/FPxxPP between β3 and β4, the sequence HPN (His-Pro-Asn) positioned 7-8 amino acids before the Cys, and a few hydrophobic residues following the Cys. Some core domains contain additional segments of residues. For example, several human E2s,

such as Ube2R1, Ube2G1 and Ube2J1, have insertions with different length in loop L7 between β4 and α2 (highlighted as grey in Figure 1.2B) and Ube2I has a significant longer loop L2 (Figure 1.2C). Mutation of e.g. the β4α2 insertion in Ube2R1 strongly decreased the formation of K48-linked polyubiquitin chains [30]. Thus these insertions can play important roles in regulating E2 catalysis.

Table 1.2: Lists of Human E2s.

Gene	Synonyms	UBLs	UniProtKB	Residues	PDB	Type
UBE2A	Rad6A, HR6A	Ubiquitin	P49459	152		Core
UBE2B	Rad6B,HR6B	Ubiquitin	P63146	152	1JAS	Core
UBE2D1	UbcH5A(UBC4/5)	Ubiquitin	P51668	147	2C4P	Core
UBE2D2	UbcH5B	Ubiquitin	P62837	147	2ESK/1W4U	Core
UBE2D3	UbcH5C	Ubiquitin	P61077	147	1X23	Core
UBE2D4	HBUCE1	Ubiquitin	Q9Y2X8	147		Core
UBE2L3	UbcH7	Ubiquitin	P68036	154	1D5F/1FBV	Core
UBE2L6	UbcH8	ISG15/Ub	O14933	153	1WZV/1WZW	Core
UBE2N	Ubc13	Ubiquitin	P61088	152	2C2V	Core
UBE2W		Ubiquitin	Q96B02	151	2A7L	Core
UBE2I	Ubc9	SUMO	P63279	158	1A3S	Core
UBE2G1	E217K/Ubc7	Ubiquitin	P62253	170	2AWF	Core
UBE2G2		Ubiquitin	P60604	165	2CYX	Core
UBE2Q1	NICE-5	Ubiquitin	Q7Z7E8	422	2QGX	N-extension
UBE2Q2	UBCi	Ubiquitin	Q8WVN8	375	1ZUO	N-extension
UBE2E1	UbcH6	Ubiquitin	P51965	193	3BZH	N-extension
UBE2E2	UbcH8	Ubiquitin	Q96LR5	201	1Y6L	N-extension
UBE2E3	UbcH9/UbcM2	Ubiquitin	Q969T4	207		N-extension
UBE2C	UbcH10	Ubiquitin	O00762	179	1I7K	N-extension
UBE2F		NEDD8	Q969M7	185	3FN1	N-extension
UBE2M	Ubc12	NEDD8	P61081	183	1Y8X	N-extension
UBE2J1	NCUBE1	Ubiquitin	Q9Y385	318		C-extension
UBE2J2	NCUBE2	Ubiquitin	Q8N2K1	259	2F4W	C-extension
UBE2R1	CDC34	Ubiquitin	P49427	236	2OB4	C-extension
UBE2R2	CDC34B	Ubiquitin	Q712K3	238		C-extension
UBE2K	HIP2, E2-25k(UBC1)	Ubiquitin	P61086	200	1YLA/3F92/3E46	C-extension
UBE2H	UbcH2,E2-20K	Ubiquitin	P62256	183	2Z5D	C-extension
UBE2S	E2-EPF5	Ubiquitin	Q16763	222	1ZDN	C-extension
UBE2U		Ubiquitin	Q5VVX9	321	1YRV	C-extension
UBE2T	HSPC150	Ubiquitin	Q9NPD8	197	1YH2	C-extension
UBE2Z	Use1	Ubiquitin	Q9H832	354		N,C-extension
UBE2O	E2-230K	Ubiquitin	Q9C0C9	1292		N,C-extension
FTS			Q9H8T0	292		N,C-extension
BIRC6		Ubiquitin	Q9NR09	4829		N,C-extension
UBE2NL		Ubiquitin	Q5JXB2	153		UBE2N-like
UBE2V1	CROC-1,UEV1	Ubiquitin	Q13404?	221	2HLW/2A4D	E2 variant 1
UBE2V2	MMS2	Ubiquitin	Q15819	145	1J74/1J7D	E2 variant 2

The precise mechanism of Ub/Ubl transfer from E2 to the lysine of the target protein is still unclear. It is generally believed that the conserved Cys of the E2 protein is the only residue that is essential for this transfer. However, Cecile Pickart and coworkers identified a conserved Asn, which is structurally near the E2 active site and which can stabilize the oxyanion intermediate formed when the Lys side chain of the target protein attacks the E2∼Ub thioester [31]. Later studies showed that other residues, such as N85, Y87 and D127 in the SUMO E2 Ubc9, can lower the effective

pKa of the active site and stimulate the transfer of SUMO by deprotonation of the target lysine [32]. Structural and sequence comparison of various E2 proteins identified a polar residue, mostly histidine, near the catalytic cysteine, that can possibly stabilize the oxyanion intermediate during the Ub/Ubl transfer [33]. More studies however will be necessary to understand the precise role of all residues involved in the catalytic mechanism.

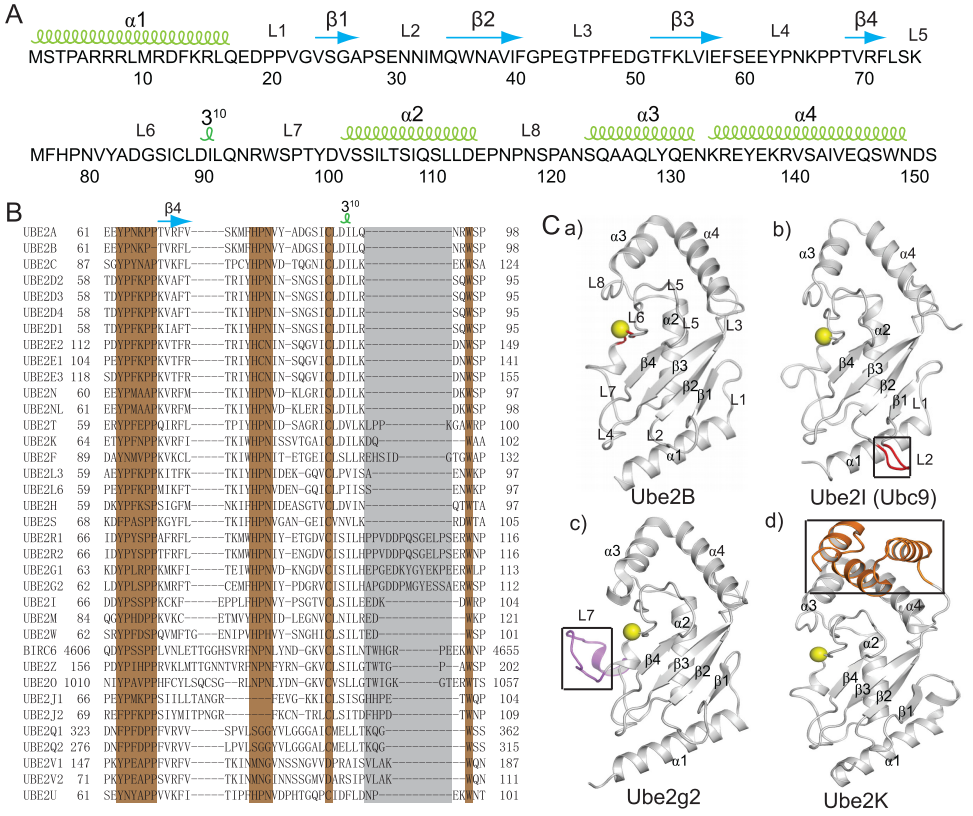

Figure 1.2: Structure of E2 ubiquitin conjugating enzymes. **A.** Sequence and secondary structure of the E2 UBC domain. Loops are labeled L1-L8; β-strands are labeled β1 to β4; and helices are labeled α1 to α4. **B.** Sequence alignment of the β3-α2 regions of human E2s. The consensus sequences are highlighted in brown. The extra insertions in the Loop L7 are highlighted in grey. **C.** (a) Schematic topology of core catalytic domain of E2 based on Ube2B (1JAS). (b) The X-ray structure of Ube2I (Ubc9) (2PE6), and the insertion in loop L2 between β1 and β2 is colored in red. (c) The X-ray structure of Ube2g2 (2CYX), and the insertion in loop L7 is colored in purple. (d) The X-ray structure of Ube2K (3E46), and the C-terminal extension is colored in orange. The catalytic cysteine is represented as a yellow ball.

E1-E2 recognition by multiple interaction surfaces

E1 enzymes activate ubiquitin (Ub) and ubiquitin-like (Ubl) proteins and facilitate the transfer of Ub/Ubl to the E2 conjugating enzymes. Generally, an E1 enzyme can charge multiple E2 enzymes with Ub/Ubl thereby expanding the E1-E2-E3 cascade. Still, the E1-E2 interaction should be specific to ensure the attachment of the right Ub/Ubl to the targets. Structural studies of the human SUMO E1-E2 [34] and NEDD8 E1-E2 [35] complexes combined with mutagenesis studies of the yeast ubiquitin E1-E2 [36] and ISG15 E1-E2 [37] complexes have provided substantial insight into the mechanism of E1-E2 recognition, but the structure of a human ubiquitin E1-E2 complex is still lacking. The structure of a typical E1, such as yeast ubiquitin E1 (UBA1), the human NEDD8 E1 (NAE1-UBA3) [35] and the SUMO E1 (SAE1-UBA2) [38], consists of three common building blocks: an adenylation domain, a catalytic domain and a ubiquitin-fold domain (UFD) (Figure * 1.3A, B). The adenylation domain binds ATP•Mg^{2+} and Ub/Ubl and activates the Ub/Ubl proteins by adenylating them at the C-terminal residue. Subsequently the adenylated Ub/Ubl protein is transferred to the cysteine of the catalytic domain forming a thioester bond. Crystal structures of intermediates at these two reaction steps were recently determined for the human SUMO E1 activating enzymes and demonstrate that the SUMO E1 catalytic domain undergoes a relative 130° rotation which allows the transfer of the adenylated SUMO (Figure * 1.3A, left) to the cysteine of the catalytic domain (Figure * 1.3A, right) [38]. This large structural change brings the catalytic Cys close to the C-terminus of SUMO. The third domain, the UFD domain, is responsible for binding the E2 enzyme, onto which the Ub/Ubl protein needs to be transferred [20].

Figure * 1.3B shows the structure of an E1-E2 complex, that of human UBA3, a NEDD8 E1, with a mutant (C111A) of Ube2M. The major E1-E2 binding surface consists of the twisted β sheet of the UFD domain of UBA3 with the helix α1 and loop L2 between strands β1 and β2 of Ube2M [35]. In addition, the N-terminal extension of Ube2M binds in a hydrophobic groove of the adenylation domain. Similar interactions can be observed in the complex of the UBE2F core domain (another human NEDD8 E2 enzyme) with the UFD domain of UBA3 (Figure * 1.3C) [39]. The structures demonstrate the importance for the E1-E2 recognition of the negatively charged C-terminal UFD and the positively charged first helix α1 of the E2 enzymes, something that is also observed in a mutagenesis study on the interaction of UFD of yeast ubiquitin E1 UBA1 and Ubc1 (the yeast E2 enzyme) [36]. Thus, all studies indicate that helix α1 and loop L2 of the E2 core domain play a key role for E1 binding. Obviously, additional interactions can come into play for E2s with N-terminal and C-terminal extensions. For example, in the case of the NEDD8 UBA3-Ube2M complex the N-terminal extension of Ube2M binds to a surface groove of the adenylation domain of UBA3 which is unique and thus highly specific for the recognition of these E1-E2

pairs [40].

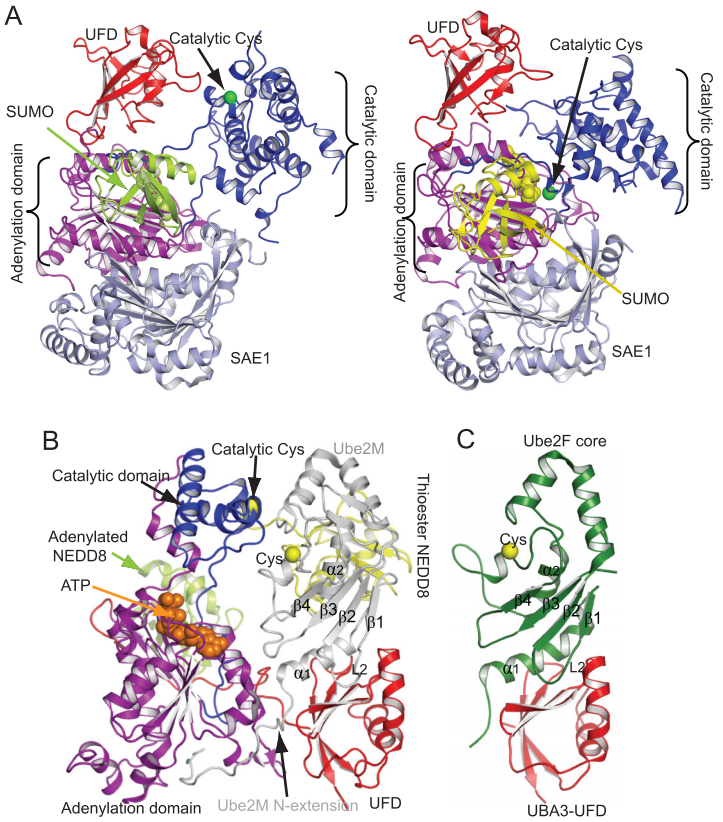

Figure * 1.3: Structure of the ubiquitin-activating enzyme E1 and of the complex with E2. **A.** Crystal structures of human SUMO E1/SUMO1-AMSN adenylate analogue (3KYC, left) and human SUMO E1∼SUMO1-AVSN intermediate analogue (3KYD, right). The UFD domain of UBA2 is colored in red, the catalytic domain of UBA2 in blue, the adenylation domain in purple, and the SAE1 in lightblue. The catalytic cysteine is represented as a green ball. SUMO is colored in limo (left) and yellow (right). **B.** Crystal structure of Human NEDD8 E1 UBA3 loaded with both NEDD8 and the E2 Ube2M (C111A)(2NVU). Ube2M (grey) is bound to the UFD domain of UBA3 (red); The thioester-linked NEDD8 (yellow) is attached to catalytic cysteine (yellow ball) of the catalytic domain of UBA3 (blue); the adenylated NEDD8 (lime) is non-covalently bound to the adenylation domain of UBA3 (purple). ATP is colored in orange. The red arrow indicates the distance between the two catalytic cysteines in E1 and E2. **C.** Crystal structure of the core domain of the complex of Ube2F (forest) with the UFD domain (red) of human NEDD8 E1 UBA3 (3FN1).

Recruitment of E2s by E3 ligases: interaction between the E2 UBC domain and the E3 RING/U-box/HECT domains

There are two major classes of E3 ligases: E3s containing a HECT-domain (homologous to E6-AP Carboxyl-terminus) and those containing a RING-finger (Really Interesting New Gene) domain. In most HECT E3s the E2s bind to the HECT domain and the activated Ub/Ubl protein is transferred from the E2 to a catalytic cysteine of the E3, before it is transferred to the target protein. In RING E3s a RING domain interacts with the E2 enzyme, but the E2 enzyme directly transfers the activated Ub/Ubl protein to the target protein, since the RING E3 has no catalytic Cys. Thus RING E3s should bind simultaneously the E2 enzyme and via another domain (or even a different protein) the target protein. In addition to these two major E3 types, a third type, U-box E3s, is highly related to the RING E3s, since the U-box domain has a similar structure and function as the RING domain [41]. Common to all E3 enzymes is the interaction of a specific domain RING, U-box or HECT, with the E2 core UBC domain [13], but the rules that define E2-E3 specificity are still not fully understood. Major steps forward were recently made by global screening of the interactions between all human E2 enzymes and a few hundred RING domains [42, 43].

Our understanding on E2-E3 recognition comes mostly from structural studies of E2-E3 complexes. The first structures that were determined by X-ray crystallography were those of the E2 enzyme UbcH7 in complex with a HECT E3 E6AP [44], and of UbcH7 with the RING E3 Cbl [45]. This was followed by NMR studies of the complexes of the RING domains of BRCA1 and of CNOT4 with the E2 enzyme UbcH5 [46, 47, 48]. Thereafter, structures of complexes of CHIP, a U-box E3 with Ubc13/Uev1A [49], of Danio rerio CHIP with UbcH5A [50], of the cIAP2 RING domain with UbcH5b [51] and of the TRAF6 RING domain with Ubc13 [52] were determined. All these structures show high similarity in the overall structures and in the elements involved in the E2-E3 interfaces (Figure * 1.4A). The E3 RING and U-box domains show a hydrophobic groove formed by loop L1, loop L2 and the central helix, which constitute the binding interface for the E2s. In addition it was seen in the c-Cbl-UbcH7 and TRAF6-Ubc13 complexes that some residues preceding the RING domain can also participate in the E2 interactions (Figure * 1.4B). On the side of the E2s, two loops and a helix play an important role: loop L4, between strand β3 and β4, loop L7, between strand β4 and helix α2, and helix α1 usually make contacts with the different E3s, both for RING, U-box and HECT E3s. The important residues involved in interface of various E2 and RING/U-box E3 pairs are summarized in Figure * 1.4B and 4C. Interestingly the studies of both E1 and E3 binding to E2s show that the helix α1 of E2 is involved in the formation of both complexes . Since the E2 enzyme cannot bind E1 and E3 using helix α1 simultaneously, the charged E2∼Ub has to dissociate from the E1 enzyme before it binds to the E3 and transfers ubiquitin to the target

protein[53].

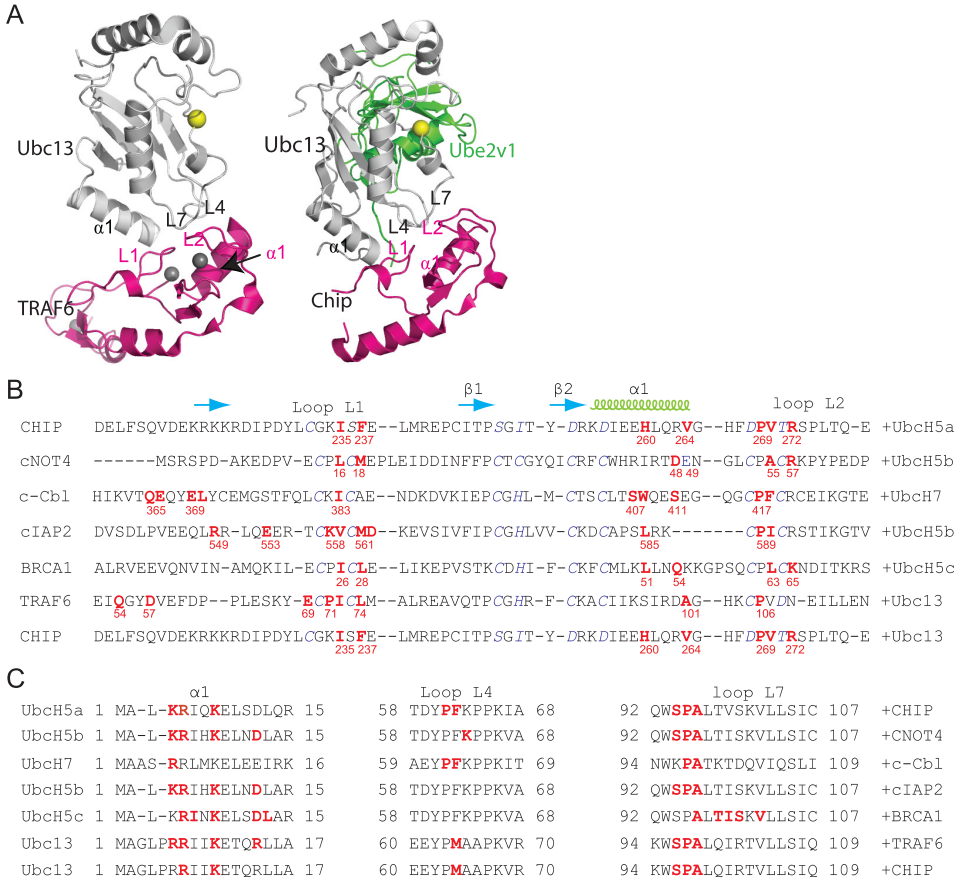

Figure * 1.4: Interactions of E2 enzymes with the E3 RING/Ubox domains. **A.** Crystal structures of TRAF6-Ubc13 (3HCT) and CHIP-Ubc13-Ube2v1 (2C2V). The E2 is colored grey and the E3 colored in deeppink. **B.** Contacts between the E2 core domain and the E3 RING/U-box domains. The important residues on the E3 RING/U-box, which are involved in binding to E2, are highlighted in bold red and the zinc-coordinating residues in the RING domain or the equivalent residues in the U-box are highlighted in italic blue. **C.** Residues of E2 enzymes involved in E3 RING/U-box binding. The major interacting residues are highlighted in bold red.

Despite high similarity in the overall structure, the detailed E2-E3 interfaces and the resulting binding affinities can vary substantially. For example, loop L4 of UbcH7 and UbcH5b plays an important role in the interaction with c-Cbl and CNOT4, respectively, but seems not to be involved in the binding of UbcH5 to cIAP2 and BRCA1/BARD1 [48, 51]. Substitution of Arg5 with Ala in UbcH5b interferes with the functional interaction with CNOT4, but not with that of APC2-APC11 [54], which

suggests that the role of each residue can be very different for different E3s. The relative orientation between E2 and E3 can also be slightly different. For example, when overlaying the U-box domain of CHIP-Ubc13/Uev1A and RING domain of TRAF6-Ubc13, there is 10 degree rotation of Ubc13 for these two complexes [52].

Although the canonical E2-E3 interfaces have been described quite clearly, it is still uncertain what the determinants of active E2-E3 pairs are. It is generally believed that the function of RING and U-box E3s is to bring the activated E2∼Ub in close proximity to the target protein in order to facilitate the ubiquitin transfer. For most active E2-E3 complexes it appears that the binding affinity between E2 and E3 pairs is relatively low (often only µM affinities), which potentially reduces specificity. However, this low affinity may be favorable for a quick dissociation of the charged E2∼Ub from the E3 ligases, which could facilitate the transfer of ubiquitin to the substrate by allowing direct contact of E2∼Ub and substrate [39, 46]. In general, there appears to be a poor correlation between E3 ligase activity and the binding affinity of E2 and E3s, which complicates our picture of E2-E3 recognition considerably. Determining the essentials of each active E2-E3 pair individually will be quite difficult while important too, given the large number of E2s and E3s, and their large variety in sequence and biological function.

Allosteric effects have been noted in the E2 enzymes. Binding of a RING E3 to E2∼Ub can induce a rearrangement in the E2 active site, which exposes the sidechain of an Asp residue essential for catalysis and conserved in many E2s [31]. It has also been found that E3 RING binding can enhance the discharge rate of ubiquitin from E2∼Ub, which was observed for UbcH5b∼Ub by binding the E3s CNOT4 and Apc2/11 [54], and for Cdc34∼Ub by binding the E3 SCF [30]. Similarly, a biochemical study of the UbcH5b I37A mutant, distant from the active site and E3-binding site, also suggests there is communication between the active site of UbcH5b and the RING-binding site [54]. One may think that these allosteric functional effects also involve major structural effects. However, structural studies show that binding E3 RING or U-box domains to E2s cause no major conformational changes [39, 45, 49, 51, 55]. Unfortunately, in all these structural studies the E2s were uncharged with ubiquitin which may indicate a difference between free E2 and activated E2∼Ub in response to the binding of E3.

Another question is how the combination of E2 and E3 enzymes determines substrate specificity and ubiquitin chain type. The combination of one E3 with different E2s can lead to different ubiquitin chain linkages. For example, the RING E3 BRCA1/BARD1 forms poly-K63 chains on BRCA1 with the heterodimeric E2s Ubc13-Mms2, while it forms poly-K48 chains with Ube2K [56]. Similarly, one E2 with different E3s can also lead to different chains, e.g. UbcH5c produces a mixture of K11, K48 and K63 linkages with the E3s APC/C, Murt, CHIP and MDM2 [57, 58], while with the E3 BRCA1-BARD1, it synthesizes predominantly K6-linked chains [59]. One

hypothesis is that many E3s contain non-covalent ubiquitin-binding domains and that this might orient ubiquitin as an acceptor for the E2∼Ub thioester reaction [60] and therefore influence the chain topology.

The covalent interaction between the E2 UBC domain and ubiquitin

In sharp contrast to the wealth of structures of E2 enzymes in free state and in complexes with E3s and E3 domains, structural insight of the E2∼Ub thioester intermediate is very limited because of its intrinsic instability. The E2∼Ub thioester intermediate can be studied directly in the NMR tube, where a covalent complex can be formed using a mixture of E2, ubiquitin, Mg^{2+}-ATP and a catalytic amount of the activation enzyme E1, and the reaction can be monitored by ^{1}H-^{15}N HSQC spectra [61, 62, 63]. Another approach is to stabilize the thioester linkage between the E2 catalytic Cys and Ub Gly76 by replacing this Gly by a Cys residues to form a disulfide linkage between the Cys sidechains [64], or by mutating the E2 catalytic Cys by a Ser to form a more stable ester complex [65, 66].

As discussed above as well, the catalytic site of E2∼Ub is highly conserved, including the catalytic Cys residue and the surrounding residues in loop L6 and L7 (Figure 1.5A, B). This conservation does not seem to position ubiquitin in a fixed orientation. NMR titrations show that only the C-terminal residues 73-76 of ubiquitin are perturbed upon formation of the E2∼Ub thioester complex, which implies that the E2∼Ub linker is rather flexible [62, 63] (Figure 1.5A). Also the crystal structure of the heterodimeric Ubc13-Mms2(C87S)∼Ub complex shows a flexible ester linkage between Ser87 of Ubc13 and ubiquitin Gly76, with no residues securing the link in any defined orientation (Figure 1.5B). This flexibility may be functional and facilitate the approach to the lysine residue of the target protein.

Noncovalent ubiquitin binding by E2s and polyubiquitin chain formation

It has been recently found that the assembly of ubiquitin chains on substrates proceeds in two separate steps, chain initiation and chain elongation [30, 56, 67, 68, 69, 70, 71]. In chain initiation ubiquitin is directly attached to the substrate, which is target selective and generally rate limiting. During chain elongation ubiquitin is subsequently attached to the native ubiquitin chain via the (processive) formation of a ubiquitin-ubiquitin isopeptide bond, which is usually faster. These two steps can be carried out by one E2 with one E3, two E2s with one E3, or two different E2s and E3s. For example, the multisubunit RING E3 ligase APC together with yeast E2 Ubc4 rapidly forms monoubiquitinated APC targets, and next this chain can be extended by the

E3 APC with yeast E2 Ubc1 via K48 linkages [70]. Another example is the *in vitro* autoubiquitination of BRCA1 by a mixture of E2s. In the chain initiation step Ube2e1, Ube2e2, Ube2e3 and Ube2w can all monoubiquitinate BRCA1, while the elongation of ubiquitin chains can occur via the heterodimeric E2s Ubc13-Mms2 and the E2 Ube2k . In contrast UbcH5c is able to both initiate and elongate ubiquitin chains on BRCA1 [56].

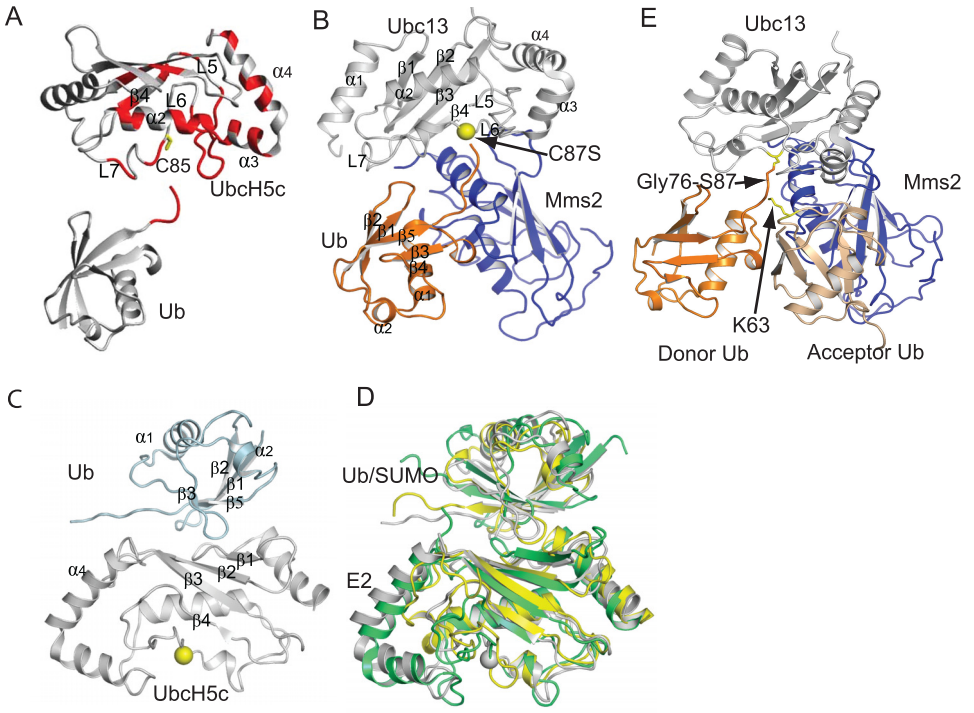

Figure 1.5: Interaction of E2 enzymes with ubiquitin. **A.** Formation of the E2∼Ub thioester linkage. The perturbed residues during formation of UbcH5c∼Ub as detected by NMR experiments in the formation of the thioester complex are colored in red. **B.** X-ray structure of yeast Mms2-Ubc13 (C87S) with covalently-attached donor ubiquitin (2GMI). Grey: Ubc13, blue: MMS2, orange: ubiquitin. **C.** NMR structure of UbcH5c non-covalently bound to ubiquitin (2FUH). Lightblue: ubiquitin, grey: UbcH5c. **D.** Comparison of the non-covalent binding geometry in different E2-Ub/Ubl complexes. The figure shows an overlay of the MMS2-Ub (1ZGU,yellow), Ubc9-SUMO (limegreen) and UbcH5c-Ub noncovalent complexes (grey). **E.** Structural overlay the MMS2-Ubc13(C87S)∼Ub(2GMI) and MMS2-Ub noncovalent complexes (1ZGU, wheat) based on an alignment of MMS2. The G76-S87 thioester bond with the donor ubiquitin and K63 of the acceptor ubiquitin are indicated.

It has been suggested that the ability of processive ubiquitin transfer to target proteins is related to the noncovalent ubiquitin binding to E2s, especially when these E2s are complexed to certain E3 ligases. For example, the S22R mutant of UbcH5c

abolishes noncovalent Ub binding and produces only monoubiquitinated BRCA1, whereas wild-type UbcH5c can interact non-covalently with ubiquitin and produces poly-Ub chains [63]. Also Ube2e1, Ube2e2, Ube2e3 and Ube2w can not bind ubiquitin noncovalently and can only monoubiquitinate BRCA1 [63]. However, the mechanism by which noncovalent ubiquitin binding is involved in chain elongation is still far from clear. In one model Brzovic et al. suggested that the noncovalent binding can accumulate multiple activated E2∼Ub in close proximity and that this self assembly causes the processive formation of poly-Ub chains [63].

A structural study of the noncovalent complex of UbcH5c and ubiquitin shows that the interaction interface consists of the surface formed by strands β1, β2, β3 and the C-terminal residues of helix α4 of UbcH5c, and the β-sheet surface of ubiquitin [63, 69] (Figure 1.5C). Similar binding surfaces have been found in non-covalent ubiquitin complexes with Mms2 and that of SUMO with UBC9 (Figure 1.5D) [69, 72, 73], suggesting that the noncovalent binding interfaces of E2s and Ub/Ubl proteins are quite conserved.

The noncovalent binding site for ubiquitin on Mms2 together with the crystal structure of the Ubc13 (C87S)∼Ub ester complex provides a model for poly-K63 chain formation. After loading the donor ubiquitin on the Ubc13-Mms2 heterodimer by the E1 enzyme (Figure 1.5B), the acceptor ubiquitin comes and will noncovalently bind to Mms2 (Figure 1.5E). This places K63 of the acceptor ubiquitin near the thioester bond of Ubc13∼Ub, which allows isopeptide formation between the C-terminus of the donor ubiquitin and K63 of the acceptor ubiquitin, leading to K63-linked diubiquitin [65]. Next, more ubiquitin can be attached to the chain in the same way enabling the poly-K63 chain formation.

A second E2 binding site in E3 ligases

It is generally thought that RING E3s mainly interact with their cognate E2s via the RING domain. This appears not always to be true. In fact, even before RING domains were known as such, in some "RING" E3 ligases other interaction regions had already been identified. The interaction of the E3 Rad18 with the E2 Rad6 depends critically on a C-terminal segment in Rad18 [74], whereas it has also a N-terminal RING domain. Later it was found that the RING domain and a C-terminal region of Rad18 (RING E3) both contribute to Rad6 interaction [75, 76].

The presence of multiple E2 interaction domains in RING E3s appears to be more common. The BRR domain (basic rich region) of RING E3 Ubr1 binds even stronger to yeast Ubc2 than its RING domain [77]. It has also been shown that a peptide segment named G2BR in the RING E3 gp78 binds to Ube2g2 (E2) and that the stable interaction of gp78 with Ube2g2 is even largely mediated by this G2BR segment

[78]. Kim et al. found that the C-terminal RING fingers in hBRE1A and hBRE1B (that form a E3 dimer) are dispensable for ubiquitination of the hBRE1 complex, and proposed that Rad6 (E2) interacted with the hBRE1 complex through a region(s) other than the RING finger domain [79]. All these cases demonstrate that the second binding site on E3s can bind to its cognate E2 even stronger than the RING domain.

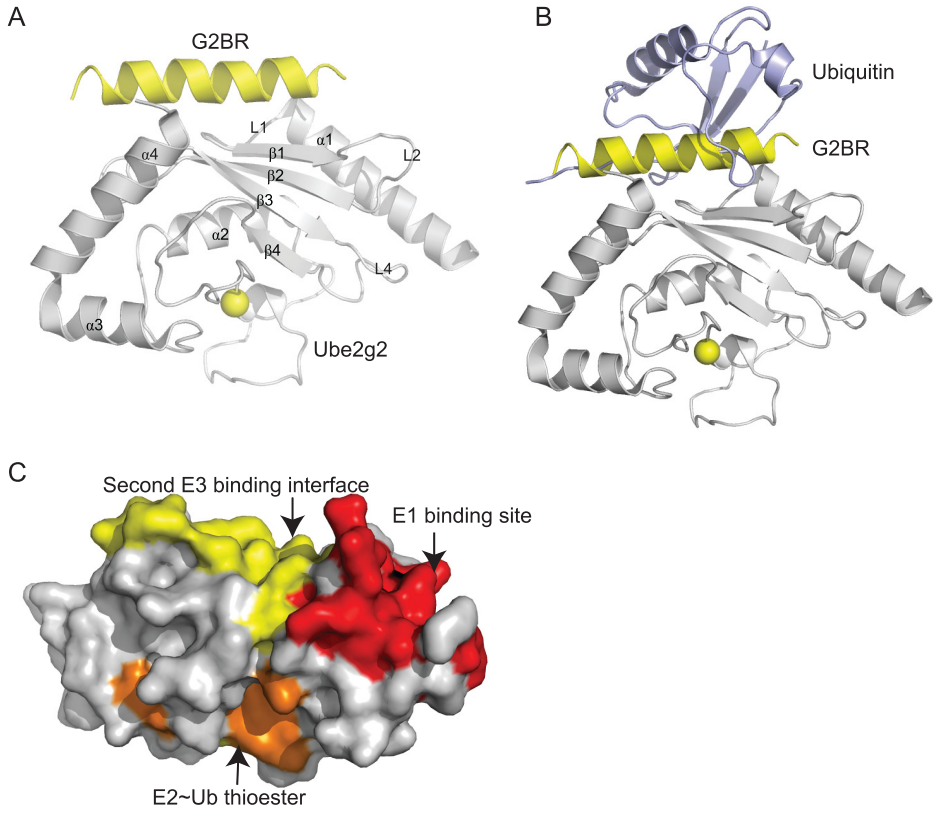

Figure 1.6: The second E3-binding site of the E2 enzymes. **A.** X-ray structure of the G2BR domain of the E3 ligase gp78 in complex with Ube2g2 (3FSH). Yellow:G2BR; Grey: Ube2g2. **B.** Comparison of the G2BR binding site on E2 and the noncovalent Ub-binding site on E2. The structures of G2BR-Ube2g2 (3FSH) and the noncovalent Ub-UbcH5c complex (2FUH) were overlayed based on their E2 structures. Lightblue: ubiquitin. **C.** Surface representation of Ube2g2 showing the E1 and the second E3-binding site on Ube2g2. Yellow: the second E3-binding surface. Red: the E1-binding surface. Orange: the thioester-linkage region.

Similarly, a structural study of the complex of the G2BR peptide segment of gp78 with Ube2g2 shows that G2BR binds to an extended region of the core UBC domain that includes the β sheet (β1-β3) surface and the C- and N-terminal ends of the α1 and α4 helices (Figure 1.6A). This binding site overlaps substantially with the noncovalent ubiquitin binding site (Figure 1.6B) and this may interfere with

poly-Ub chain formation, since the binding affinity of G2BR for Ube2g2 is much higher than that of ubiquitin [81]. However, the two E2 binding sites of gp78 can bind two Ube2g2∼Ub complexes which would allow the formation of K48-linked polyubiquitin chains directly on the active-site Cys of Ube2g2 [78, 80]. This integral poly-K48 chain can then subsequently be transferred to the target substrate. The poly-Ub chain formation directly on Ube2ge might explain why Ube2g2-gp78 can polyubiquitinate substrate without non-covalently binding to ubiquitin.

E2 enzymes can normally not bind at the same time to E1 and RING E3 enzymes, since in both cases the E2 helix α1 is involved in binding [53]. However, the second interaction surface on E2 enzymes for E3s, which is not overlapping with the E1 binding surface, enables on-site recharging of E2s by E1 (Figure 1.6C).

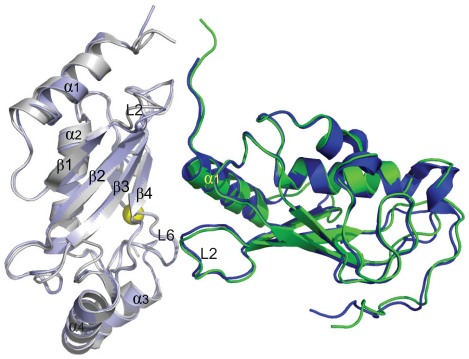

Figure 1.7: Structures of E2 heterodimers. Structural overlay of Ubc13-Uev1A (2C2V) and Ubc13-MMS2 (1J7D). Grey and green represent Ubc13 and Uev1A, respectively. Lightblue and blue represent Ubc13 and MMS2, respectively.

E2 dimerization

It was reported that yeast E2 Cdc34∼Ub thioester can self-associate in vivo and form dimers via symmetrical E2-E2 interactions [82] and that UbcH5c∼Ub can self-associate to facilitate the poly-Ub chain formation [63]. However, in general the presence of E2 oligomers and implication for ubiquitination is not very clear. Structures were described for Ubc13 (Ube2N) in heterodimeric complexes with the E2 variants Ube2v1 (Uev1A) and Ube2v2 (Mms2) that lack the active Cys residue [73]. The overall structures and the dimeric interfaces of Ubc13-Uev1A and Ubc13-Mms2 are highly similar (Figure 1.7). The interface consists of the first helix α1 and loop L2 located between β1 and β2 of Uev1A and Mms2, and the surface created by the β2-β4 strands, loop L2 and loop L6 of Ubc13. Since the E2 dimerization interface of Uev involves

an interface similar to the noncovalent ubiquitin binding site, E2 dimerization could possibly interfere with polyubiquitin chain formation.

Rad6-Rad18 ubiquitination and DNA repair

Ubiquitination is not only involved in proteolytic degradation, but in many cellular pathways as well, including DNA synthesis and DNA repair [10, 83]. The ubiquitination of the protein PCNA (proliferating cell nuclear antigen) is a well-known example [84]. PCNA has an important role in DNA replication as the auxiliary protein of polymerase δ, the enzyme responsible for replication of chromosomal DNA. Upon encountering DNA damage replication is interrupted and the E2/E3 enzymes Rad6/Rad18 are recruited to the stalled replication forks where they monoubiquitinate PCNA at K164 [71]. This causes an exchange of polymerase δ (polδ) by the translesion polymerase η (polη), thereby enabling DNA synthesis across the DNA damage site, the so-called translesion DNA synthesis (TLS) (Figure 1.8) [85, 86]. Subsequently a second set of E2 and E3 enzymes, Ubc13-Mms2 and Rad5, can form a K63-linked polyubiquitin chain onto the monoubiquitinated PCNA [71, 87], and thereby promote the error-free damage avoidance pathway [71, 88]. How Rad6/Rad18 favors monoubiquitination and how Ubc13-Mms2/Rad5 favors polyubiquitination of PCNA, are unanswered questions. In Chapters 4 and 5 of this thesis, we studied the complexes of the E2 Rad6b with the RING E3 Rad18. We show that the Rad18 RING domain forms a homodimer structure and this RING dimer can form a canonical RING-E2 complex with two Rad6b E2s. Surprisingly, in the intact Rad18 dimer only one Rad6b binding site is available. Using X-ray crystallography and NMR spectroscopy we also determined the structure of the complex of Rad6b with R6BD, the C-terminal secondary E2 binding domain of Rad18, and analyzed the interaction regions of Rad6b with ubiquitin. We found that R6BD binds Rad6 at a surface similar to that bound by non-covalently bound ubiquitin. On the basis of these results we propose in Chapters 4 and 5 a mechanism for the monoubiquitination of PCNA by Rad6/Rad18.

The ubiquitin system, disease and drug discovery

The human ubiquitin system targets thousands of proteins for degradation or regulation and mediates a variety of cellular functions, including many diseases associated proteins. Defects in these crucial regulatory processes have been associated with a large number of human diseases including cancers, severe neurological and muscular disorders and a wide array of immune and inflammatory responses [89, 90]. Specific cancers can

result from the stabilization of oncoproteins and growth promoting factors or by the destabilization of tumor suppressor genes. For example ubiqutin targets n-Myc, c-Myc, c-Fos, c-Jun and Src are all oncoproteins, which, when not properly removed from the cell, can induce malignancies. Similarly, destabilization of tumor suppressor proteins such as p53 and p27 can also cause malignant cell growth. A considerable effort in drug discovery is therefore to identify inhibitors of components of the ubiquitination pathway. Possible drug targets include the proteasome, but also the E1 enzymes, E3 ligases and deubiquitination enzymes.

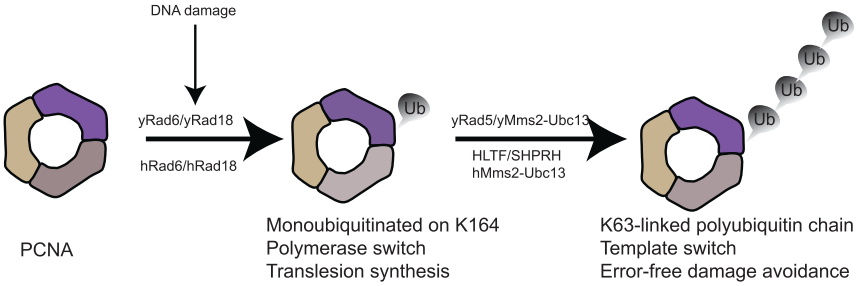

Figure 1.8: Ubiquitination of PCNA in DNA damage response.

The first drug developed for targeting the ubiquitin proteasome system is bortezomib (Velcade). Bortezomib is a small tripeptidic inhibitor of the 20S proteasome and can be used for treating relapsed multiple myeloma and mantle cell lymphoma [91]. The relative selectivity of killing tumor cells vs normal cells may be surprising, but could possibly be associated to preventing pro-apoptotic factors permitting the activation of programmed cell death. Bortezomib targets all ubiquitinated proteins destined for the proteasome, and attacking a single E3 ligase could possibly lead to the stabilization of a single ubiquitinated protein. Higher selectivity could both improve therapeutic effectiveness and reduce non-specific side effects.

Thus E3 ligases and deubiquitination enzymes with a high protein selectivity can potentially be attractive drug targets [91]. One example is the oncogenic protein MDM2 (Murine double minute 2). MDM2 is a RING E3 ligase that is a major regulator of p53 via its proteosomal degradation [92]. p53 is a tumor suppressor, and p53 mutations are observed in a large fraction of human tumors [93]. Therefore overexpression of MDM2, as found in many human tumors, effectively impairs the tumor suppressive effect of p53. Inhibition of the MDM2-p53 interaction can stabilize p53, so selective inhibitors could possibly be used in cancer therapy. One of the first small molecules

that were found to inhibit the MDM2-p53 interaction is the cis-imidazole derivative Nutlin. Nutlin can occupy the p53-binding pocket on MDM2 and displace p53 from it [94]. An example of an E1 targeted drug is MLN4924, a small molecule that inhibits the NEDD8-activating enzyme (NAE). The therapeutic applications of both Nutlin and MLN4924 have progressed considerably with early phase clinical trials and phase I clinical trials, respectively [94, 95], which demonstrates the considerable potential of new drugs targeting the ubiquitin system.

Outline of this thesis

This thesis describes structural and functional studies on the interaction network of E2 conjugating enzymes: the complex of the RING domain of the E3 ligase c-Cbl RING with the E2 enzyme UbcH5b and that with UbcH7, and the complexes of the E2 Rad6b with the RING E3 Rad18 and ubiquitin. **Chapter 1** presents an overview of the ubiquitin system. In this overview I focus on the human E2 conjugating enzymes and their different partners encountered in the ubiquitination pathway. I also describe several structural studies that form the basis of models for the specificity of E2 enzymes in the ubiquitination pathway. In **Chapter 2** I describe an effective method for producing RING/U-box E3 domain proteins in quantities suitable for structural and biophysical studies. In **Chapter 3**, I studied the interaction of the E2 enzymes UbcH5b and UbcH7 with the RING domain of the proto-oncogenic protein c-Cbl. I studied both the ubiquitination activities of both enzymes and their interaction affinities for the c-Cbl RING domain, and found that there is no simple relationship between affinity and ubiquitination activity. In **Chapter 4** and **Chapter 5**, I described the studies on E2/E3 complex of Rad6b/Rad18, a project in which I collaborated with Titia K. Sixma and Richard G. Hibbert of the Netherlands Cancer Institute in Amsterdam. In **Chapter 4**, I describe the X-ray structure of the homodimer of the Rad18 RING domain, and analyzed the interaction of this RING dimer and that of the full-length Rad18 homodimer with Rad6b. In **Chapter 5**, I present the structures of the complex of Rad6b with Rad18 R6BD domain and describe the interactions of Rad6b with covalently and noncovalently attached ubiquitin. These studies form the molecular basis for the recognition of Rad6 by Rad18, which provides an explanation why Rad18 together with Rad6 is specific for monoubiquitination of PCNA. The thesis ends with a summary of my studies.

Chapter 2

Strategy for production of correctly folded E3 RING domains

Anding Huang[1], Rob N. de Jong[1,2], Gert E. Folkers[1], Rolf Boelens[1]

[1] Department of NMR Spectroscopy, Bijvoet Center for Biomolecular Research, Utrecht University, Padualaan 8, 3584 CH, Utrecht, The Netherlands.

[2] Current address: Genmab B.V., Yalelaan 60, 3584 CM Utrecht, The Netherlands.

submitted

Abstract

RING domains of E3 ubiquitin-ligases are involved in specific interactions with E2 ubiquitin conjugating enzymes and thus play an essential role in the ubiquitination pathway. Protein production of the Zn^{2+} containing and cysteine rich RING domains for molecular studies frequently turns out to be problematic. We compared the expression and solubility of 14 E3 RING/U-box domains fused to the N-terminal tags of His_6, His_6-GB1, His_6-Trx and His_6-GST at small scale and analyzed their correct folding after purification by NMR spectroscopy. The addition of GST, Trx or GB1 to the N-terminal His_6 tag significantly improved both the expression and solubility of target proteins as compared to His_6 tag alone. More importantly most of the metal affinity chromatography purified proteins were largely unfolded as judged by ^1H-^{15}N HSQC analysis. We demonstrate that imidazole used in purification of RING proteins can cause proteins unfolding. In contrast, using glutathione affinity chromatography, the His_6-GST fused RING and U-box domains were purified as correctly folded proteins with high yields. Our data demonstrates that GST-fusion affinity chromatography is a better method for expression and purification of Zn^{2+} containing proteins than IMAC.

Introduction

The RING domain is one of the most common zinc binding motifs in human proteins and was first identified in the protein product of the human gene RING1 (really interesting new gene 1) [96]. RING domain proteins play a critical role as the E3 ubiquitin-ligase enzymes in the ubiquitination pathway and the activity of most E3 RING ligases is intrinsic to the RING domain [97]. RING domain proteins contain a cysteine-rich motif defined as Cys-X_2-Cys-X_{9-39}-Cys-X_{1-3}-His-X_{2-3}-Cys-X_2-Cys-X_{4-48}-Cys-X_2-Cys , where X can be any amino acid [98, 99]. In this canonical C3HC4 motif, one zinc ion is bound in a unique cross-brace arrangement to four cysteines (Cys1, Cys2, Cys5 and Cys6), and the other to three cysteines and one histidine (Cys3, His4, Cys7 and Cys8), which maintains a well-defined fold. Over time, several variants of this motif have been identified, such as the RING-H2 motif in which Cys at position 5 is replaced by a histidine [100], and the C4C4 motif in which all the zinc bounded residues are cysteines [101]. There is little sequence conservation in the other residues than zinc ligation Cys/His residues. RING domain structures adopt a similar fold with the conserved Cys/His residues binding to two zinc ion, but the structure outside the zinc binding motif differs considerably. Each RING domain exhibits unique structural characteristics that may affect the specificity for recruitment

of E2 ubiquitin-conjugating enzymes or substrate recognition. Therefore, although dozens of RING domain structures have been studied by X-ray crystallography or NMR, structural studies are needed to understand the rules for E2-E3 recognition. In addition to the RING type E3s, another type of E3s called U-box E3s is involved in ubiquitination. U-box domain of E3 proteins is structurally similar to the RING domain, but it lacks the eight canonical zinc-coordinating residues. Instead, the U-box is stabilized through two centers composed of hydrogen bonds and salt bridges [102, 103].

The RING/U-box containing E3 ligases are considered to be adaptor molecules with the RING/U-box domains responsible for interaction to E2 and another domain for substrate recruitment, thus the specific interaction between E2 and E3 is essential for substrate recognition [98]. Although genome wide interaction maps of human E2/E3-RING/U-box have been generated by yeast two-hybrid screens [104, 105], the mechanism underlying these interactions at an atomic level remains to be elucidated. One particular complication is that one E2 enzyme can interact with multiple E3s, and one E3 can interact to several E2s. Moreover, strong physical interactions of E2-E3 pairs have a poor correlation with enzyme activity in the target ubiquitination [106]. Thus, additional studies will be needed for understanding the redundancy and specificity of E2-E3 interactions. A requirement for such studies is sufficient quantities of purified E2 and E3 proteins.

In this study, we focus on the recombinant expression of soluble and correctly folded RING and U-box domains from 14 E3 proteins which might form functional E2-E3 pairs with UbcH5a, b, c. These highly promiscuous E2 enzymes that have been studied extensively, and show activity with different E3s in a broad number of *in vitro* ubiquitination reactions [107]. Other than these 14 E3s, we also included the Rad18 RING domain which is a cognate partner of Rad6b (E2) and can monoubiquitinate PCNA to initiate the error-prone DNA repair pathway [108]. These targets were cloned into 4 vectors with different fusion tags, since fusion tags are considered to improve the solubility of proteins [109]. The expression and solubility of the selected RING and U-box domains with 4 fusion tags were compared at small scale. Selected His_6, His_6-GB1 fused proteins were expressed at large scale and purified by immobilized Ni^{2+}-affinity chromatography and His_6-GST fused proteins by glutathione-agarose based affinity chromatography. The folding of the purified proteins was analyzed using ^{1}H-^{15}N HSQC NMR spectra.

Material and methods

Expression plasmids construction

All DNA fragments encoding the selected proteins were amplified by PCR using a home-made human cDNA library with synthetic oligonucleotide primers [110]. Each primer contained an extended sequence in front of the gene specific sequence GCCGCGCG-GCAGCCTG for the forward primer (LICFW) and CAAGAAGAACCCCTCA for the reverse primer (LICRV). The AMPure PCR purification method (Agencourt) was used to purify DNA fragments. After purification, these PCR products were treated with T4 polymerase and dATP as described in a previous study [111]. This will create overhangs compatible with those of the vectors used for the ligation independent cloning (LIC). Construction of the single tag pLICHIS plasmid and the dual tag His_6-GB1 (pLICHISGB1), His_6-Trx (pLICHISTRX) and His_6-GST (pLICHISGST) plasmids have been described before [111]. The vectors and inserts are annealed by mixing ∼200 ng of PCR product and ∼10 ng of T4 treated vector followed by incubation at room temperature for 20 min. The annealed plasmids DNA were transformed to Escherichia coli DH5α competent cells, and the cells were incubated in 100µL Luria Broth (LB) without any antibiotics at 37°C for 45 min on a rotating wheel (150 rpm). A total of 75µl of the transformation mixture was transferred to 12-well LB plates containing 50µg/ml ampicillin and allowed to grow overnight at 37°C. For the transformations to the expression strains, such as BL21 Rosetta 2 (Novagen), the transformation mixture was plated on LB plates containing 50µg/ml ampicillin and 35µg/ml chloramphenicol. The selected RING E3 domains were cloned into these 4 vectors with N-terminal His_6, His_6-GB1, His_6-Trx and His_6-GST fusion tags. Rad18 RING proteins were cloned into a His_6-GST fusion tag. The encoding frames of these plasmids were verified by sequencing.

Recombinant protein expression and solubility tests

Expression and solubility tests of target proteins with the 4 different fusion tags were carried out by growing Escherichia coli BL21 Rosetta 2 strain (Novagen). A colony was picked and grown in 3 ml LB containing antibiotics, and when the bacteria culture reached OD_{600} of 0.5-0.7, induced by the addition of 0.5mM of IPTG and 100µM of $ZnCl_2$. The bacteria were grown overnight at 18°C after IPTG induction, the bacterial pellet, taken from a 0.1ml sample, was suspended in 20µl SDS-PAGE sample buffer (whole cell lysate sample). 2 mL of the bacterial culture was lysed in 200µL lysisbuffer containing 50mM Tris-HCl PH8.0, 300mM NaCl, 20%, Sucrose, 50µM $ZnCl_2$, 0.5mM PMSF, 0.2% Triton X-100, 5mM DTT, 0.1 mg/ml lysozyme and EDTA-free protease inhibitor cocktail (Sigma). After two freeze-thaw steps (-80°C /0°C) and 2 times 5s pulses with a Soniprep 150 sonicator, the cell lysate was cleared by centrifugation

for 15 min at 14,000 rpm at 4°C, and 5µl was taken (soluble fraction). Subsequently the lysate was transferred to another tube and the pellet was resuspended in the same volume of lysis buffer. After sonication for 5 seconds 5µl sample was taken (insoluble fraction). Samples were loaded together on SDS-PAGE gel and visualized by Coomassie staining.

For the Rad18 RING proteins, we used pLICHISGST vectors containing the target genes which were introduced in the following expression strains: Escherichia coli BL21 (DE3), Rosetta 2, Rosetta2- pLysS, Tuner and HMS174 (Novagen). The observations of total expression levels as well as soluble protein under different conditions were carried out as described above.

Large scale expression and protein purification

Large scale expression of ^{15}N-labeled RING E3s was performed in 0.5 liter minimal medium[112] with 0.25 g ^{15}N-NH4Cl as described before [110], with the following adaptations. When the culture reached an OD_{600} of 0.6, protein expression was induced by the addition of 0.4 mM IPTG; to ensure the presence of zinc in the protein 100µM $ZnCl_2$ was added simultaneously. The bacteria were grown overnight at 18°C and lysed in 10 ml buffer containing 50mM Tris-HCl, pH 8.0, 300mM NaCl, 20% sucrose, 100µM $ZnCl_2$, 5mM DTT, 0.1% Triton X-100, 0.5mM PMSF, EDTA-free protease inhibitor cocktail (Roche) and 0.3 mg/ml lysozyme.

His_6-tagged and His_6-GB1-tagged RING E3 fusion proteins were purified on a Nickel-charged Poros MC column (PerSeptive Biosystems) as described before [110]. The buffer contained 50 mM Tris-HCl pH 7.5, 100µM $ZnCl_2$ and 10mM β-mercaptoethanol and elution was performed using 800mM imidazole. GST fusion protein purification was carried out by binding the cleared lysate onto glutathione-agarose beads (Sigma) in a binding buffer (50mM Tris-HCl pH 7.5, 100mM NaCl, 100µM $ZnCl_2$, 0.2mM PMSF, 5mM DTT) on a rotating wheel for 16 hours at 4°C(4 rpm). Washing was performed by an increasing salt gradient from 400mM to 1M NaCl in binding buffer. Following washing in thrombin buffer (50mM Tris-HCl pH 7.5, 100mM NaCl, 100µM $ZnCl_2$, 1mM DTT), the GST tag was removed on glutathione-agarose beads by cleavage in the presence of 2 U of thrombin (Sigma) per milligram protein at room temperature for 2 hours and thereafter kept at 4°C until cleavage was complete. The precise amount of thrombin, cleavage time and temperature needed optimization for each target. To prevent non-specific binding of the cleaved proteins to agarose beads, 500 mM NaCl was added to the binding buffer to elute the cleaved proteins. Following inactivation of thrombin by the addition of 0.5mM PMSF (final concentration), the protein samples were exchanged to binding buffer and concentrated using a 5-kDa cutoff spinconcentrators (Amicon ultra-15) to a final concentration of 0.1-1 mM.

NMR spectroscopy

2D ^{1}H-^{15}N HSQC spectra were recorded on Bruker Avance 500 or 600 spectrometers at 298K. All these spectra were processed using XwinNMR3.5 (Bruker) and analyzed using the program SPARKY. Recording times varied depending on the exact concentration of the samples, typically ∼0.2-2 hours. For the imidazole titrations, ^{1}H-^{15}N HSQC spectra of 200µM c-Cbl RING (358-437) in binding buffer were recorded at 298K alone and in the presence of imidazole, increasing from 100mM to 800mM with 100mM each step.

Results and discussion

Cloning, expression and solubility of RING and U-box domains

11 E3 RING domains and 3 U-box domains of human E3 ligases which have been identified as potential partners of the E2 UbcH5a/UbcH5b/UbcH5c were selected for expression examination (Table 2.1). A single domain boundary was chosen for each protein by extending 10-20 amino acids to the RING domain on the basis of sequence homology and secondary structure prediction. His_6, GB1 [113], Trx [114] and GST [115] tags were used as N-terminal soluble fusion partners of the selected E3s rather than the larger MBP and NusA fusions, since the larger tags tend to mask the poor solubility of their fusion partners after removal of the tag [116]. The same amount of PCR products of the 14 targets were hybridized with these vectors by ligation independent cloning, resulting in 14, 8, 14 and 14 targets that were successfully cloned into His_6, His_6-GB1, His_6-Trx and His_6-GST plasmids, respectively. We did not attempt to clone the remainder of the GB1 fusion proteins as preliminary ^{1}H-^{15}N HSQC spectra of the first set of purified proteins revealed unfavorable behavior (see below).

Expression plasmids were transformed into Rosetta 2 for small scale expression and solubility screening. The total cell extract and cleared lysate from 30µL of LB culture were loaded on Coomassie-stained SDS-PAGE, and the intensities of the over-expressed proteins were compared. The effects of His_6, His_6-GB1, His_6-Trx and His_6-GST tags on the expression and solubility of the 14 target proteins were compared as summarized in Table 2.1. With the His_6 fusion, 7 out of 14 proteins could be expressed and 5 appeared to be soluble. The 8 targets that were successfully cloned in the His_6-GB1 vector were expressed and soluble. The proteins fused to the His_6-Trx and the His-GST tag reached similar scores for both total expression and solubility (Figure 2.1). Based on the intensities of soluble expression level on the SDS-PAGE, the order of soluble expression level of the targets was Trx>GB1>GST>His_6 (Supplementary Figure 2S.1). Overall, the numbers of soluble protein constructs were 5, 8, 12, and 10 for His_6,

Table 2.1: Cloning, expression and solubility of select E3s RING and U-box domain after fusing to pLICHIS, pLICHISGB1, pLICHISTrx and pLICHISGST vectors.

Target	Protein Name	E3 type	Boundary	pLICHIS	pLICHIS GB1	pLICHIS Trx	pLICHIS GST
1	AO7	RING	129-213	+/-	+/+	+/-	+/+
2	KF-1	RING	607-685	-	nc	+/+	+/-
3	MDM2	RING	133-181	+/+	nc	+/+	+/+
4	PJA1	RING	584-643	+/+	+/+	+/+	+/+
5	SNURF	RING	117-190	+/+	nc	+/+	+/+-
6	TRC-8	RING	534-598	-	nc	+/+	+/+-
7	RMA1	RING	1-75	-	nc	+/+	-
8	Nrdp1	RING	1-66	-	+/+	+/+	+/+
9	TOPORs	RING	91-156	+/+	+/+	-	+/+
10	CHIP	U-box	225-303	+/-	+/+	+/+	+/+
11	E4A	U-box	1000-1075	-	nc	+/+	+/+
12	E4B	U-box	1147-1218	-	+/+	+/+	+/-
13	c-Cbl	RING	358-437	-	+/+	+/+	+/+
14	hRING2	RING	40-101	+/+	+/+	+/+	+/+

(+/+) expressed/soluble, (+/-) expressed/insoluble, (-) no expression, (nc) No Cloning.

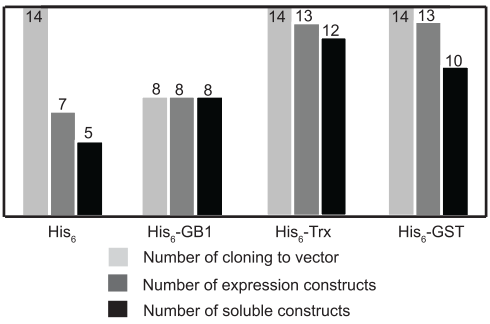

Figure 2.1: Analysis of the small scale expression of target proteins in the 4 vectors. Numbers of target proteins those were successfully cloned, expressed and soluble in Rosseta 2 as a function of the used expression vector.

His_6-GB1, His_6-Trx and His_6-GST, respectively, indicating that GB1, Trx and GST significantly improved expression and solubility of RING and U-box domain proteins compared to His_6 tag alone. Of the 14 targets, all were solubly expressed in at least one of the vectors, clearly demonstrating the advantage of performing small scale expression screening tests using distinct fusion tags to obtain soluble RING domain proteins. These results are in good agreement with earlier studies however the N-terminal His tag seems to perform worse here than in many other studies [109, 117, 118].

Unstructured His_6 and His_6-GB1 tagged RING domains after purification by Ni^{2+} affinity chromatography

Purification can cause problems for target proteins, such as denaturation, inactivation

or proteolysis, as they are exposed to nonnatural conditions during the process. Purification of RING domains can be even more problematic, since modification of critical cysteine or histidine amino acids in the zinc coordination sphere will result in zinc release and alternation of conformation [119, 120]. Thus, for large scale production and purification of RING domain, as needed for NMR studies, the following precautions are generally taken: (a) phosphate buffers should be at a low concentration to avoid precipitation of Zn^{2+}-phosphate; (b) use of metal chelators, such as EDTA or EGTA, should be minimized; (c) the pH should not be lower than 6 to 6.5 in order to prevent the protonation of the Zn^{2+} coordinating residues and subsequent loss of the metal ions [121].

We recorded ^{1}H-^{15}N HSQC spectra which are often referred to as the fingerprint of proteins to monitor the foldedness of purified proteins. We started with the large scale expression of His_6 and His_6-GB1 fused proteins, since they can be efficiently purified by Ni^{2+} affinity chromatography without an extra proteolysis step to remove the fusion tags given their small size and the low risk of disturbing the analysis of the target proteins by HSQC. The His_6 tag is often largely invisible in ^{1}H-^{15}N HSQC, while GB1 shows a group of characteristic signals representing a well folded protein of 56 amino acids.

Four selected His_6 fused proteins appeared at the correct molecular size on SDS-PAGE after purification (data not shown). However, ^{1}H-^{15}N HSQC recorded after buffer exchanging showed that PJA1 and TOPORs were unstructured judged by their poor HSQC spectra with the majority of resonances, in fact, only a few residues were detectable and being broad with little dispersion in the chemical shift possibly reflecting an unfolded oligomeric state (Figure 2.2A). The resonances on the spectrum of the hRING2 spectrum were better resolved than most other His-tag proteins, but the majority of signals are in a narrow range of 7.5-8.5 ppm suggesting that hRING2 was not completely correct folded either (Figure 2.2A). Using the same purification method as for His_6-tagged proteins, four His_6-GB1 tagged proteins appeared denatured in ^{1}H-^{15}N HSQC spectra, for example His_6-GB1-TOPORs and His_6-GB1-CHIP in Figure 2.2B. All these spectra displayed a similar pattern, in which the majority of the well-dispersed peaks corresponded to those from the fully folded GB1 domain (Figure 2.2Ba), while the remaining poorly dispersed peaks in the centre of the spectra are indicative for an incorrectly folded protein.

The observation that most purified proteins with His_6 or His_6-GB1 tags appeared unfolded suggests a common reason for this behavior. Knowing the importance of zinc for folding of RING domains we reasoned that the presence of an excess of imidazole during lysis and/or purification could interfere with zinc binding, due to its ability to bind to transition metals [122]. We therefore studied the effect of imidazole on fold of the RING domain.

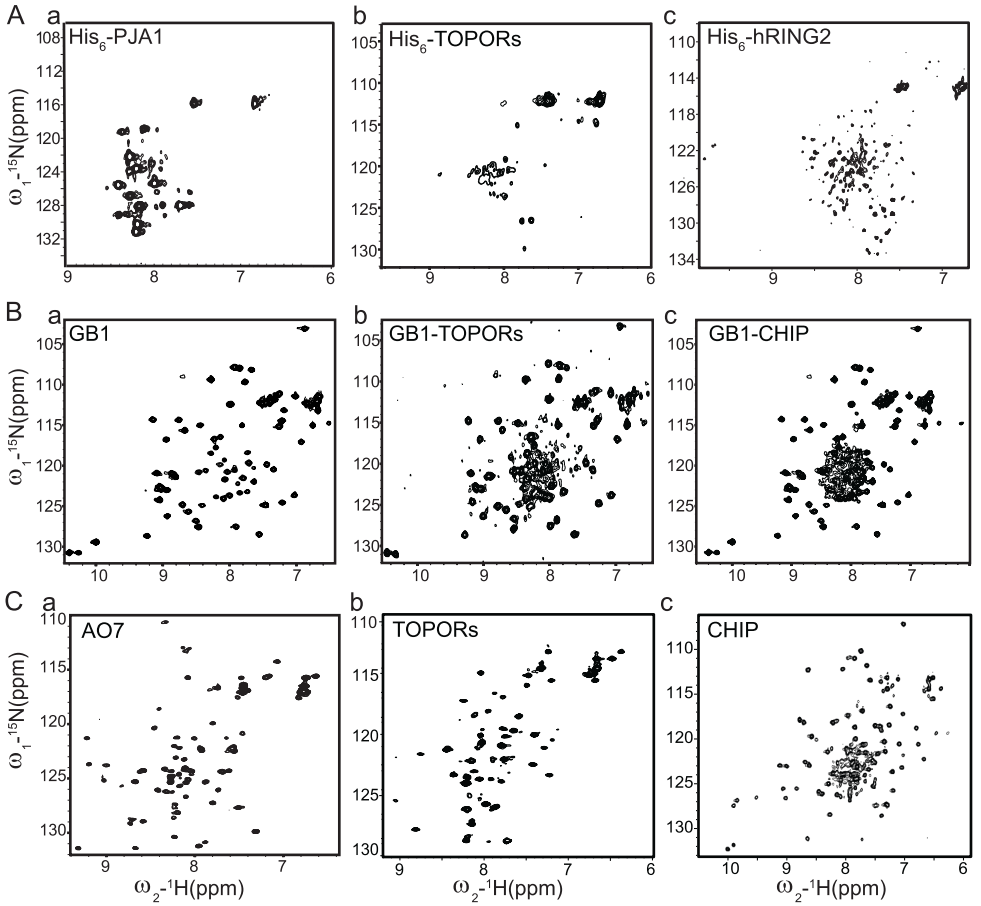

Figure 2.2: Large scale expression of selected proteins and examination by ^{1}H-^{15}N HSQC spectra. **A.** ^{1}H-^{15}N HSQC spectra of purified His_6 tagged RING domains. **B.** ^{1}H-^{15}N HSQC spectra of GB1 and GB1-tagged RING and U-box domains. **C.** ^{1}H-^{15}N HSQC of RING and U-box proteins purified from His_6-GST vector.

Imidazole can unfold RING domains

Imidazole is commonly used for eluting target proteins from Ni^{2+} affinity columns, as it binds to Ni^{2+} and competes with His6-tagged proteins for Ni^{2+} binding (Ni^{2+}/His_6-tagged protein, KD=10^{-6} M at neutral pH [123]). Taking into account of the similar stability between Zn^{2+} and Ni^{2+} for imidazole [124] and the binding affinity of Zn^{2+} with Cys/His residues in zinc finger, for example 10^{-5} M to 10^{-8} M for TFIIIA at pH 7.0 [125], high concentration of imidazole might compete with the Cys/His for zinc binding and thus unfold the zinc finger proteins. Considering the similarity between zinc finger and RING finger proteins, we tested the possible unfolding of c-Cbl RING domain, which is a well behaved and stable protein, by addition of imidazole

and followed the changes by ^{1}H-^{15}N HSQC spectra. We found that upon addition of 400mM imidazole to c-Cbl RING intensity of some peaks decreased, while in the presence of 800mM imidazole this RING domain fully lost the chemical shift dispersion, the characteristic of a well-folded protein (Figure 2.3). Thus, in agreement with the ability of imidazole to bind transition metals, purification of RING domains using high concentrations of imidazole has a potential risk to unfold unstable RING domains. The successful purification of Human NOT4 [101] and EL5 [119] RING domains using 400mM imidazole could be explained by their high stability, similar as c-Cbl RING, which remained largely correctly folded in the presence of 400mM imidazole. Although a lower amount of imidazole in the elution step might rescue several proteins, the elution efficiency will be greatly reduced and optimization of the required imidazole concentration would be time consuming. To overcome these problems, we decided to continue with the GST-tagged targets.

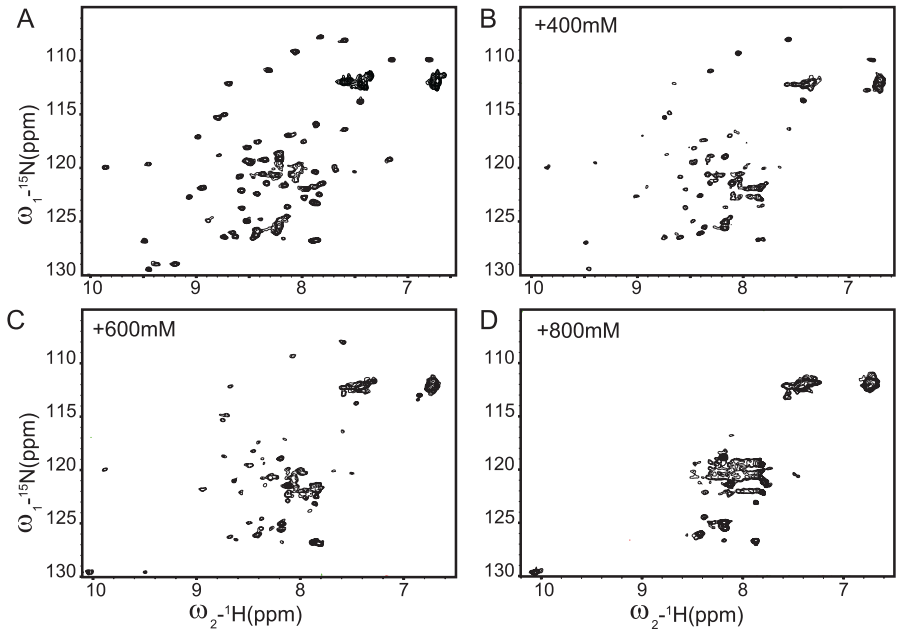

Figure 2.3: Titration imidazole to c-Cbl RING domain. ^{1}H-^{15}N HSQC spectra of c-Cbl RING domain in the presence of 0mM imidazole (**A**), 400mM imidazole (**B**), 600mM imidazole (**C**) and 800mM imidazole (**D**).

Expression of folded RING and U-box domains using a His$_6$-GST expression vector

For His$_6$-GST fused RING and U-box domains, imidazole-caused unfolding can be

circumvented by avoiding Ni^{2+}-affinity chromatography we therefore subsequently tested whether RING domain GST fusion proteins could be purified using glutathione affinity chromatography. This has a number of disadvantages: the tag has to be removed for the structural study since GST is relatively big, the tag might solubilize a poorly folded domain causing the target protein to precipitate after tag-removal and finally the protease cleavage site between the GST moiety and target could be inaccessible for protease digestion resulting in a low yield. To test large scale His_6-GST-RING and His_6-GST-U-box expression and purification using glutathione-agarose beads, six proteins were selected. We recovered 2-5 mg of target protein after removal of GST tag from one liter of M9 minimal medium for TOPORs, c-Cbl and CHIP, and 80% of the GST tags could be successfully removed on the glutathione-agarose beads by thrombin. We did not calculate the yield of AO7, since only one purification trial was performed on AO7.

Well dispersed HSQC spectra indicated that the four proteins were correctly folded after purification and removal of their tags (Figure 2.2C, 2.3A), including TOPORs and CHIP which were unstructured when expressed as His_6 or His_6-GB1 tagged protein and purified by IMAC. In addition, structural and functional studies of c-Cbl RING, expressed and purified as described here, have been conducted, showing that the presented method permits preparation of functional protein [126].

The above strategy was used to produce a soluble Rad18 RING domain. Rad18 RING domains with 8 different boundaries based on the RING domain position (residues 25-63) and the long loop (residues 64-200) were cloned into the pLICHISGST expression vector (Table 2.2). Of those 5 His_6-GST-tagged Rad18 RING constructs containing the most N-terminal loop (residue 1-15) (Figure 2.4A line 1-5), could be expressed solubly in BL21 Rosetta 2. To further enhance the amount of produced Rad18 RING, we examined different bacterial strains including Escherichia coli BL21 (DE3), Rosetta 2, Rosetta 2- pLysS, Tuner and HMS174 (Novagen) at small-scale. Similar solubility however was observed for all these different strains (data not shown). In the end, Rad18 RING (1-103) and RING (1-200) domains were purified successfully, and the RING (1-103) domain was produced as a correctly folded protein suitable for further study (Figure 2.4B).

Overall although GST tag purification using glutathione-agarose beads is not as convenient as His-tag purification by Ni^{2+} affinity chromatography, it clearly circumvents the denaturation of RING domain caused by imidazole dependent zinc removal. A similar setup for all target proteins and subsequent GST cleavage on beads can speed up the GST purification significantly. Thus, the GST tag can be a general good choice for production of RING proteins, not only to improve the expression and solubility but also for purification. Of the four fusion tags, His_6-Trx was the best in the enhancement of soluble expression level, but Trx is not as convenient as GST being

a purification tag.

Table 2.2: Domain boundaries selected for Rad18 RING expression.

Construct	Boundary	Molecular Weight
1	1-76	37 kDa
2	1-103	40 kDa
3	1-194	50 kDa
4	1-200	51 kDa
5	1-228	54 kDa
6	16-76	36 kDa
7	16-103	39 kDa
8	16-194	48 kDa

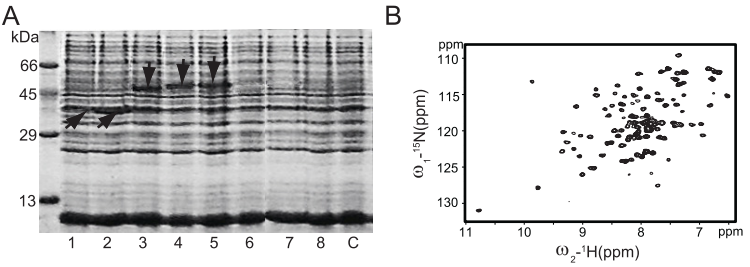

Figure 2.4: Expression of Rad18 RING domain. **A.** Soluble fraction from overexpression of the 8 Rad18 RING constructs cloned to pLICHISGST vector in Rosseta 2. 1-8 refers to construct number in Table 2.2. **B.** ^{1}H-^{15}N HSQC spectrum of Rad18 RING (residues 1-103).

Conclusions

We compared four common fusion tags to improve expression, solubility and foldedness of 14 E3 RING and U-box domains. At small-scale, all targets expressed as soluble proteins, and the addition of GB1, Trx or GST to the fusion His_6 tag significantly improved the expression and solubility as compared to His_6 tag alone. We found that high concentrations of imidazole can unfold RING domains due to competition with the coordinating Cys/His residues, therefore not suitable for either solubility enhancement or purification of RING E3 proteins. In contrast, the GST fusion tag was shown to significantly improve the expression and solubility of RING and U-box domains, and was demonstrated as a reliable purification tag for production with good yields. Considering the similarity between RING domain and other zinc binding motifs, it is likely that GST is also an efficient fusion tag for producing zinc finger proteins in general.

Acknowledgements

We would like to thank Mark Daniels, Johan van der Zwan and Dr. Rainer Wechselberger for laboratory and technical support. This work was financially supported by the Netherlands Organization for Scientific Research, Chemistry Council (NWO-CW) and by European Commission funding through the SPINE2-COMPLEXES project.

Supplementary data

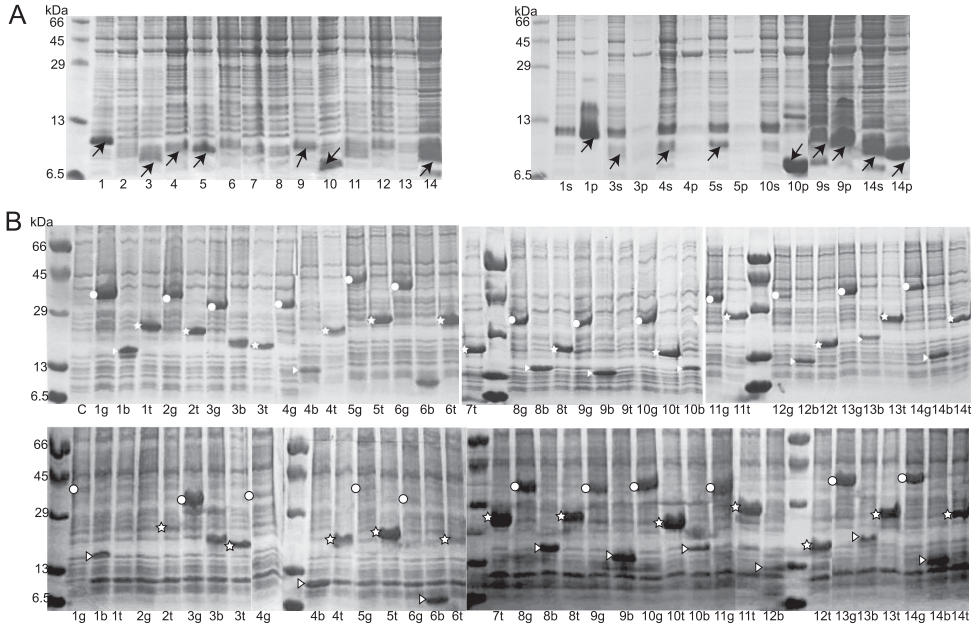

Figure 2S.1: Supplementary Figure: SDS-PAGE gel analysis of small scale expression of target proteins in the 4 vectors. **A.** Total cell lysate (left panel), soluble and insoluble fraction (right panel) from overexpression in Rosseta 2 of the selected E3 RING and U-box domain sequences that were cloned into the pLICHIS vector. 1-14 refers to the target number as depicted in Table 2.1, s-soluble, p-insoluble. **B.** Total cell lysate (upper panel) and soluble fraction (lower panel) from overexpression of selected E3 RING and U-box domains cloned to pLICHISGST, pLICHISGB1 and pLICHISTRX vectors in Rosseta 2. 1-14 refers to target number in Table 2.1, g-GST tag (○), b-GB1 tag (▷), t-Trx tag (★).

Chapter 3

E2-c-Cbl recognition is necessary but not sufficient for ubiquitination activity

Anding Huang[1], Rob N. de Jong[1,3], Hans Wienk[1],
G. Sebastiaan Winkler[2,3],H. Th. Marc Timmers[2]and Rolf Boelens[1]

[1] Department of NMR Spectroscopy, Bijvoet Center for Biomolecular Research, Utrecht University, Padualaan 8, 3584 CH, Utrecht, The Netherlands.

[2] Department of Physiological Chemistry, University Medical Center Utrecht, Universiteitsweg 100, 3584 CG, Utrecht, The Netherlands.

[3] Current address: Genmab B.V., Yalelaan 60, 3584 CM Utrecht, The Netherlands (R.N.de J.), and School of Pharmacy, University of Nottingham, University Park, NG7 2RD Nottingham, U.K. (G.S.W).

JMB, 385, 507-519 (2009)

Abstract

The E2 ubiquitin conjugating enzymes UbcH7 and UbcH5B both show specific binding to the RING domain of the E3 ubiquitin-protein ligase c-Cbl, but UbcH7 hardly supports ubiquitination of c-Cbl and substrate in a reconstituted system. Here, we found that neither structural changes nor subtle differences in the E2-E3 interaction surface are possible explanations for the functional specificity of UbcH5B and UbcH7 in their interaction with c-Cbl. The quick transfer of ubiquitin from the UbcH5B∼Ub thioester to c-Cbl or other ubiquitin acceptors suggests that UbcH5B might functionally be a relatively pliable E2 enzyme. In contrast, the UbcH7∼Ub thioester is too stable to transfer ubiquitin under our assay conditions, indicating that UbcH7 might be a more specific E2 enzyme. Our results imply that the interaction specificity between c-Cbl and E2 is required, but not sufficient for transfer of ubiquitin to potential targets.

Introduction

Post-translational modification by ubiquitin is a major mechanism for regulating protein function in eukaryotes. The general enzymatic cascade of this pathway comprises three enzymes known as E1 (ubiquitin-activating enzyme), E2 (ubiquitin-conjugating enzyme), and E3 (ubiquitin-protein ligase enzyme). The first step in this cascade is the ATP-dependent formation of a thioester bond between ubiquitin and E1, after which ubiquitin is transferred to the catalytic cysteine of an E2 enzyme forming an E2∼Ub thioester. Next, the E3 catalyzes the transfer of the ubiquitin from the E2 to a lysine residue of the substrate, with which it forms an isopeptide bond. While HECT domain E3 ligases mediate this step by formation of a HECT-ubiquitin thioester intermediate, RING domain E3 ligases facilitate a direct transfer of ubiquitin from E2 to the substrate via noncovalent interactions with the E2∼Ub and the substate [127]. In yeast, the substrate can be tagged by a single ubiquitin or ubiquitin chains which can vary in length and linkage specificity. The functions of chains linked through K48 and K63 of ubiquitin have been established. The K48-linked chains are shown to target proteins for degradation via the 26S proteasome, while K63-linked chains recruit binding partners during inflammation or DNA repair [128].

The E2 enzymes are the key enzymes in the ubiquitin and ubiquitin-like pathways. More than 30 structures of E2s from various organisms are available, and all these E2 proteins share a topologically conserved α/β-fold core domain of ∼150 residues. Four α-helices (α1-α4) compose one face of the protein, and a four stranded antiparallel β-sheet (β1-β4) sits on the back of the enzyme between helices α1 and α2 (Figure 3.4). Every E2 core domain can bind three other proteins: the E1 ubiquitin activating

enzyme, a cognate E3 ligase enzyme, and activated ubiquitin via a labile thioester linkage. E2 enzymes can gain additional functionality via association with additional domains or subunits [129, 130].

The complex of c-Cbl and UbcH7 was the first RING E3-E2 structure to be solved [131], but further structural insight into E2-E3 interactions comes from the HECT E3 E6-AP complexed to UbcH7 [132], the NMR based model of the RING E3 CNOT4 bound to UbcH5B [133] and the U-box domain E3 CHIP/Ubc13-Uev1a complex [127, 134]. All these complex structures show equivalent elements in the E2-E3 interface and similarities in overall structure. The core interface is formed by a hydrophobic groove on the E3 and two main regions on E2: loop L1, located between the strand β3 and β4, and loop L2, connecting the strand β4 and the helix α2. In sharp contrast to the wealth of knowledge on E2 structures, the best structural insight of the E2∼Ub thioester intermediate is limited to models based on NMR chemical shift perturbation data due to the inherent instability of the thioester complex [130, 135].

The human genome encodes a few E1s [127, 136], around 30 E2s, several hundred of E3s and thousands of substrates for ubiquitin, which makes the ubiquitination pathway very versatile and highly complex. An E3 may have more than one substrate and some substrates can be recognized by multiple E3s [137]. The large abundance of E3s relative to E2s implies that E2s can function with multiple E3 ligases, but the inverse situation also exists. For example, the RING E3 complex SCF shows *in vitro* poly-ubiquitination activity with both CDC34 and Ubc4 [138, 139], and the activity of the E3 APC is observed with both UbcH10 and UbcH5A, C [140, 141].

It is generally assumed that the binding ability of E2-E3 is the determinant of functional E2-E3 pairs, because decreasing the interaction between E2 and E3 also diminishes their poly- or mono-ubiquitination activity *in vitro*. Interestingly, Brzovic et al. found that the BRCA1/BARD1 E3 heterodimer can interact with UbcH5C and UbcH7 with similar affinity and a similar interface, but only UbcH5C was active in Ub-ligase activity assays [142]. Other examples of E3s that can physically interact with some E2s but fail to support ubiquitin transfer to targets include the RING E3 heterodimer Ring1b/Bmr1 [143] and the U-box E3 CHIP [134]. These results suggest that binding between E2-E3 pairs does not suffice for function. To address this paradox, we have analyzed and compared the c-Cbl/UbcH5B and c-Cbl/UbcH7 complexes both at a structural and functional level.

The E3 ubiquitin ligases of the Cbl family are key regulators of signaling by many surface receptors. From the N- to C-terminus, c-Cbl contains a tyrosine kinase binding (TKB) domain, a linker region and a RING domain, followed by an extensive proline-rich region and an ubiquitin associated domain (UBA). The UBA domain of Cbl-b, a homolog of c-Cbl, has recently been shown to bind ubiquitin noncovalently, promote Cbl-b UBA dimerization and is required for RTK ubiquitination in vivo [144]. The

RING domain can recruit the E2 and function as an E3 ligase [145]. The c-Cbl RING E3 ligase can regulate receptor kinases via their ubiquitin conjugation, and catalyze the ubiquitination of c-Cbl itself as well. This autoubiquitination of E3 enzymes is suggested to represent a regulatory mechanism to control the abundance of Ub protein ligases in cells, since E3 autoubiquitination mediates their proteasome dependent degradation [146, 147]. Here, we studied the binding and functional specificity of UbcH5B and UbcH7 to c-Cbl RING using NMR structural analysis, chimeric UbcH5B/UbcH7 proteins and *in vitro* activity assays, mostly by studying autoubiquitination of the c-Cbl RING domain. We found that although both UbcH5B and UbcH7 can bind specifically to the c-Cbl RING domain, only UbcH5B can facilitate ubiquitination of c-Cbl and substrate, which suggests that the binding specificity between E2-E3 pairs does not necessarily suffice for their functional specificity.

Results

Ub-charged UbcH7 cannot mediate the autoubiquitination of c-Cbl

Early studies indicated that c-Cbl can ubiquitinate EGFR and Src in cooperation with UbcH7 [148, 149], while more recent work showed that c-Cbl promoted EGFR and Src ubiquitination in a UbcH5B dependent fashion [150, 151]. We tested if c-Cbl can form functional complexes with UbcH7 and/or UbcH5B using an *in vitro* autoubiquitination assay, which is a characteristic commonly used to identify functional E2-E3 pairs [152]. To enable accurate quantitation of ubiquitinated c-Cbl, ^{32}P-Ub-K63, in which all lysine residues except for K63 were mutated to arginines, was used in our assays to allow only mono-ubiquitination of c-Cbl. Figure 3.1A shows the efficient autoubiquitination of the c-Cbl linker and RING domain (aa 358-437) in the presence of UbcH5B (lanes 4-8). In contrast, UbcH7 was not active in this system even at very high protein concentration (lanes 9-13). These observations confirm the more recent results [150, 151] and suggest that the UbcH7/c-Cbl pair might be a nonproductive E2-E3 complex. Similar results were obtained using native ubiquitin allowing poly-ubiquitination (data not shown).

To exclude a possible deficiency in our E2 isolates, we tested the integrity of our E2 enzyme preparations in an E2 activation assay (Figure 3.1B). Both UbcH5B and UbcH7 showed efficient formation of ubiquitin-thioester linkages. We also tested the E2 specificity of c-Cbl ubiquitination using a larger c-Cbl construct (47-447) that was previously co-crystallized with UbcH7 [131] and observed that UbcH7 failed to support its ubiquitination as well (Figure 3.1C). Finally, we examined whether UbcH7 and UbcH5B can support the c-Cbl induced ubiquitination of Src, a nonreceptor-type protein tyrosine kinase. Our data show that Src was only ubiquitinated by UbcH5B (Supplementary Figure 3S.1). These data demonstrate that the c-Cbl-UbcH7 complex is a non-productive E2-E3 complex *in vitro*, while under the same conditions the c-Cbl-

UbcH5B complex is productive. This indicates that the physical binding between an E2 and an E3 does not suffice for function. Therefore, we decided to test a number of factors that might explain the different functionality of UbcH5B and UbcH7 complexed to the c-Cbl RING domain.

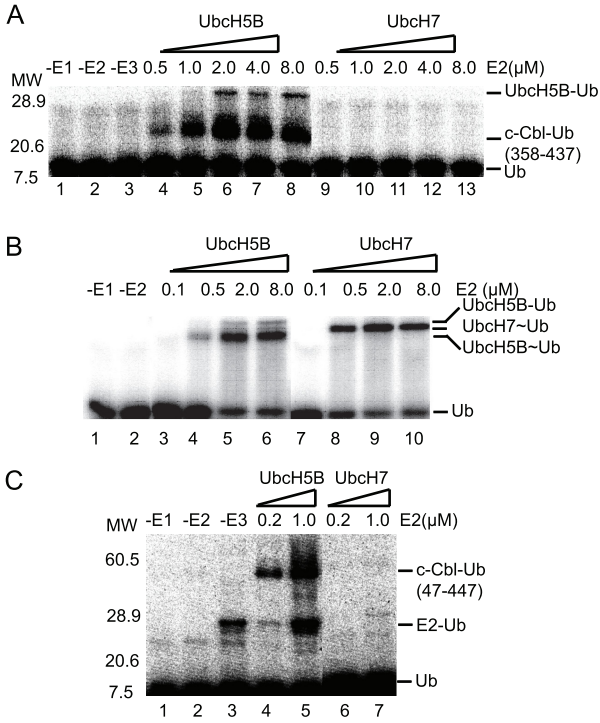

Figure 3.1: UbcH7 does not support autoubiquitination of c-Cbl. Ubiquitin modification via isopeptide bonds resists DTT treatment and is indicated as –Ub, while ubiquitin modification via thioester linkages is sensitive to DTT and denoted with ∼Ub. **A.** Autoubiquitination of c-Cbl linker and RING domain (358-437) with UbcH5B and UbcH7. E3 ligation assays were performed using increasing amounts of E2 enzyme and a radiolabeled ubiquitin mutant incapable of K48 linked polyubiquitin chain formation. Reaction products were separated by reducing SDS-PAGE. **B.** Activation of UbcH5B and UbcH7. E2 ubiquitin conjugation assays of UbcH5B and UbcH7 were performed at increasing E2 concentrations, in the absence of E3 ligase; reaction products were separated using non-reducing SDS-PAGE. Activity of purified UbcH5B and UbcH7 is confirmed by the formation of thioester intermediates, indicated as UbcH5B∼Ub and UbcH7∼Ub. **C.** Autoubiquitination of c-Cbl TKB and RING domain (47-447) with UbcH5B and UbcH7. E3 ligation assay products were analyzed by reducing SDS-PAGE.

c-Cbl RING interacts with similar residues to UbcH5B and UbcH7

First, we tested the possibility that the two E2s might interact with subtly different c-Cbl protein interfaces. We addressed this question by NMR, because the changes in

a [^{1}H,^{15}N]-HSQC protein spectrum are a very sensitive marker to map residues that interact with other factors. We studied the interaction between E2 enzymes and c-Cbl using ^{15}N-labeled c-Cbl (358-437), which contains both the RING domain and the N-terminal H1 linker region previously implicated in E2 binding [131]. In the following discussion, c-Cbl refers to c-Cbl (358-437) unless specified otherwise.

To identify differences between UbcH7 and UbcH5B binding to c-Cbl, we recorded a series of [^{1}H-^{15}N]-HSQC spectra of c-Cbl to which increasing amounts of unlabeled UbcH7 and UbcH5B had been added. The c-Cbl backbone amide peaks sensitive to UbcH7 (Figure 3.2A) binding belong essentially to the same residues that are also in the crystal structure in close proximity to UbcH7. The most perturbed residues in the NMR spectra of the complexes occurred in two c-Cbl regions: residues 383-387 in loop L1, and residues 404-420 in the helix H2 and loop L2 of the RING domain. In contrast to the crystal structure, we have no indications of UbcH7 interaction with residues in the c-Cbl linker H1 region. A comparison between the c-Cbl residues implicated in binding to UbcH5B and to UbcH7 shows that both E2s use a very similar protein interface (Figure 3.2A, B, Supplementary Figure 3S.2). This data indicates that c-Cbl interacts with UbcH5B and UbcH7 in a structurally highly similar fashion.

The titrations of c-Cbl with UbcH5B show fast exchange behaviour for all NMR signals, whereas the titrations with UbcH7 show fast exchange behaviour for most signals and intermediate exchange for signals with large changes in NMR chemical shifts. This allowed an estimation of the binding affinities of c-Cbl for UbcH5B and UbcH7 by fitting the curves of the chemical shift changes upon titration with the two E2s (Figure 3.2C). Fitting the binding curves (assuming a 1:1 stoichiometry) for three representative residues of c-Cbl gave dissociation constants (Kd) of 170 $\pm$ 96 µM and 13 $\pm$ 3.8 µM for UbcH5B and UbcH7, respectively. The larger error in the case of UbcH5B is due to the low solubility of 0.4 mM of UbcH5B that prevents full saturation of c-Cbl. The overall resonance shifts in c-Cbl that can be reached upon full saturation with UbcH7 and UbcH5B are very similar (Figure 3.2). The observed NMR exchange in the titrations indicates that the higher affinity for UbcH7 is largely due to a lower dissociation rate of the c-Cbl-E2 complex. The observation, that c-Cbl bound stronger to UbcH7 might be explained by induced conformational changes in the c-Cbl structure that could affect E2 specificity. However, binding of the two E2s to c-Cbl did not cause chemical shift perturbations for residues distant from the E2 binding site, suggesting that no global c-Cbl conformational changes occurred upon binding. To address this question in more detail, we solved the free solution structure of c-Cbl and compared it with the c-Cbl-UbcH7 complex determined by X-ray crystallography.

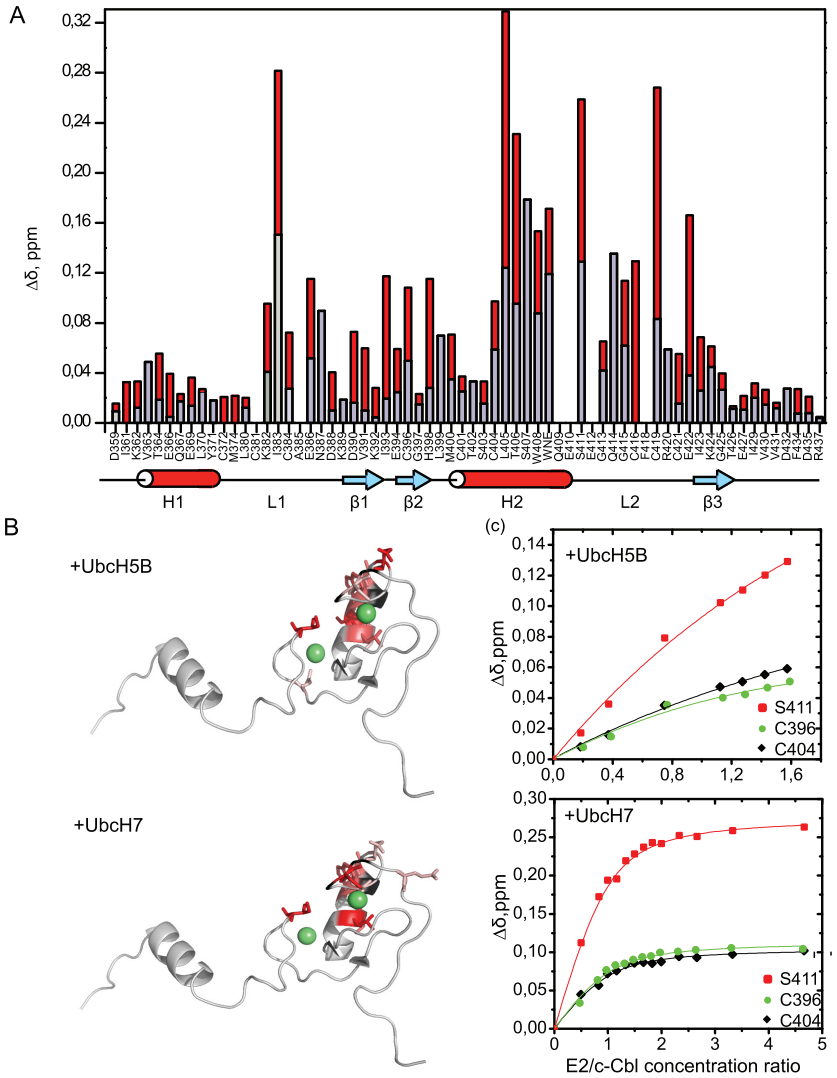

Figure 3.2: Mapping of c-Cbl RING amino acids implicated in binding with UbcH5B and UbcH7. **A.** Chemical shift changes of 15N-c-Cbl (358-437) by addition of unlabeled UbcH5B were colored grey. The larger chemical shift changes of c-Cbl by titration with UbcH7, comparing to UbcH5B, are presented in red. Dotted lines indicate chemical shift perturbation threshold (0.08ppm for UbcH5B, 0.12ppm for UbcH7). **B.** UbcH5B (top) and UbcH7 (bottom) chemical shift perturbations mapped on the c-Cbl crystal structure (PDB ID: 1FBV). Chemical shift changes are colored from white to red (maximal shift). Sidechains colored black indicate signals that were missing or disappeared during titration. **C.** Chemical shift perturbations of C396, C404 and S411 residues in c-Cbl by addition of unlabeled UbcH5B (top) and UbcH7 (bottom) against the molar ratio of E2:c-Cbl RING were fitted to standard 1:1 binding curves.

The c-Cbl RING domain does not show conformational changes upon E2 binding

We obtained a high-resolution c-Cbl solution structure based on 1128 nuclear Overhauser effect (NOE)-derived distance restrains and 58 dihedral angles (Table 3.1). The RING motif is composed of two large Zn^{2+}-binding loops, a short three-stranded anti-parallel β-sheet and a central α-helix (Figure 3.3A). The overall structure of the central c-Cbl Ring motif as determined by NMR is very similar to other RING domain structures. A superposition of the solution structure of the free c-Cbl RING domain to the c-Cbl RING domain in the UbcH7 bounded complex shows that the structures are highly similar (Figure 3.3B). One minor difference between both structures is the conformation of Pro395, which resides between β-stand 1 and 2. The NMR data demonstrate it adopts a cis-conformation in solution instead of the trans conformation in the crystal structure. The linker H1 region also forms an α-helix in solution, but its orientation is not well defined with respect to the RING domain. This may be explained by the absence of the N-terminal TKB domain, which might stabilize this helix by direct interactions with the linker helix H1 Tyr368 and Tyr371 important in c-Cbl phosphorylation [153]. Taken together, these data indicate that there is no evidence for a conformational change upon c-Cbl RING binding to UbcH7.

Table 3.1: Structural statistics of the c-Cbl (358-437) structure ensemble

Number of NMR restraints used in the structure calculation	
Short-range (|i-j|<=1	669
Medium-range(1<|i-j|<5)	135
Long-range(|i-j|>=5)	324
Total NOE restraints	1128
Phi+psi dihedral restraints	58
Coordinated RMSD from mean for residues 377-430 (Å)	
All backbone atoms	0.5
All heavy atoms	1.0
WHATCHECK	
First- generation packing quality	-2.37
Second-generation packing quality	-0.97
Ramachandran plot appearance	-3.05
chi-1/chi-2 rotamer normality	-0.82
Backbone conformation	-5.16
Number of bumps per 100 residues	32.32
PROCHECK	
Most favored regions	78.9
Allowed regions	19.1
Generously allowed regions	1.4
Disallowed regions	0.6

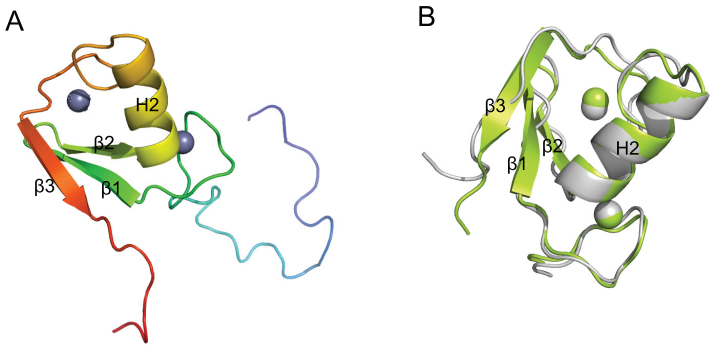

Figure 3.3: NMR solution structure of c-Cbl linker and RING domain (358-437). **A.** Free NMR solution structure of c-Cbl linker and RING domain. **B.** The solution structure of free c-Cbl RING finger domain (lime) superimposed on the crystal structure of the c-Cbl RING finger domain (grey) complexed to UbcH7 (PDB ID: 1FBV).

UbcH5B and UbcH7 bind c-Cbl with similar interfaces

Next, we tested if the functional specificity of the E2-E3 complexes could be caused by structural differences in the E2 enzymes upon binding to c-Cbl. We studied the consequences of c-Cbl binding using NMR titration experiments reciprocal to those presented in Figure 3.2. Unlabeled c-Cbl RING was added stepwise to 15N-labeled UbcH5B and UbcH7 from a 1:5 to a final 2:1 molar ratio. The largest chemical shift perturbations in UbcH5B and UbcH7 were located in the first helix H1, loop L1 between β-strands 3 and 4 and loop L2, connecting β-strand 4 and helix H2 (Figure 3.4). UbcH7 displayed larger chemical shift changes than UbcH5B, in agreement with our observations on the c-Cbl side (Figure 3.2). Already at a 1:5 molar ratio of c-Cbl: UbcH7, the majority of the UbcH7 L2 signals disappeared completely. The peaks belonging to L1 residues F63 and K64 disappeared at lower molar ratios, but reappeared and shifted with increasing amounts of c-Cbl. We did not observe significant changes in the proximity of the catalytic cysteine upon c-Cbl binding to UbcH7.

The chemical shift perturbations in UbcH5B observed upon c-Cbl addition were generally less pronounced. Most of the L1 and L2 resonances disappeared when the molar ratio approached 1:1. Some residues with low peak intensities disappeared upon complex formation, most likely caused by the increased size and lower tumbling rate of the complex. No significant chemical shift changes were observed in the proximity of the catalytic cysteine. In summary, these data suggest that UbcH5B and UbcH7 bind to c-Cbl with a similar interaction surface, and importantly, there was no evidence that c-Cbl binding induced changes in the catalytic center.

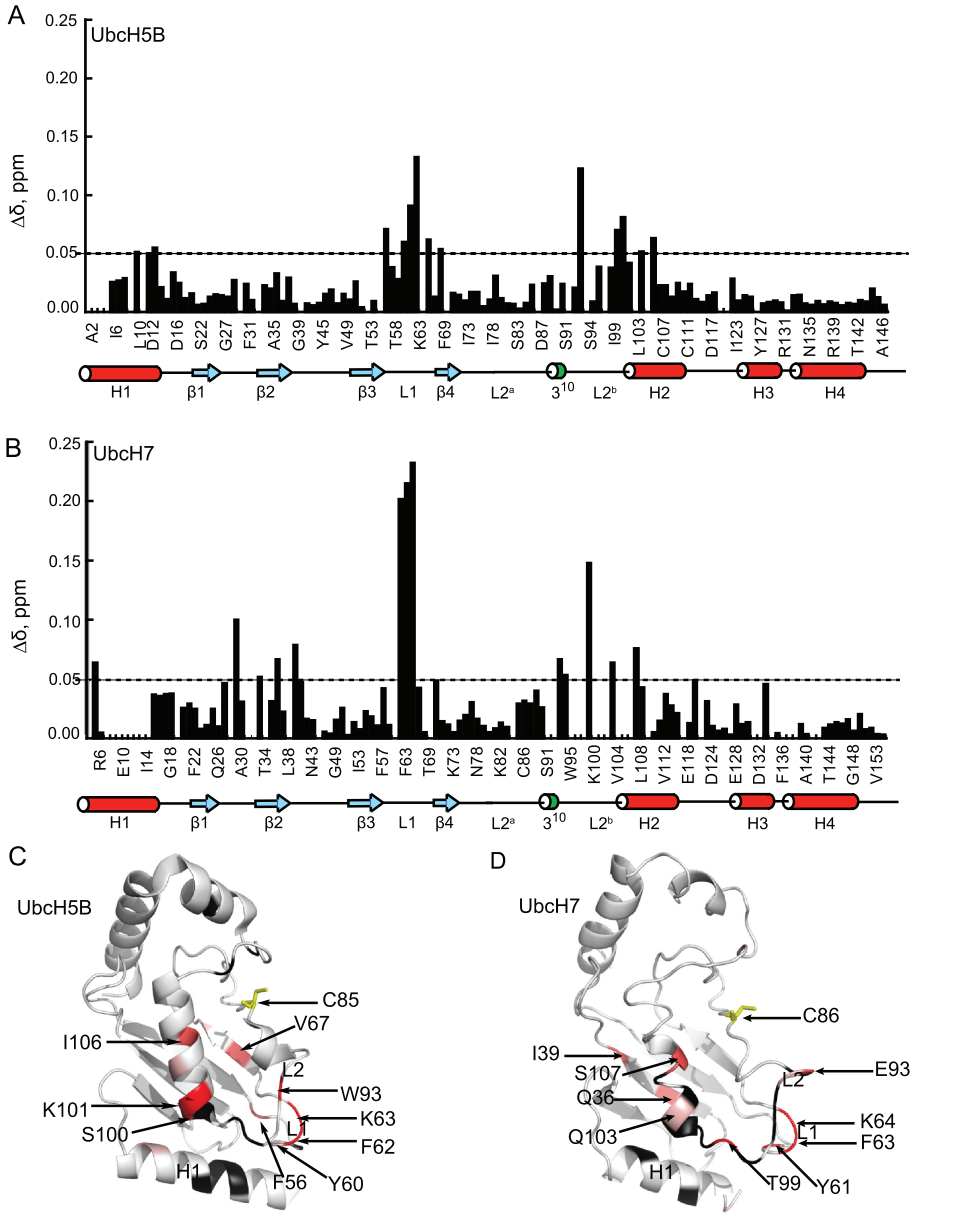

Figure 3.4: UbcH5B and UbcH7 interaction surfaces with c-Cbl mapped by NMR chemical shift perturbation. ^{15}N -labeled UbcH5B (**A**) and UbcH7 (**B**) were incubated with increasing amounts of unlabeled c-Cbl (358-437). UbcH5B (**C**) and UbcH7 (**D**) NMR chemical shift perturbations upon c-Cbl addition were mapped on their structures (PDB ID: 1W4U and 1FBV). Chemical shift changes are colored from white (below threshold of 0.05 ppm) to red (maximal). Sidechains colored black indicate signals that were missing or disappeared during titration. The catalytic cysteine is indicated in yellow.

Table 3.2: E3 interaction motifs in UbcH5B, UbcH7 and three chimeric proteins.

	helix H1	loop L1	loop L2
UbcH5B	MALKRIHKELNDLARD	FPTDYPFKPP	QWSPALTI
UbcH7	MAASRRLMKELEEIRKC	FPAEYPFKPP	NWKPATKT
7H1	MAASRRLMKELEEIRKC	FPTDYPFKPP	QWSPALTI
7L1	MALKRIHKELNDLARD	FPAEYPFKPP	QWSPALTI
7L2	MALKRIHKELNDLARD	FPTDYPFKPP	NWKPATKT

The E2-E3 binding interface does not determine the functional specificity of the E2-E3 interaction

Structural and mutagenesis studies of a number of E2s have identified three regions important for binding to the E3s: the first helix H1, loop L1 and loop L2. Also UbcH5B and UbcH7 interact with the c-Cbl RING domain using these same three regions (Figure 3.4). The mechanism of the E2-E3 interaction is structurally conserved, but specific E2-E3 pairs use subtle variations of a fundamentally similar contact interface [131, 132, 134], which could explain the different consequences of UbcH7 and UbcH5B binding. It is currently disputed whether the specificity of E2s is dependent upon the composition of their L1 and L2 loops. To further characterize the importance of the E3 interaction regions H1, L1 and L2, and to test if any of these three regions causes the functional specificity of the E2 for the c-Cbl RING finger, we created three chimeric UbcH5B/UbcH7 proteins that have a UbcH5B framework with a small part of UbcH7 at the E3 interface (Table 3.2). In chimera 7H1, we replaced helix H1 of UbcH5B with helix H1 of UbcH7. Likewise, in the 7L1 and 7L2 mutants, we swapped UbcH5B loops L1 and L2 with the corresponding loops of UbcH7.

First, we confirmed proper folding of the three chimeric proteins with [^{1}H, ^{15}N]-HSQC spectra (Supplementary Figure 3.3A). The HSQC spectra are highly similar for residues not directly neighboring the substituted motif, which shows that the mutants adopt highly similar conformations. Second, we determined the averaged dissociation constants (Kd) of 7L1 and 7L2 by titration experiments as described in Figure 3.2. Chimera 7L1 and 7L2 displayed a Kd of approximately 26 ± 9.6 μM and 110 ± 41 μM, respectively (Supplementary Figure 3.3B). Next, we evaluated the chimeras by a number of functional assays. In an E2 activation assay, chimeras 7H1 and 7L1 formed thioester linkages to ubiquitin with UbcH5B wild type like efficiency (Figure 3.5A, C). Chimera 7L2 possessed slightly less E2∼Ub active protein than wild type UbcH5B. The changes in L2 might induce subtle conformational changes to the catalytic region because of its closer proximity. All three chimeras could ubiquitinate c-Cbl with an efficiency comparable to that of wild type UbcH5B (Figure 5b,d), while even the lower amount of 7L2∼Ub did not compromise efficient transfer of ubiquitin

from 7L2 to c-Cbl. Although the c-Cbl binding affinity of 7L1 and 7L2 is higher than that of UbcH5B, this stronger interaction did not inhibit the ubiquitination of c-Cbl. For these E2/E3 complexes, there appears no direct correlation between the binding affinity and ubiquitination ability. Together, these observations indicate that the inability of UbcH7∼Ub to transfer ubiquitin to c-Cbl is not related to differences in mode and strength of E2/E3 interaction.

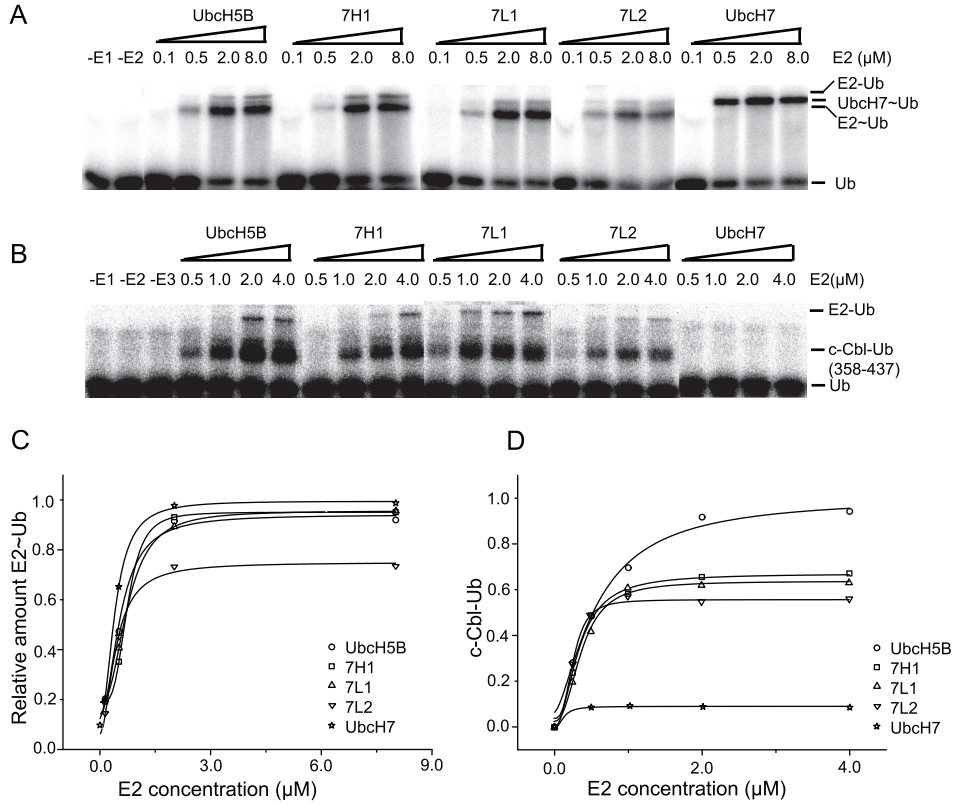

Figure 3.5: Analysis of the E2/E3 interaction surface using chimeric UbcH5B/UbcH7 proteins. **A**. E2 conjugation assays (see legend to Figure 3.1B) of the three chimeras 7H1, 7L1 and 7L2. The activity of these three chimeras was confirmed by the formation of thioester intermediates indicated as E2∼Ub. Reaction products were separated by non-reducing SDS-PAGE. **B**. Autoubiquitination activity assays (see legend to Figure 3.1A) of c-Cbl RING domain by the three chimeric E2 enzymes 7H1 7L1 and 7L2. Reaction products were separated by reducing SDS-PAGE. All three chimeras can support c-Cbl RING autoubiquitination with an efficiency similar to that of wild type UbcH5B. E2-Ub and c-Cbl-Ub are indicated. **C**. Quantitation of reactions shown in (A). **D**. Quantitation of reactions shown in (B).

The UbcH5B∼Ub thioester shows greater reactivity than UbcH7∼Ub

Since we ruled out both structural changes and subtle differences in the interaction

region as possible explanations for the functional specificity of UbcH5B and UbcH7 in their interaction with c-Cbl, we focused on the intrinsic catalytic properties of the two E2 enzymes. Therefore, we studied the E2 reactivity of transferring the E2∼ubiquitin thioester to different ubiquitin acceptors including water, buffer and thiol, which is called release rate here. After charging the E2 with ubiquitin, we assayed the time course of ubiquitin dissociation from E2∼Ub. By adding apyrase, we depleted the ATP needed for E1 activity and monitor E2∼Ub dissociation in the absence of E2 recharging.

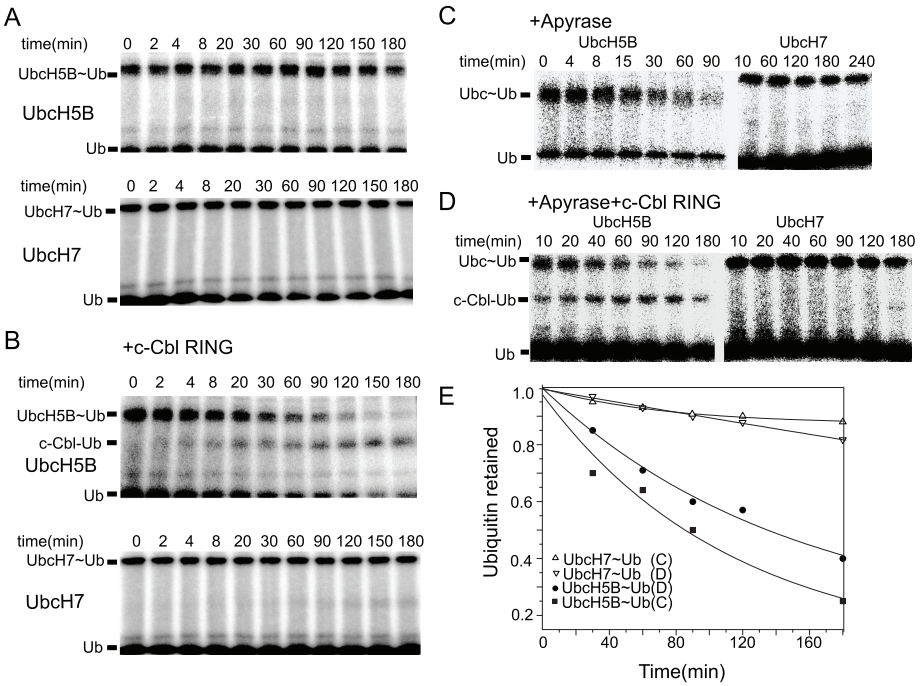

Figure 3.6: Ubiquitin thioester stability measurements. **A**. UbcH5B or UbcH7 were charged with ubiquitin by incubating with E1, ubiquitin, and ATP for 30 minutes. Subsequently, samples were taken at the indicated time points and separated using non-reducing SDS-PAGE. **B**. After a 30 min preincubation as described for (A), c-Cbl was added at the start of the sampling timecourse. **C**. After the 30 min preincubation as described for (A), apyrase was added at the start of the sampling timecourse to deplete ATP and block E1-dependent ubiquitin charging of E2. **D**. As described in (C) with addition of c-Cbl at the start of the sampling timecourse. **E**. Quantitation of reactions shown in (C) and (D). The upper 2 lines are the timecourses of UbcH7∼Ub amount without and with addition of c-Cbl RING. The lower 2 lines are the timecoures of UbcH5B∼Ub amount with and without addition of c-Cbl RING.

Under recharging conditions, the levels of UbcH5B∼Ub and UbcH7∼Ub were stable for more than three hours, since E2∼Ub formation and dissociation are in

steady state (Figure 3.6A). The addition of c-Cbl enhanced the ubiquitin release rate of UbcH5B∼Ub, but not of UbcH7∼Ub (Figure 3.6B). When recharging was blocked by the addition of apyrase, UbcH5B∼Ub released ubiquitin from its thioester 10 times faster than UbcH7 (Figure 3.6C, E). The addition of c-Cbl slightly slowed down ubiquitin release from UbcH5B (Figure 3.6C, D), In contrast, CNOT4 and Apc2/11 can enhanced the rate of ubiquitin release from UbcH5B∼Ub [154]. The release rate of ubiquitin from UbcH7∼Ub in the absence of recharging was not affected by the presence of c-Cbl (Figure 3.6E).

The quick transfer of ubiquitin from UbcH5B∼Ub to c-Cbl and to other acceptors suggests that UbcH5B might be a more active and relatively pliable E2, which could explain why many RING E3s can be ubiquitinated by UbcH5B. We also examined the ubiquitin release rate of the three UbcH5B/UbcH7 chimeras, and found that they behaved like the wild type UbcH5B (data not shown). In contrast, UbcH7∼Ub is too stable to release ubiquitin to ubiquitin acceptors under our assay conditions, which indicates that UbcH7 could have a more restricted specificity. This intrinsic stability of the E2∼Ub thioester intermediate is unique for each E2, which suggests that understanding the factors that influence E2∼Ub thioester stability will help to understand E2 specificity.

Discussion

In our experiments, we found that UbcH5B can support the *in vitro* autoubiquitination of c-Cbl and the c-Cbl-facilitated substrate ubiquitination, and UbcH7 not. NMR titrations of c-Cbl to UbcH5B and UbcH7 did not show structural distinctions that could explain the functional differences. More likely, the different reactivity of the thioesters UbcH5B∼Ub and UbcH7∼Ub might explain why c-Cbl/UbcH7 is almost "nonproductive" *in vitro*. The E2∼Ub thioester intermediate is a key intermediate in the ubiquitination pathway, which is the actual substrate for ubiquitin ligases and substrates. Unfortunately, the transient nature of this thioester makes it very difficult to study its interactions with E3. The NMR study of the formation of S22R-UbcH5C∼Ub thioester showed that chemical shift perturbations on UbcH5C were not solely a consequence of direct contact with Ub, but also induced by allosteric effects [130], which might explain the different properties of E2∼Ub and E2 in their interaction with E3 or substrate.

Electrostatic potentials of UbcH5b and UbcH7 A comparison of the electrostatic potential surface of UbcH7 and UbcH5B reveals striking differences (Figure * 3.7). Protein Interaction Property Similarity Analysis (PIPSA) is a measure of electrostatic potential similarity and ranges from -1 on full anti-correlation to 1 on perfect correlation between two potentials [155]. Autoubiquitination of BRCA1 could be facilitated by Ube2w, UbcH6 and UbcH5, but not by UbcH7 [156]. UbcH5B has much less

electrostatic potential similarity to UbcH7 (0.394) than it has to UbcH6 (0.678) and Ube2w (0.613). The biggest difference in electrostatic potential between UbcH5B and UbcH7 is observed at the β-sheet implicated in noncovalent ubiquitin binding (Figure * 3.7), which corresponds to the fact that only UbcH5B can noncovalently bind to ubiquitin [130]. Interestingly, the E2∼Ub thioester interfaces of UbcH5B and UbcH7 also display differences: although both are negatively charged, UbcH7 is more negatively charged both close to the catalytic cysteine as well as at the residues expected to bind Ub upon thioester formation [135]. The increased stability of the UbcH7∼Ub thioester might be explained by this superior complementarity to the positively charged Ub thioester interface.

Functional specificity of UbcH5B and UbcH7

The intrinsic high stability of the UbcH7∼Ub thioester intermediate could explain why UbcH7 fails to transfer ubiquitin to c-Cbl, but also suggests that other accessory factors might be needed to help the release of ubiquitin from the UbcH7∼Ub thioester to its substrates or E3. For example, the auxiliary protein Smad7 can recruit UbcH7 to the HECT E3 Smurf2, and regulates the catalytic activity of Smurf2 at the level of E2 recognition [146]. Also ubiquitination of Trk by UbcH7 and the TRAF6/E3 was carried out in the presence of p75 and p62 [157].

Although the E3 interacts with E2 on the common interface composed of helix H1, loop L1 and loop L2, E3s have their own preference for the binding position on E2s. For example, K63 of UbcH5B, F63 of UbcH7 and M64 of Ubc13 in loop L1 were important in the interactions with CNOT4, c-Cbl and CHIP respectively [131, 134, 159], while the loop L2 residues of UbcH5C showed bigger perturbations upon binding to BRCA1-BARD1 [156]. The mechanism underlying the E2-E3 interactions and functions is not well understood, but it seems that dynamic, transient and modest affinity interactions are more productive. Similarly as observed for the BRCA1/BARD1, the stronger binding of c-Cbl to UbcH7 did not facilitate ubiquitin transfer. Also, in the case of E6AP/UbcH7, there was no correlation between the increased formation of ubiquitin-E6AP and enhanced binding affinity of UbcH7 and mutant E6AP [160]. These results imply that the ubiquitination pathway might not be optimized for one particular pairwise interaction, but is rather designed to function in its entirety. Together with our comparison of UbcH5B and UbcH7 in c-Cbl ubiquitination, this indicates that binding specificity only compromises a part of the functional specificity of E2 enzymes. Does the binding specificity of E2-E3s form the basis for their functional specificity? We believe the answer is yes, although the physical interaction between a functional E2-E3 pair is required, yet not necessarily sufficient to transfer ubiquitin to substrates.

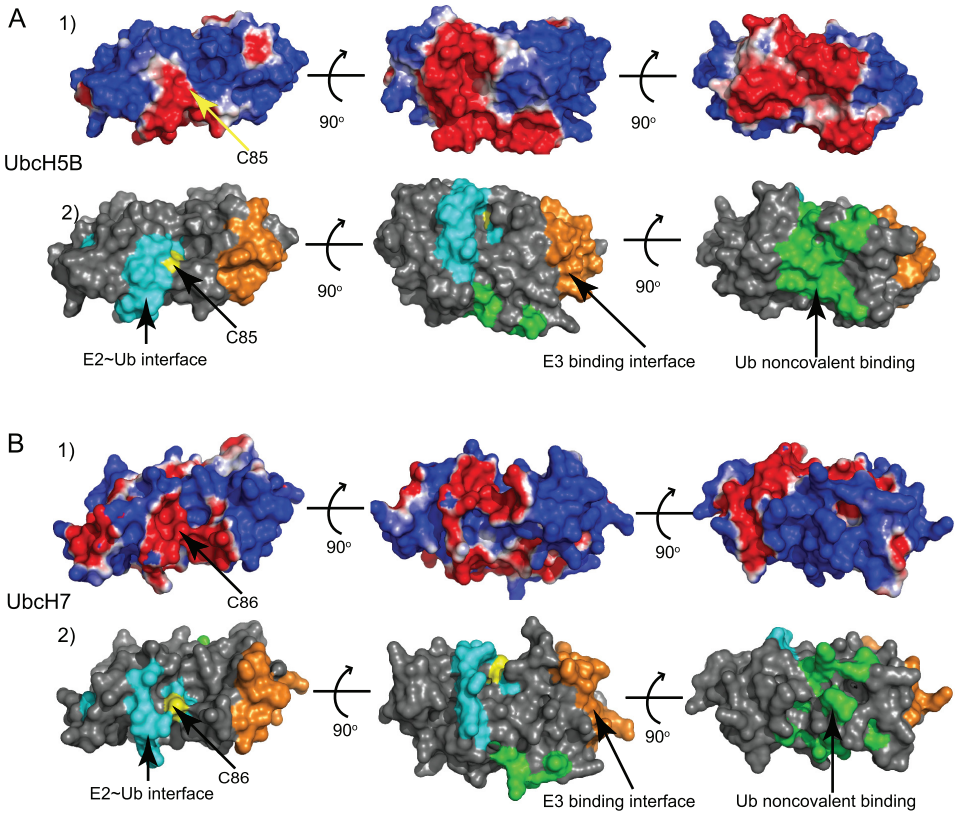

Figure * 3.7: Comparison of surface properties of UbcH5B and UbcH7. **A**. Top: electrostatic surface potential of UbcH5B was calculated using the APBS plugin to PyMol and indicated as a charge scale from negative (red) to positive (blue). Bottom: surface representation of interaction sites on UbcH5B. The catalytic site (yellow), E2∼Ub binding interface (cyan), E3 binding interface (orange), and the non-covalent Ub-binding interface on UbcH5B (green) are indicated. **B**. UbcH7 electrostatic surface potential (top) and interaction sites (bottom), colored as indicated under (A).

Materials and Methods

Construction of Plasmids

The construct of wild-type human UbcH5B was amplified from a human cDNA library and cloned into the plasmid pLICHIS, a pET15B derived expression vector, by Enzyme-free cloning [161]. The chimera 7H1, 7L1 and 7L2 (Table 3.2) plasmids were amplified from the plasmid pLICHIS-UbcH5B, and further details are provided as Supplementary material. The fragment enconding the c-Cbl linker and RING domain (358-437) was cloned from a human cDNA library into pLISHISGST vector

[161]. Correct constructions of these plasmids were confirmed by DNA sequencing. The plasmid of UbcH7 has been described before [158]. The pGEX4T1 expression plasmid containing c-Cbl (47-447) was a kind gift of Dr N. P. Pavletich (Memorial Sloan-Kettering Cancer Center).

To allow ^{32}P labeling of ubiquitin, a protein kinase A recognition site was introduced in the normal enzyme free cloning short forward 5' and LIC forward 5' primers to generate ^{32}P-labeled Ub-K63, in which all lysine residues were mutated except for K63. PCR A was amplified from pET14b-Ub-K63 vector (kindly provided by Dr R. Baer, Columbia University) with short forward 5' TGCGTCGTGCATCTGTTatgcagatcttcgtgaagac and LIC reverse 5' CAAGAAGAACCCCTCAcccacctctgagacggagtac. PCR B was performed with LIC forword 5' GCCGCGCGGCAGCCTGCGTCGTGCATCTGTTatgcagatcttcgtgaagac and short reverse 5' TCAcccacctctgagacggagtac. The hybridized PCR product of PCR A and B was cloned into the pLICHIS vector.

Recombinant Protein Expression and Purification

Overexpression and lysis of ^{15}N and ^{13}C/^{15}N-labeled c-Cbl were accomplished by growing Escherichia coli BL21(DE3) Rosetta 2 strain (Novagen) containing the pLICHISGST-Cbl (358-437) expression vector in minimal medium mainly as described before [162]. Further details are provided as Supplementary material. Purification was carried out by binding the lysate supernatant to gluthation-agarose (Sigma) in buffer B (50mM KH_2PO_4/K_2HPO_4 pH 7.3, 100mM NaCl, 100µM $ZnCl_2$, 0.2mM PMSF, 5mM DTT), washing with buffer B plus 900mM NaCl, and changing to buffer C (50mM KH_2PO_4/K_2HPO_4 pH 7.3, 100mM NaCl, 100µM $ZnCl_2$, 1mM DTT) for GST cleavage. The GST tag was cleaved on the gluthation-agarose beads by addition of 2 U of thrombin (Sigma) per milligram protein at room temperature for 1 hr and kept at 4°C for overnight. Protein was eluted by buffer B plus 500mM NaCl. Thrombin was inactived by addition of 0.5mM PMSF (final concentration). The c-Cbl sample was exchanged to buffer B and concentrated to final concentration of 1.0-1.2 mM using a 5-kDa cutoff spinconcentrator (Amicon ultra-15).

The unlabeled and ^{15}N-labeled His-tagged UbcH5B and the 7H1, 7L1 and 7L2 chimera were expressed in Escherichia coli BL21 (DE3) and purified on a Nickel-charged Poros MC column (PerSeptive Biosystems) [162]. The overexpression of unlabeled and ^{15}N-labeled GST-UbcH7 in Escherichia coli BL21 (DE3) were performed as described [158] and buffer exchanged to buffer B.

NMR spectroscopy and structure calculation

NMR experiments were carried out on Bruker AVANCE 600 and 700 spectrometers equipped with triple-resonance z-gradient probes. Standard spectra for resonance assignment and structure determination [163] on c-Cbl (aa 358-437) were recorded at

298 K in a buffer containing 50mM KH_2PO_4/K_2HPO_4 pH 7.3, 100mM NaCl, 100μM $ZnCl_2$, 0.2mM PMSF, 5mM DTT, 95%/5% H_2O/D_2O and a small amount of complex protease inhibitor (Roche). All NMR spectra were processed using XwinNMR3.5 (Bruker) and analyzed using the program SPARKY [164]. Structure calculations were performed using the program CYANA [165]. The final structures were validated with WHATIF [166] and PROCHECK [167]. Molecular images were generated with PyMol [168]. Structural coordinates of the 20 lowest energy structures were deposited in the Protein Data Bank under access code 2K4D. NMR chemical shift assignments were deposited in the Biological Magnetic Resonance Bank (BMRB) database under entry 15796.

NMR titrations

Unlabeled UbcH5B and UbcH7 were prepared in buffer B. For the binding titrations, the [^{15}N-^{1}H]-HSQC spectra of 100 μM c-Cbl (358-437) in buffer B were recorded at 298 K and in complex with different stoichiometric ratios of UbcH5B and UbcH7 (1:0.25 to 1:1.5 for UbcH5B, and 1:0.5 to 1:5 for UbcH7). Combined chemical shift perturbations were calculated using the equation, $\Delta\delta ppm = ((\Delta\delta HN)^2 + (\triangle\delta N/5)^2)^{1/2}$ [154]. The chemical shift changes were plotted against the molar ratio of Ubc:c-Cbl and fitted to standard 1:1 binding curves using the program Origin 8.0. For the reciprocal binding titrations, 15N-labeled UbcH5B and UbcH7 were prepared in buffer B at a concentration of 100 μM, and c-Cbl was added to them until a final ratio of c-Cbl:Ubc of 2:1. The 1H and 15N backbone assignments of UbcH5B and UbcH7 were from Biological Magnetic Resonance Data Bank (BMRB) entries 6277 and entry 15498 [169, 170], respectively.

^{32}PLabeling of Ubiquitin

pLICHIS-Ub-K63 containing an N-terminal His-tag and Protein Kinase A site was expressed in E. coli BL21 (DE3). Purified ubiquitin was labeled in a 100μL reaction containing 4μL [γ^{32}P]-ATP, 4μL PKA (5U/μl, Sigma P2645), 40-80μg protein in buffer 20mM Hepes/KOH pH 7.5, 100mM NaCl, 12mM $MgCl_2$ and 1mM DTT. After 30 min incubation at 30°C, ^{32}P-Ubiquitin was purified using magnetic Ni-beads (Promega) to separate radiolabeled protein from free label.

Enzymatic assays (*In vitro* Ubiquitination assay and thioester release assay)

The standard reactions (15μl) of a E2∼Ub thioester formation assay contained 0.028μM E1, 0.5μM-10μM E2, 0.2μM ($\sim$1*10^4 cpm) ^{32}P-Ub in a buffer 50mM Tris-HCl pH7.5, 50mM NaCl, 5mM $MgSO_4$, 5mM ATP, and incubated for 30 min at 30°C. For the c-Cbl autoubiquitination assay, 4 μM c-Cbl (358-437) or c-Cbl (47-447) was added to the

reactions and incubated for 90 min. In the competition assay, the indicated amounts of UbcH5B, UbcH7 and c-Cbl were included in the E2 activity reaction. For the release assays, 0.2 unit/μl apyrase was added to deplete ATP after the E2∼Ub thioester formation. Samples were taken at the indicated times, stopped by adding reducing or nonreducing SDS sample buffer, separated by 12% SDS-PAGE and subjected to autoradiography.

Footnotes

The abbreviations used are: E1, ubiquitin-activating enzyme; E2, ubiquitin-conjugating enzyme; E3, ubiquitin-protein ligase; Ub, ubiquitin; Ub-K63, ubiquitin with all lysine residues mutated to arginine except for K63

Acknowledgements

We would like to thank Dr. E. AB for help with structure calculations, Dr. Tammo Diercks and Dr. Rainer Wechselberger for expert NMR assistance, Dr. Gert E. Folkers, M. Hilbers and J. van der Zwan for laboratory and technical support. This work was supported by grants from the Netherlands Organization for Scientific Research (NWO-CW TOP 700-52-303 and 700-53-103) and by European Commission funding through the SPINE2–COMPLEXES project LSHG–CT–2006–031220. G.S.W and H.Th.M.T. were supported by grants from the Netherlands Organization for Scientific Research (NWO-MW Pionier 900-98-142) and the European Union (6FP LSHG-CT-2004-502950).

Supplementary material

Construction of 3 Chimera Plasmids

The chimera 7H1 (Table 3.2) encoding a fusion of UbcH7 (1-16) and UbcH5B (15-147) was amplified from the plasmid pLICHIS-UbcH5B by using a 5'primer containing a linking site and a sequence encoding UbcH7 (1-16), and cloned into the pLICHIS vector as the wild-type UbcH5B. The 7L1 plasmid was produced by site-directed mutagenesis. Plasmid 7L2 encoding a fusion of UbcH5B (1-90), UbcH7 (92-100) and UbcH5B (100-147) was generated using two PCRs reactions: the first amplified UbcH5B (1-90) with a 3'primer encoding the sequence of UbcH7 (92-100); the second contained UbcH5B (100-147) with a 5'primer complementary to the 3' primer of the first reaction. The two PCR products were hybridized and cloned into pLICHIS vector.

Recombinant Protein Expression and Purification

Overexpression of ^{15}N and $^{13}C/^{15}N$-labeled c-Cbl was accomplished by growing Escherichia coli BL21(DE3) Rosetta 2 strains (Novagen) containing the pLICHISGST-Cbl (358-437) expression vector in minimal medium as described before 24, with the following adaptations. Induction took place at A_{600}=0.6 by addition of 0.4mM isopropyl-β-thiogalactopyranoside (IPTG), and bacteria were grown 16 hr at 18 °C and lysed in buffer (50mM Tris-HCl pH 8.0, 300mM NaCl, 20% sucrose, 100μM $ZnCl_2$, 5mM DTT, 0.1% Triton-100, 0.5mM PMSF, protease inhibitor cocktail(Roche), 0.3 mg/ml Lysozyme). After freeze-thawing and sonication, lysates were centrifuged at 15,000 rpm in a Sorvall SS34 rotor for 45 min at 4 °C.

Src autophosphorylation and ubiquitination assays

^{32}P labeling of Src was carried out in a 26μl reaction containing 600ng Src (Sigma S5439) and 4μL [$\gamma^{32}P$]-ATP at 30°C for 30 min in buffer (20mM Hepes/KOH pH 7.5, 3mM $MnCl_2$). The ubiquitination assay of Src was performed as described in the autoubiquitination of c-Cbl (47-447), except that 3μl ^{32}P labeling Src reaction was added and unlabeled Ub-K63 was used instead of the ^{32}P-Ub-K63.

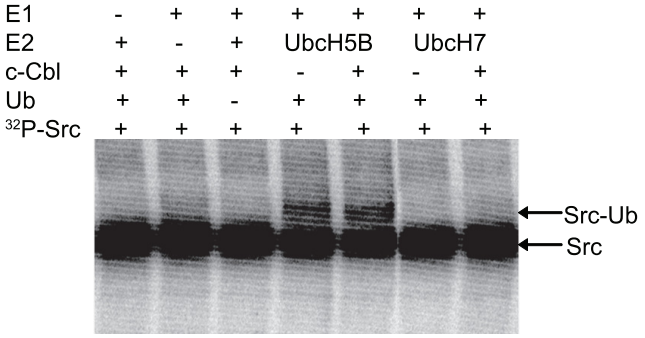

Figure 3S.1: UbcH7 was defective in supporing c-Cbl mediated ubiquitination of Src. Src-Ub and Src are indicated. In this assay, UbcH5B can ubiquitinate Src in the absence and presence of c-Cbl.

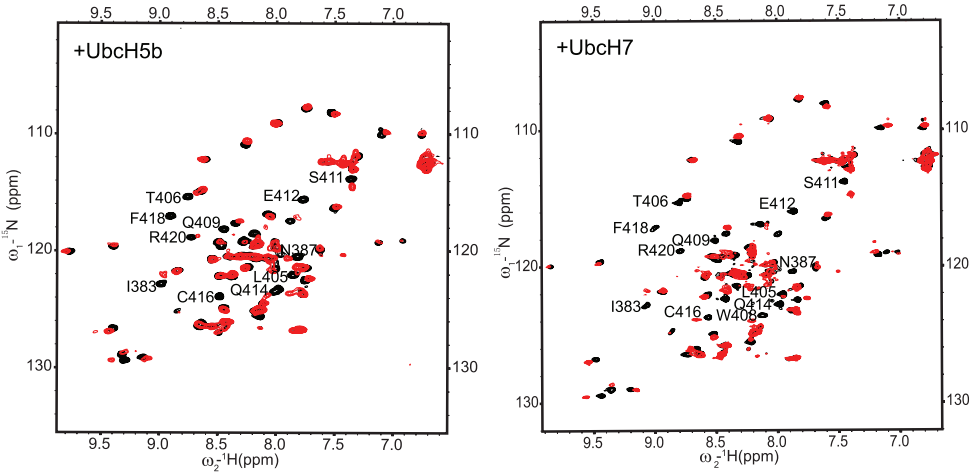

Figure 3S.2: Overlaid [^{1}H,^{15}N]-HSQC of ^{15}N -c-Cbl linker H1 and RING domain in the absence (black) and presence (red) of 1.5 equivalent of UbcH5b or and UbcH7 as indicated.

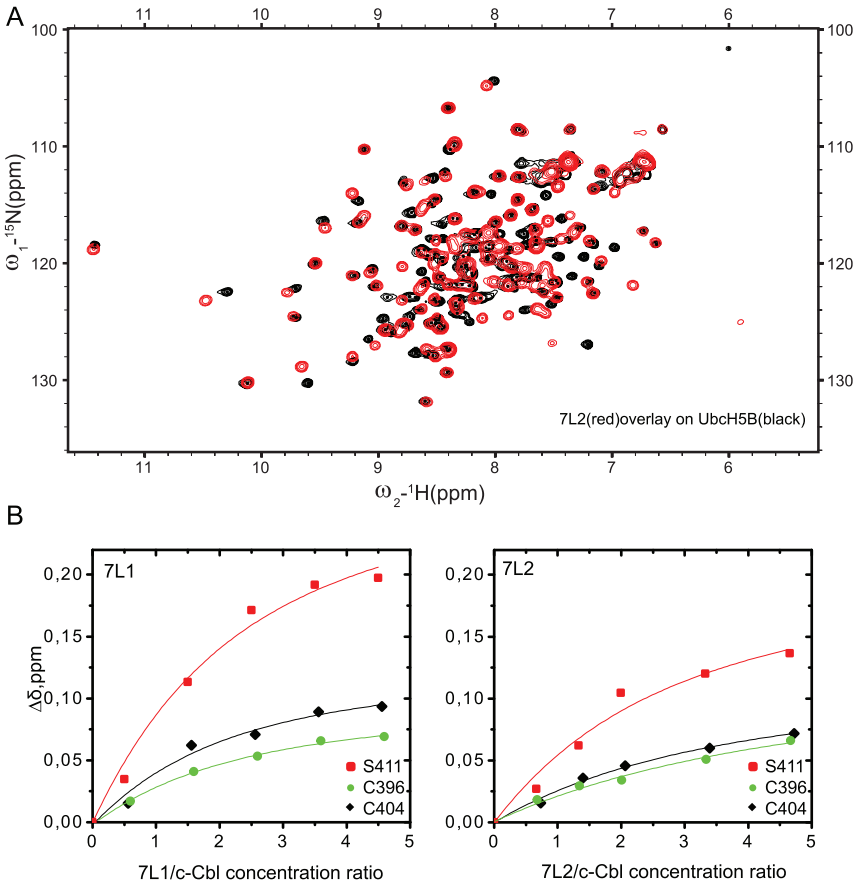

Figure 3S.3: **A**. Overlaid ^{1}H, ^{15}N-HSQC of UbcH5B (black) with chimera 7L2 (red). **B**. Chemical shift perturbations of C396, C404 and S411 residues in c-Cbl by addition of unlabeled 7L1 (left) and 7L2 (right) against the molar ratio of E2:c-Cbl RING were fitted to standard 1:1 binding curves.

Chapter 4

Symmetry and asymmetry of the RING-RING dimer of Rad18

Anding Huang[1*], Richard G. Hibbert[2*], Rob N. de Jong[1,3], Devashish Das[1], Titia K. Sixma[2] and Rolf Boelens[1]

[1] Department of NMR Spectroscopy, Bijvoet Center for Biomolecular Research, Utrecht University, Padualaan 8, 3584 CH, Utrecht, The Netherlands.

[2] Division of Biochemistry and center for Biomedical Genetics, Netherlands Cancer Institute, Plesmanlaan 121, 1066 CX Amsterdam, The Netherlands.

[3] Current address: Genmab B.V., Yalelaan 60, 3584 CM Utrecht, The Netherlands.

*These authors contributed equally to this work

Manuscript in preparation

Abstract

The human ubiquitin-conjugating enzyme Rad6 (E2) and ubiquitin-ligase enzyme Rad18 (RING E3) complexes are involved in the monoubiquitination of PCNA in response to DNA damage and play a crucial role in translesion DNA synthesis. The connection between the oligomeric states of Rad18 and Rad6 and monoubiquitination of PCNA is not clear. We studied the structure of the Rad18 RING domains, and the complex formation with Rad6. We show that the N-terminal RING domain of Rad18 is responsible for dimerization. The three-dimensional structure of the Rad18 RING homodimer, solved by X-ray crystallography shows dimer interactions through the four-helix bundle composed of helices adjacent to the RING domains and through the canonical RING domains. Using NMR spectroscopy and site-directed mutagenesis, we show that the Rad6b binding site for the Rad18 RING domain strongly resembles that of other E2-E3 RING/U-box complexes and the Rad18 RING dimers can bind two Rad6b E2 enzymes. In contrast, binding studies of full-length Rad18 homodimer with Rad6b show that Rad18 homodimer can bind only to a single Rad6b enzyme. This asymmetry has been observed in heterodimeric E3 ligases, and once in the homodimeric U-box E3 CHIP [171]. Our results indicate that this asymmetry could be more common in E3 homodimers.

Introduction

Protein modification by ubiquitin or ubiquitin-like proteins conjugation through the E1-E2-E3 enzyme cascade has been involved in not only proteolytic degradation but also modulation of protein function [172], including cell-cycle control, DNA replication and DNA repair. Almost all DNA repair pathways are regulated in some way by ubiquitination or SUMOylation [173, 174]. Ubiquitination of proliferating cell nuclear antigen (PCNA), a DNA polymerase sliding clamp involved in DNA synthesis and repair that encircles DNA as a homotrimer, plays an essential role in the DNA repair pathway [175].

DNA lesions can halt the progression of DNA replication forks, which may lead to more severe damages, such as DNA double-strand breaks (DSB) or cell death unless synthesis resumes. Post-replication repair mechanisms (PRR) can overcome such replication blockage and allow DNA replication to continue [176, 177, 178]. In *Saccharomyces cerevisiae*, *RAD6* and *RAD18* encode a ubiquitin-conjugating enzyme E2 and a ubiquitin ligase E3 – the central players in PRR [179]. For mammals, two yeast *RAD6* related genes named *RAD6A* and *RAD6B* and a single *RAD18* homologue are involved in DNA damage tolerence [180, 181, 182]. The PRR pathway contains two

major processes, translesion synthesis (TLS) and error-free template switch combined with recombination [183]. A Rad6-Rad18-dependent ubiquitination of PCNA functions to initiate and choose the different subpathways [184, 185]. When DNA is damaged, Rad6/Rad18 are recruited to stalled replication forks and monoubiquitinate PCNA at K164 at stalled replication folks in an RPA-dependent manner [186], which makes a polymerase exchange from the replicative polymerases, such as δ (polδ) to one of the translesion polymerases at the stalling sites, thereby inducing TLS [176, 187, 188]. A second pair of E2/E3 enzymes, such as Ubc13-Mms2/Rad5 in yeast, can sequentially carry out K63-linked polyubiquitination chain formation from the monoubiquitinated PCNA, and promote an error-free damage avoidance pathway [185, 189].

Rad18 has been shown to exist as a dimer and to form a stable complex with Rad6b *in vitro* [179, 184, 190, 191, 192]. Early studies in yeast showed that the C-terminal region of Rad18 was involved in this complex formation with Rad6 [179, 193]. For human Rad18, this C-terminal region, was later mapped more precisely to residues 340-395, and called the Rad6 binding domain (R6BD) [187, 191]. In addition, it was noted that the N-terminal RING domain (25-74) could interact with Rad6 as well [181, 190, 191]. It has been found that the two Rad6 interaction regions on Rad18 are non-overlapping [191].

The importance of the E3 ligase enzymes in ubiquitin pathway is manifested in conferring specificity by recognizing a target and by facilitating ubiquitin transfer to this target. Different types of E3 ubiquitin ligases have been identified previously: RING, U-box and HECT-domain containing proteins [194]. These domains are involved in recognizing specific E2s [195]. However in contrast to the HECT domain, the RING and U-box E3s do not attach activated ubiquitin themselves, but only bring the E2∼ubiquitin thioester and substrate in close proximity and in this way transfer the activated ubiquitin to the target substrate [195]. The folds of the RING and U-box domains, both 40-60 amino acids, are structurally highly similar. In the RING domain the fold is maintained by eight conserved Cys/His residues which bind to two zinc ions [196], but the U-box domain has the same fold without coordinating two metal ions [194, 197]. The mode of interaction of both RING and U-box domains to the E2 core UBC domain is very similar and involves a common interface [195, 196].

Many E3 ubiquitin ligase enzymes are known to form homo- and hetero-oligomeric species [173, 196]. The E3 ligases can dimerize or multimerize via different domains, and there are some examples where the dimerizations are mediated by the RING/U-box domains, such as heterodimers BRCA1-BARD1[198], RING1b-BMI1 [199] and MDM2-MDMx [200]. Some RING domains can form homo-dimers, such as RAG1 [201], cIAP [202], TRAF6 [203], as well as the Prp19 [204] and CHIP U-box proteins [171]. The functional significance of homo- and hetero-dimeric complexes in ubiquitin ligase signaling has been demonstrated[198, 200, 205], but whether both of the E3

monomers are capable of E2 binding and E3 activity is still a question. Theoretically, E3 proteins in the state of dimer could interact with two E2 proteins, since each RING/U-box domain can bind one E2. However, for the RING domain heterodimer E3s BRCA1-BARD1[206], RING1b-BMI1[199], it has been shown that only one of the two RING domains can bind E2 and has E3 activity. More surprisingly, the U-box dimer of CHIP binds two E2s in the absence of the TPR domain[171, 207], but the full-length CHIP dimer displays that only one U-box domain recruits E2 since the other U-box domain is occluded by the N-terminal TPR domain[171]. Other E3 homodimers might possess similar behaviour as CHIP dimer. For this reason, we studied the structure and E2 complexes of the Rad18 RING domain and analyze the stoichiometry of full-length Rad18 with Rad6 in this context.

Results and discussion

The N-terminal Rad18 RING domain forms a homodimer

Dimerization of the full-length Rad18 has been demonstrated in yeast and human[184, 190, 191], but the dimerization interface is not clear so far. Earlier studies proposed that ZnF domain of the human Rad18 was important for dimerization [190], while later work by Notenboom et al. [191] found that neither ZnF nor the C-terminal domain of Rad18 was responsible for dimerization of Rad6/Rad18 complex, but mapped this to the region comprising residues 1-199 of Rad18 containing the N-terminal RING domain. To examine whether the RING domain of Rad18 is able to dimerize, we expressed and purified the RING domain of human Rad18 (1-121) and performed multi-angle static light-scattering (MALLS) measurements to analyze its molecular weight. The MALLS profile of Rad18 RING (1-121) in Figure * 4.1B fits to a molecular weight of ∼28 kDa, which is consistent with a dimeric state of the Rad18 RING that has a molecular weight of 13.5 kDa for one monomer. Rad18 RING (1-99) shows a similar MALLS profile (data not shown). Combining this with the previous results of the dimerization interface studies by Notenboom et al. [191], we propose that full-length Rad18 dimerizes through the interface of RING domain.

Crystal Structure of Rad18 RING homodimer

To characterize the structure of the dimeric Rad18 RING domain, we crystallized Rad18 (1-99) and solved the crystal structure to 1.8 Å resolution (Figure * 4.1C, Table 4.1). The structures of the two RING monomers are nearly identical with RMSD (root-mean-square deviations) of 0.6 Å over 86 Cα atoms. The electron densities of the first eight and last five residues are missing, suggesting that these residues are disordered. Each monomer subunit of Rad18 RING contains a central RING motif (residue 24-76) and two anti-parallel ∝-helices flanking at the N-terminus (residues

14-23, α1) and C-terminus (residues 77-91, α4) (Figure * 4.1C). The core RING motif adopts a characteristic fold similar to other RING domains comprising a three-stranded anti-parallel β-sheet (β1, β2 and β3), a central α-helix (α2), a 3_{10}-helix (α3), and two long loops (L1, L2) that are stabilized by coordination of two zinc ions with consensus Cys/His residues in a cross-brace composition, of which the first zinc coordinates two cysteines from loop L1 (Cys25 and Cys28) and other two cysteines from α2 (Cys46 and Cys49), and the second zinc with three cysteines and one histidine (Cy41, His43, Cys60 and Cys63) (Figure * 4.1C, * 4.2A). The anti-parallel α1 and α4 helices at N- and C-terminus pack against each other and extend from the core RING motif. The relative orientation of the helices with respect to the core RING is determined mainly by the helices contacting with residues in the loop L1 and β1 of core RING (Figure * 4.1D). (Tyr31 and Phe32 in the loop L1 interact with both N-terminal and C-terminal residues Asp20, Leu23, Arg24, Val82 and Arg89. The first β-sheet residues Ile34 and Ala35 have contact to C-terminal resides Leu78 and Asp79.)

Table 4.1: Data collection, phasing and refinement statistics of Rad18 RING Homodimer.

Data Collection Statistics		1-99	
Number of Crystals1	1		
Spacegroup		C121	
Unit Cell: a, b, c, (Å)	104.68	29.34	69.72
alpha, beta, gamma	90.0	125.0	90.0
Resolution Limits (High)	42.9-1.8 (1.84-1.80)		
Completeness		99.4 (98.2)	
Number of unique reflections	31646 (2339)		
Multiplicity		9.1 (2.9)	
Low resolution Rmerge	0.014		
Rmerge		0.105 (0.929)	
<I/sigma>	18.3 (1.59)		
Wilson B factor ($Å^2$)	19.6		
Model Refinement Statistics			
R factor	0.175		
R free		0.218	
Number of Protein Atoms	1404		
Number of Waters	113		
Ramachandran Plot			
- favoured		97.08%	
- outliers		0.00%	
RMS bond, Z-bond (Å)	0.0123, 0.496		
RMS angle, Z-angle (deg)	1.308, 0.585		

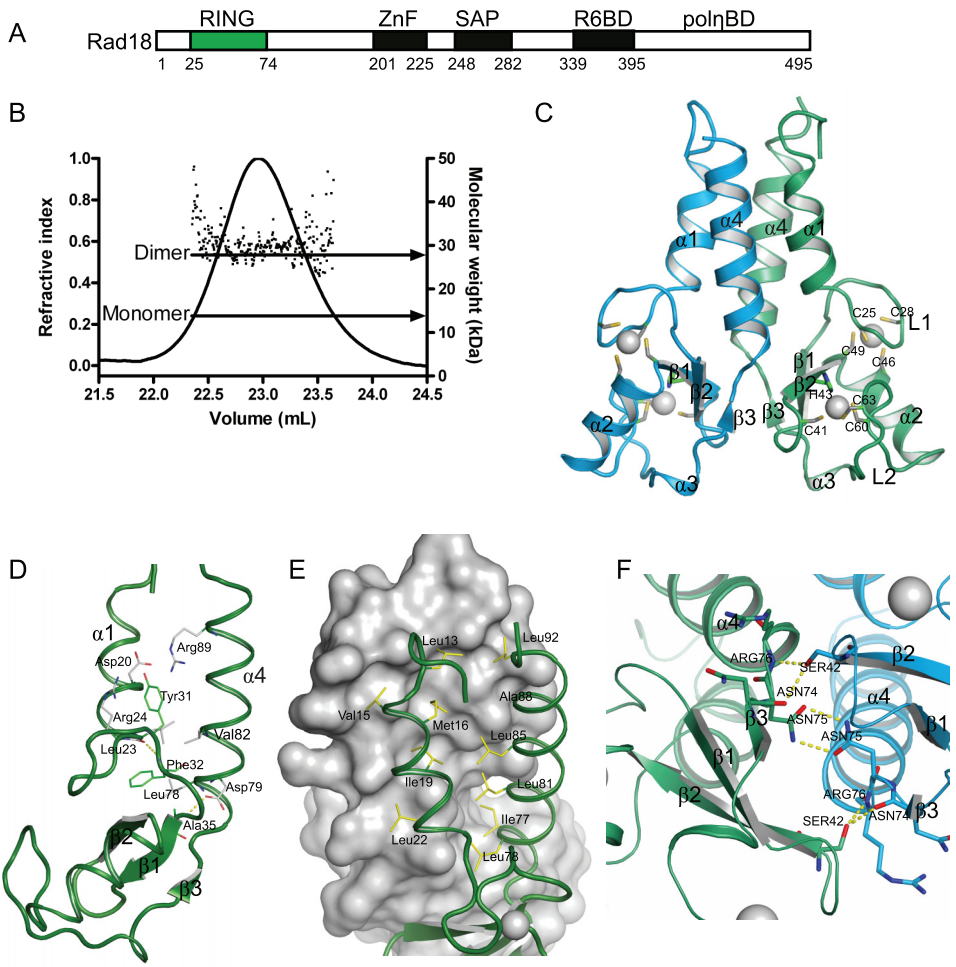

Figure * 4.1: Structure of the Rad18. **A.** Domain organization of Rad18. **B.** Oligomeric state of Rad18 (1-121) RING. MALLS profile showing refractive indices for monomeric and dimeric Rad18 RING domains. **C.** Secondary structure cartoon of the Rad18 RING (1-99) homodimer. The secondary structure elements are labeled. **D.** Detailed view on the interaction between helices α1, α4 and the RING core motif. The yellow dashes indicate stabilizing hydrogen bonds. **E.** Detailed view on the interaction at the dimerization interface of the four-helix bundle consisting of α1, α4, α1' and α4' at the C- and N-terminus of Rad18 RING (1-99). **F.** Hydrogen bonding network of the dimerization interface of the central core RING motif.

The structure of Rad18 RING illustrates a symmetric dimer with a buried interface of 1131 Å^2, which is primarily hydrophobic. Dimerization is mediated by both the N- and C-terminal helices and the core RING motif. The N- and C-terminal helices combined as a four-helix bundle forms the major homo-dimerization interface, which is governed by an extensive hydrophobic packing including Gly12, Leu13, Val15, Met16,

IleE19, Leu22, Ile77, Leu78, Leu81, Ser84, Leu85, Phe87, Ala88, and Leu92 from the both monomers (Figure * 4.1E). The second dimerization interface is located in the core RING motif and is largely augmented by 6 hydrogen bonds formed through a symmetric interaction (Figure * 4.1F, Supplementary Table 4S.1).

Comparison of Rad18 RING to other RING/U-box domain dimers

As outlined in the materials and methods, we compared the Rad18 RING fold to all available structures in the PDB. From the resulting list, we chose the closed matching proteins, which like the Rad18 RING are all dimeric (Supplementary Table 4S.3). For these proteins we next made a structural pairwise comparison to Rad18 RING dimer. The proteins that provide highest similarity to Rad18 RING are the CHIP U-box homodimer (RMSD of 1.42 Å), the RING homodimer TRIM37 (RMSD of 1.74 Å) and RING heterodimer RING1b/BMI1 (RMSD of 1.86 Å). Also the BRCA1/BARD1 and MDM2/MDMx heterodimers and cIAP2 homodimer have a relatively good matching. The U-box homodimer Prp19 has a high Q-score too, but it lacks the N- and C-terminal helical extensions. Several other RING dimers, with low matching scores, have helical extensions, that are oriented differently.

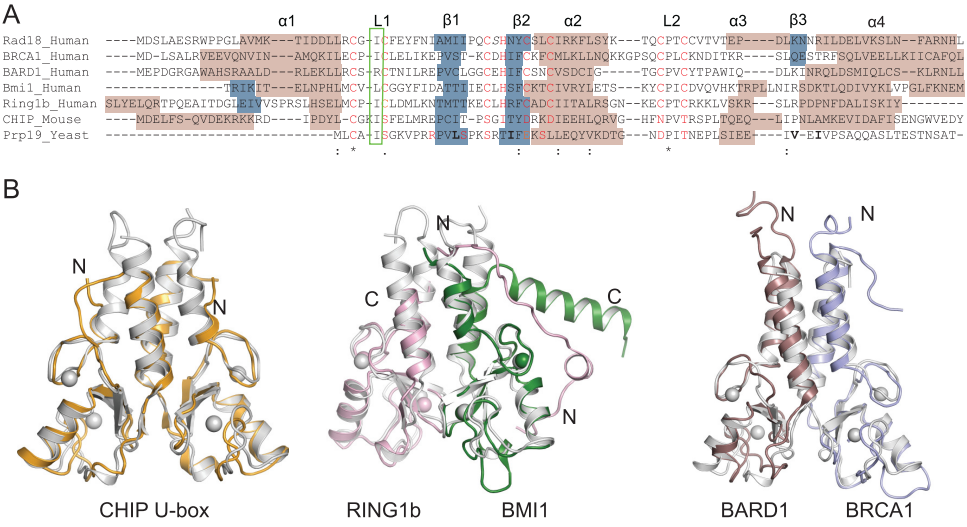

Figure * 4.2: Comparison of the Rad18 RING with other RING/U-box domains. **A.** Sequence alignment of Rad18 RING with other RING/U-box domains. Secondary structures are labeled and shaded (helix-light pink, s-blue). Zinc coordinating residues are highlighted in red. The green box indicates I27 of Rad18 in loop L1. **B.** Superposition of the structures of Rad18 RING dimer (grey) with CHIP U-box domain (2C2V, orange, left panel), of Rad18 RING dimer (grey) with RING1b/BMI1 (2CKL, middle panel), and of Rad18 RING dimer with BRCA1/BARD1 (1JM7, right panel).

The structure of the Rad18 RING dimer is very similar to that of BRCA1/BARD1

and TRIM37. In all three, the N- and C- terminal helical extensions located outside the RING domain show a similar four-helix bundle that forms a major part of the dimerization interface (cf. Figure * 4.2B). The CHIP U-box has a similar dimer structure, despite shorter helical extensions. The RING1b/BMI1 heterodimer also highly resembles that of the Rad18 RING dimer, but their helical extensions are shorter than in the Rad18 RING. A major part of the interface is quite distinct and highly asymmetric, with the long N-terminal loop of RING1b in contact with both the RING domain and the C-terminal helix of BMI1.

The interaction between Rad18 RING and Rad6b

A NMR structure of free Rad6b has been presented before [208]. The experimental conditions in that study were different from what was suitable for our studies on the interaction of the Rad18 RING and Rad6b. Therefore we re-analyzed the NMR spectra of the Rad6b by Heteronuclear multidimensional NMR for our experimental conditions. Under these conditions we also solved the solution structure of free Rad6b. A summary of the structural and restraint statistics is presented in Supplementary Table 4S.2. The twenty lowest-energy final structures are superimposed with the average RMSDs for backbone and all heavy atoms are 1.04 Å and 1.69 Å, respectively, and the ribbon representation is depicted in Supplementary Figure 4S.1A. The solution structure of Rad6b shows a canonical E2 core fold, with a four-stranded anti-parallel β sheet at one side and four α-helices with a short 3_{10} helix at the opposite side. The structure superimposes to the previous one (PDB: 1JAS) with a backbone RMSD of 1.9 Å. The main differences between both structures are the slightly positional difference in the first helix and last two helices.

In case of Rad18 both its RING domain and the R6BD domain have been implicated in recruiting Rad6b [181, 190, 191, 193]. In this study we focus on the complex formation between the Rad18 RING and Rad6b. To identify the residues that are involved in Rad18 RING binding to Rad6b, we recorded a series of ^{1}H-^{15}N HSQC spectra of ^{15}N-labeled Rad6b to which increasing amounts of unlabeled Rad18 RING were added, from 0.3:1 to a final 1.5:1 molar ratio (Figure * 4.3A, Supplementary Figure 4S.1B). During the titration of Rad6b with Rad18 RING most resonances show a fast to intermediate exchange behaviour, indicating relatively fast off-rates, which agrees with the weak value of the dissociation constant, as measured by ITC (see below). The largest chemical shift perturbations are located in three regions that are part of the canonical E2-E3 RING binding interface: the first helix α1, loop L1 between β3 and β4, and loop L2 connecting β4 and α2. Most residues that show large chemical shift changes, such as R11 and D12 in helix α1, K66 in loop L1, S97 and T99 in loop L2 are directly at the interface with the RING domain (Figure * 4.3B). As compared to other available E2-E3 binding interfaces there are a relatively high

proportion of hydrophobic residues, such as L9, M10 and F13 in helix α1, involved in binding to Rad18 RING domain. We did not observe direct chemical shift changes at the catalytic cysteine of Rad6b, but binding of the RING domain also caused relatively large chemical shift changes at residue N37, which is quite distant from the canonical E3 binding site, suggesting that there might be subtle conformational change underlining Rad6b by RING binding. We also noted small but significant shift changes at I91, R95 and W97 which is not distant from the catalytic cysteine.

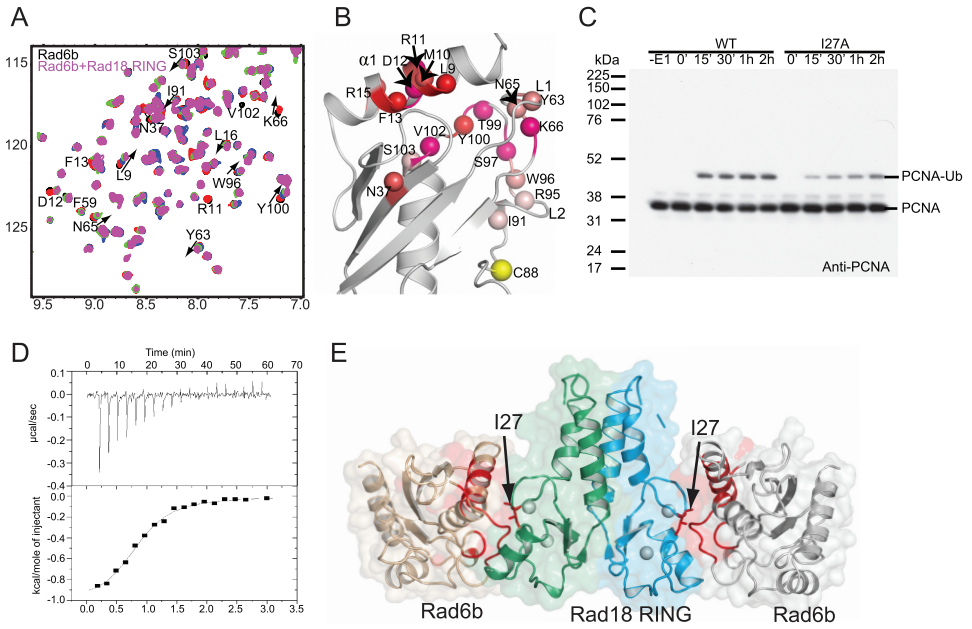

Figure * 4.3: Rad18-Rad6b complex formation. **A.** NMR titration of Rad6b and Rad18 RING dimer. The figure shows an overlay of representative regions of ^{1}H-^{15}N HSQC spectra of Rad6b in the absence (black) and presence of increasing concentrations of unlabeled Rad18 RING domain (ratios of Rad6b:Rad18 RING=1:0.3 [red];1:0.6 [blue]; 1:1 [green]; 1:1.5 [magenta]). **B.** Chemical shift mapping of the Rad18 RING domain binding site on Rad6b. Residues experiencing significant NMR chemical shift changes (>0.034 ppm) are colored with a linear gradient from white (<0.034ppm) to red (=0.1ppm). Spheres represent the nitrogen atoms of the affected residues. **C.** Ubiquitination of PCNA by Rad18 (I27A) and Rad6b. **D.** ITC binding study of Rad18 RING dimer with Rad6b. Analysis of the ITC data shows a Kd (Rad18 RING dimer: Rad6b) of 35µM. **E.** Structural model of Rad6-Rad18 RING complex. The model is obtained by aligning the structure of Rad18 dimer and Rad6b with CHIP dimer and UbcH5, respectively, with the complex CHIP-UbcH5 structure (2OXQ). The Rad6b residues located in the Rad18 binding interface by NMR titration experiment are colored red. The sidechain of the mutated residue I27 of Rad18 is indicated in red.

The interaction specificity of E2 and E3 can regulate the ubiquitin conjugation of substrate, since mutations of some residues in the E2/E3 contact surface resulted in

loss of conjugation activity [199, 206]. In the presence of ubiquitin-activating enzyme E1, ubiquitin and Mg^{2+}/ATP, Rad6/Rad18 can catalyze monoubiquitination of PCNA in an *in vitro* ubiquitination assay [209, 210]. Isoleucine in loop L1 region of E3 RING/U-box domain (Figure * 4.2A), such as I26 in human BRCA1 [206] and I53 in mouse RING1b [199], has been most consistently implicated in E2-E3 interactions and their conjugation activity. Therefore, we mutated the corresponding isoleucine of Rad18 to alanine (I27A) and found that it greatly decreased the monoubiquitination of PCNA and polyubiquitination of Rad18, indicating that I27 of Rad18 RING is crucial for Rad18 E3 ligase activity (Figure * 4.3C), similar to other E3s.

All E2-E3 RING/U-box complexes show conserved interface and common structural folds for the RING/U-box and the UBC domains [195, 196]. The above data indicate that Rad6-Rad18 RING domain interaction is similar to other E2-E3 interactions too. Thus we can build a model of Rad6-Rad18 RING structure by aligning the structure of Rad18 RING dimer and two Rad6b with CHIP dimer and UbcH5, respectively, in the crystal structure of CHIP-UbcH5 complex [207] (Figure * 4.3E). The structure model shows most residues of Rad6b implicated in the Rad18 binding by NMR are present on the Rad6-Rad18 interface in the model. The mutation I27A of Rad18 is right in the heart of the interaction.

Using isothermal titration calorimetry (ITC) we found that Rad18 RING (residue 1-99) can bind to Rad6b with a dissociation constant (Kd) of 35μM. The interaction was both entropically and enthalpically favorable (ΔH=-1037 cal/Mol, ΔS=17.3 cal/Mol.deg). The interaction showed a stoichiometry of one Rad18 RING monomer per molecule of Rad6b (N=0.84±0.02). This indicates that each RING domain dimer binds to two Rad6b molecules (Figure * 4.3D), as demonstrated in their structure model. This agrees with the NMR titration experiments of the Rad18 RING dimer to ^{15}N -labeled Rad6b (Figure * 4.3A), which showed the appearance of a single set of resonances only, again, indicating that the symmetric RING dimer binds two Rad6b molecules and remains symmetric after complex formation.

Asymmetry in the full-length Rad18 dimer

Though binding of intact Rad18 with Rad6 has been established in previous studies [179, 191], the stoichiometry of the complex of Rad18 and Rad6b is not known. To establish this, we expressed Rad18 in the absence of Rad6b and showed that it was still dimeric. We then tested for its interaction with two variants of Rad6b, His_6-tagged Rad6b and Strep2-tagged Rad6b. There was no noticeable difference in their interaction affinity with Rad18 based on analytical gel filtration and pull down assays (Supplementary Figure 4S.2). Next, we mixed the Rad18 protein with a mixture of equal amounts of His_6-tagged Rad6b and Strep2-tagged Rad6b and pulled down Rad6b/Rad18 complexes via the Strep2-tag. In this pulled-down we could not detect

any His_6-tagged Rad6b via coomassie staining or by western blots against the His-tag (Figure 4.4A, lane 7-9). This shows that the Rad18 homodimer only binds to a single Rad6b molecule.

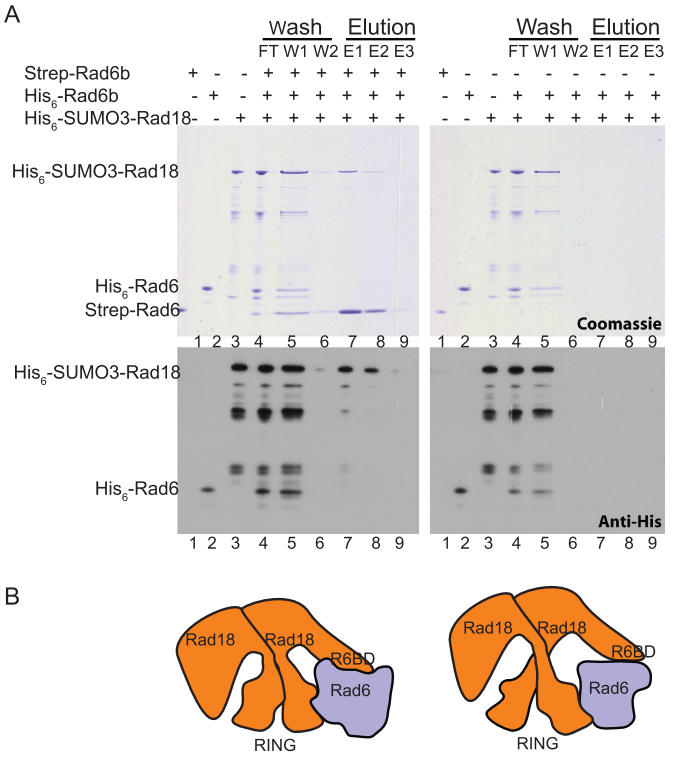

Figure 4.4: Complex formation of full-length Rad18 and Rad6b. **A.** Pull-down experiments to study the stoichiometry of full-length Rad18 homodimer with Rad6b. The left panel shows the incubation of SUMO-tagged full-length Rad18, His_6-tagged Rad6b and Strep2-tagged and then pulled down via the Strep2-tag. The results were analyzed by coomassie stained SDS-PAGE (upper panel) and by immunoblot using His1 monoclonal antibody (lower panel). The right panel is the control experiment by leaving out Strep2-tagged Rad6b. **B.** Schematic models of the Rad6-Rad18 complex. Model of the left: Rad6b binds to Rad18 RING and R6BD domains of the same monomer. Right: Rad6b binds to RING and R6BD domains of different monomers.

The fact that full-length Rad18 homodimer binds only one single Rad6b, whereas the Rad18 RING-domain homodimer can bind two Rad6b molecules, suggests that intact Rad18 forms an asymmetric dimer, in which the first binding site for Rad6 is accessible but the second binding site is closed (Figure 4.4B). Rad18 has a secondary binding domain, the R6BD domain, that bind at the opposite sides of Rad6b (unpublished data), suggesting that these bindings can occur simultaneously. Assuming that these two binding sites of Rad18 are available in the full-length Rad18 dimer, this could

lead to two possible models for generating asymmetric binding. In one model, Rad6b binds to the RING and R6BD domains of the same Rad18 monomer (*in cis*), and in the other model to RING and R6BD of different monomers (*in trans*) (Figure 4.4B). In both cases the other RING and R6BD binding sites are not available for Rad6b binding anymore.

An asymmetric homodimer has been observed before in the crystal structure of the CHIP dimer, for which only one U-box domain can interact with E2 and the other U-box domain is occluded by the N-terminal TRP domain [171]. Similar asymmetry was also observed in the heterodimer BRCA1/BARD1 [206] and RING1b/BMI1 [199], where only one of the two E3s could bind to E2. This asymmetry thus appears a common property of several E3 ligases, not only in heterodimeric complexes, but with CHIP as a founding member of an asymmetric E3 homodimer family and Rad18 as the next example.

Whether the observed asymmetry has a function, is yet unclear. It could have a regulatory role, where additional protein modificators or regulatory processes could change the E3 ligase activity, by activating the asymmetric dimer and exposing the second E2 binding site to speed up the efficiency of Rad6/Rad18 facilitated ubiquitination of PCNA. Alternatives are differential roles in other ubiquitination pathways, involving different E2 enzymes.

Conclusion

Although Rad6 and Rad18 belong to the first ubiquitination enzymes studied in detail, and extensive functional and biochemical studies have been performed, both on intact proteins and domains of their complexes, structural aspects of the Rad18/Rad6 complex at atomic level is lacking. Now, we determined the crystal structure of symmetric RING homodimer of Rad18, and showed that this protein dimerizes through an interface containing a four-helix bundle and a secondary interface involving the canonical RING motifs. This interaction interface strongly resembles that one seen before in the BRCA1/BARD1 heterodimer and in the CHIP homodimer. NMR titrations, ITC and a structural model show that the Rad18 RING dimer can in principle bind two Rad6b molecules. The full-length Rad18 homodimer, however, shows binding with only a single Rad6b molecule, indicating that full-length Rad18 is an asymmetric dimer like the CHIP homodimer or becomes one upon Rad6b binding. Rad18 can be placed in a class of dimeric RING E3 ligases whose RING domains can, in principle, bind to two E2 enzymes, but for which only a single site is occupied. It is plausible that the second site may be rendered accessible by a conformational change, following a post-translational modification, for example. This could provide an activation signal for the E3.

Materials and methods

Molecular cloning

Full-length Rad18, Rad18 (1-99) and Rad18 (1-121) were cloned into a pSUMO3 vector (SUMOPRO). Alternatively, His-tagged Rad18 was cloned into pET28a (Merck Chemicals). The I27A point-mutant of Rad18 was made by Quikchange site-directed mutagenesis (Stratagene). Untagged, His-tagged and Strep2-tagged Rad6b were cloned into vectors pCDF1b, pACYC-Duet and pET28a, respectively (Merck Chemicals).

Protein expression and purification

Unlabelled proteins were expressed in a Bl21 (DE3) cell line using LB media and the recommended concentration of appropriate antibiotics. Protein expression was induced with 0.25mM IPTG. All purification steps and biochemical experiments were performed in a buffer containing 10mM Hepes pH 7.5, 150mM NaCl, 2μM $ZnCl_2$ and 0.5mM TCEP unless stated otherwise. Rad6b/Rad18 complexes were co-expressed via the pCDF1b/pET28a vectors and first purified via a His_6-tag on Rad18 using Talon beads (CloneTech), eluting with 200mM imidazole. Initial purification was via a 6mL Heparin column (GE Healthcare), with a step elution into a buffer containing 440mM NaCl, followed by Gel Filtration with a S200 16/60 column (GE Healthcare). His-SUMO3-tagged -Rad18 (FL) -Rad18 (1-99) and -Rad18 (1-121) were also purified via Talon beads and a Heparin Column (eluting with a buffer containing 600mM NaCl). The SUMO-tag was cleaved from Rad18 (1-121) and Rad18 (1-99) using Senp2 protease and removed with Talon beads, while the RING domain was further purified via Gel Filtration using an S75 10/300 column (GE Healthcare). His_6-Rad6b and Strep2-Rad6b were purified via Talon beads or StrepTactin resin (Novagen) followed by Gel Filtration using an S75 16/60 column.

Multi-angle static light-scattering (MALLS)

MALLS experiments were performed at 4°C on a Mini-Dawn light scattering detector (Wyatt Technology) online with a Superdex S75 10/30 column in 10mM Hepes pH 7.5, 150mM NaCl 2μM $ZnCl_2$ and 0.5mM TCEP. Refractive index and light scattering detectors were calibrated against toluene and BSA.

Crystallization and Structure calculation

Rad18 (1-99) readily crystallized as clusters of crystals in conditions containing 15-25% PEG 3350 or PEG-MME-2K and several Sulfate and Acetate salts. A micro-seeding approach was used from these conditions. A seed solution was prepared by harvesting the microcrystals in 30μL of mother liquor and vortexing for 10x10 seconds. 200nL Rad18 1-99 (concentration 700μM) was mixed with 100nL mother liquor (10%-18%

PEG3350 or PEG-MME-2K, 50-100mM Ammonium Acetate and 100mM Bis-Tris pH 5.5) and 20nL of seed solution was added. A vapour diffusion experiment was performed to yield diffraction-quality crystals with space group C121. Cryoprotection was achieved by soaking single crystals in a solution containing 35% PEG-MME-2K, 50mM Ammonium Acetate and 100mM Bis-Tris pH 5.5 for 30s. Data were collected on a single crystal that diffracted up to 1.8 Å resolution at 100 K on European Synchrotron Radiation Facility beam line ID23-1 (λ=1.2828 Å). Data were processed with XDS.

The structure was solved using the anomolous signal from four zinc ions that were coordinated by the RING dimer, using SHELXC and Phaser. Rebuilding was performed with ARP/wARP and Coot, and refinement was with REFMAC. The quality of the model building was assessed using MolProbity. Crystallographic parameters are summarized in Table 4.1. All structure figures were generated using Pymol.

Structure comparisons of RING/U-box dimers

The DALI server [211] was applied to search for similar structures as Rad18 RING monomer in the PDB. The closed matching proteins that are dimeric were chosen to do pairwise comparison with Rad18 RING dimer by SSM [212]. For those proteins that have more than one structure in PDB, the best matched structure was selected for our analysis. The RING/U-box dimers in Supplementary Table 4S.3 are ordered according to the Q-score.

NMR (Rad6b)

The ^{15}N-labeled and ^{13}C, ^{15}N-labeled His-tagged Rad6b were expressed in *Escherichia coli* BL21 (DE3) and purified on a Nickel-charged Poros MC column (PerSeptive Biosystems), and final samples were exchanged to buffer containing 50mM KH_2PO_4/K_2HPO_4 (pH 8.0), 300mM NaCl, 1mM DTT, 95%/5% H_2O/D_2O and a small amount of complex protease inhibitor (Roche). NMR experiments were carried out on Bruker AVANCE 600 and 750 spectrometers equipped with a triple-resonance z-gradient probe. The spectra for resonance assignment and structure determination of Rad6b were recorded by a standard set of NMR experiments at 310 K. All NMR spectra were processed using XwinNMR3.5 (Bruker) and analyzed using the program SPARKY. Structure calculations were performed using the program CYANA. The final structures were validated with WHATIF and PROCHECK. Molecular images were generated with PyMol.

NMR titration

Unlabeled Rad18 RING and ^{15}N-labeled Rad6b was prepared in buffer 50mM Tris-HCl pH7.5, 100mM NaCl, 3mM DTT. For the binding titrations, the ^{1}H-^{15}N HSQC spectra

of 200μM Rad6b in buffer containing 50mM Tris-HCl pH7.5, 100mM NaCl, 3mM DTT, 95%/5% H_2O/D_2O were recorded at 310 K alone and in complex with different ratios of Rad18 (from 1:0.3 to 1:1.5). Combined chemical shift perturbations were calculated using the equation, $\Delta\delta ppm = ((\Delta\delta HN)^2 + (\triangle\delta N/5)^2)^{1/2}$.

Strep2-pull down

Pull-down experiments were performed in 10mM Hepes pH 7.5, 150mM NaCl, 2μM $ZnCl_2$ and 0.5mM TCEP. 100μM SUMO-tagged full-length Rad18, 25μM His_6-tagged Rad6b and 25μM Strep2-tagged Rad6b were incubated on ice for 10 minutes in a total volume of 100μL. Alternatively, a control sample was prepared in the absence of Strep2-Rad6b. Both samples were incubated on ice for 10 minutes with 30μL of pre-washed StrepTactin resin (Novagen) and loaded onto gravity flow columns (BioRad). The beads were washed with 2x500μL 10mM Hepes pH 7.5, 500mM NaCl, 2μM $ZnCl_2$ and 0.5mM TCEP and protein complexes that contained Strep2-Rad6b were eluted from the beads using 3x100μL of 10mM Hepes pH 7.5, 150mM NaCl, 2μM $ZnCl_2$, 3mM desthiobiotin and 0.5mM TCEP. Samples were analyzed by coomassie stained SDS-PAGE using 10% NuPAGE gels in a MOPS buffer system (Invitrogen). Alternatively samples were immunoblotted using His1 monoclonal antibody (Sigma) and analyzed.

Isothermal Titration Calorimetry

ITC experiments were performed with an ITC200 Micro Calorimeter (GE Healthcare) at 25°C. Stock solutions of Rad6 and Rad18 (1-121) were prepared by Gel Filtration into a buffer containing 10mM Hepes pH 7.5, 150mM NaCl, 2μM $ZnCl_2$ and 0.5mM TCEP and were degassed before use. The sample cell contained Rad18 1-121 (368 μM), which was titrated with Rad6b (3648μM) using 2.5μL injections. The injections after saturation were used to determine the background signal. Corrected data were analyzed using software supplied by the ITC manufacturer to calculate the dissociation constant (Kd). Parameters were obtained for a model describing one set of binding sites, using nonlinear least-squares fitting.

Ubiquitination assay

Rad6b ubiquitin chain formation assays were performed at 32°C in buffer containing 50mM Tris (pH 8.0), 100mM NaCl, 10mM $MgCl_2$ and 0.1mM DTT. Reactions were performed with 80nM Uba1, 3μM Rad6b/Rad18(WT) or Rad6b/Rad18(I27A), 3μM PCNA and 12μM ubiquitin. Reactions were started by addition of 3mM ATP and at the indicated time points samples were denatured in reducing loading buffer. Samples were run on NuPAGE gels using a MOPS buffer system (Invitrogen), immunoblotted and analyzed.

Acknowledgements

We thank Ludovic Carlier for his technical supports in NMR experiments, Anastassis Perrakis for assistance with crystallography and Vincent Breukels with ITC data collection. This work was financially supported by the Netherlands Organization for Scientific Research, Chemistry Council (NWO-CW) and by European Commission funding through the SPINE2-COMPLEXES and RUBICON projects.

Supplementary Material

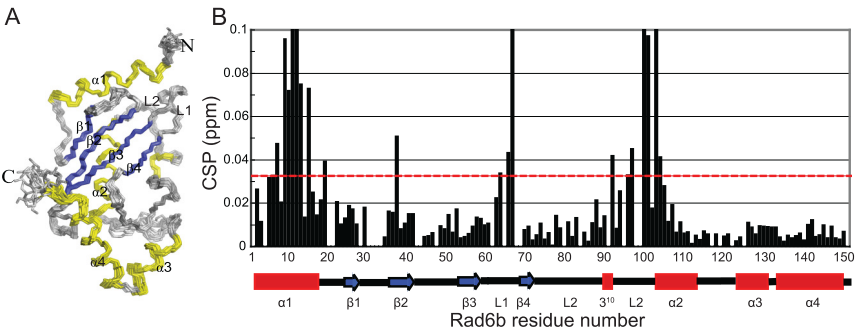

Figure 4S.1: **A**. Stereoview of the ensemble of 20 NMR structures. Helices are shown in yellow and sheets in blue. **B**. Chemical shift perturbation (CSP) chart of Rad6b titration with Rad18 RING.

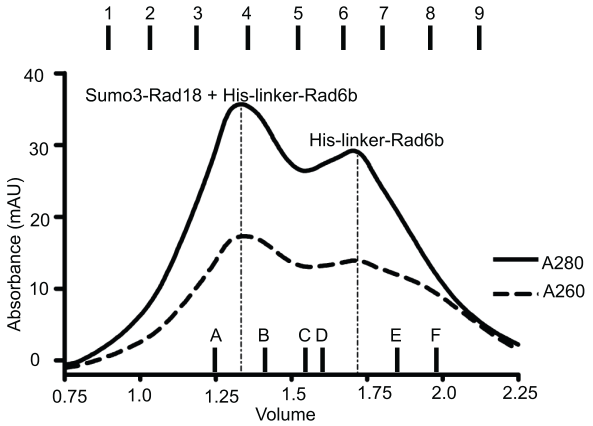

Molecular weight standards

	kDa	Retention
A Ferritin	440	1.23
B Aldolase	158	1.39
C Conalbumin	75	1.54
D Ovalbumin	44	1.58
E Ribonuclease A	14	1.85
F Aprotinin	6.5	1.96

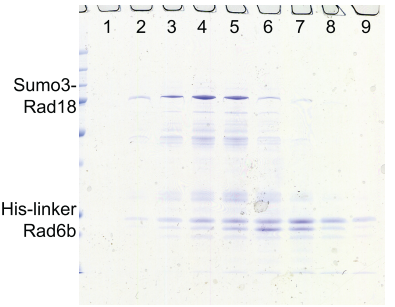

Figure 4S.2: Sumo tagged Rad18 interaction with His tagged Rad6b. Analytical gel filtration shows that Sumo tagged Rad18 interacted with His tagged Rad6b and they were co-eluted.

Table 4S.1: H-bonds and contacts on the RING homodimer interface.

Chain A	Chain B	Distance (Å)
GLY12	LEU92	
LEU13	LEU13	
VAL15	PHE87, ALA88	
MET16	MET16	
THR18 OG1	SER84 O	4.467
THR18 O	SER84 OG	4.588
ILE19	SER84, LEU85	
LEU22	ILE77, GLU80, SER84	
PRO39	LYS73	
SER42	ASN74, ASN75, ARG76	
SER42 OG	ASN74 O	2.771
SER42 OG	ARG76 N	2.857
SER42 OG	ILE77 N	4.696
ASN44	ILE77	
ASN44 ND2	ASN75 OD1	4.685
LYS73	PRO39	
ASN74	SER42	
ASN74 O	SER42 OG	2.916
ASN75	ASN75	
ASN75 ND2	ASN75 OD1	3.025
ASN75 OD1	ASN44 ND2	4.686
ASN75 OD1	ASN75 ND2	2.965
ARG76	SER42	
ARG76 N	SER42 OG	2.897
ILE77	LEU22, LEU78	
ILE77 N	SER42 OG	4.66
LEU78	ILE77	
LEU81	LEU81	
SER84	THR18	
LEU85	ILE19	
PHE87	VAL15	
ALA88	VAL15	
LEU92	LEU13, VAL15	
PHE95	PRO11	

Table 4S.2: Structural statistics for the solution structure of Rad6b

Restraint information	
Short-range (|i-j|<=1)	1143
Medium-range (1<|i-j|<5)	419
Long-range (|i-j|>=5)	693
Total NOE restraints	2255
TALOS-derived dihedral angle restraints φ+ψ	210
Coordinated RMSD from mean (Å)	
All backbone atoms	0.87
All heavy atoms	1.39
Structure Z-scores	
1st generation packing quality	-2.22
2st generation packing quality	-3.46
Ramachandran plot appearance	-2.21
chi-1/chi-2 rotamer normality	-0.62
backbone conformation	-2.16
Ramachandran Quality Parameters (%)	
Residues in most favored regions	88.79 ± 1.95
Residues in Allowed regions	10.60 ± 2.04
Residues in generously allowed regions	0.40 ± 0.61
Residues in disallowed regions	0.20 ± 0.36

Table 4S.3: SSM pairwise comparison of Rad18 RING dimer with other RING/U-box dimer structures.

PROTEIN	PDB	Q-score	P-score	Z-score	RMSD	Nalign
CHIP	2oxq	0.6	9.5	9.2	1.42	136
TRIM37	3lrq	0.6	8.3	8.5	1.74	151
RING1b-BMI1	2ckl	0.39	4.5	6.9	1.86	135
Prp19	2bay	0.35	4.6	6.3	2.38	105
BRCA1-BARD1	1jm7	0.28	0.5	2.7	2.40	127
cIAP2	3eb5	0.27	0.0	1.0	2.91	109
MDM2-MDMx	2vje	0.25	0.0	1.4	2.72	99
Hdm2	2hdp	0.19	0.0	1.6	3.37	97
TRAF6	3hcs	0.16	2.3	6.5	2.43	121
UHRF2	1z6u	0.15	0.2	4.8	2.32	99
UHRF1	3fl2	0.13	0.0	5.3	1.84	85
Rag1	1rmd	0.11	0.0	5.6	2.14	81

Q-score: the quality of alignment, which balances the effect of RMSD-Nalgn. Q-score reaches 1 in the case of identical structures. P-score: the probability of achieving the same or better quality of match at a chance, and P-score lower than 3 indicates statistically insignificant matches. Z-score: the statistical significance of a match in terms of Gaussian statistics. RMSD: root mean square deviation of Cα atoms of matched residues at best 3D superposition of the two structures. Nalgn: number of matched residues.

Chapter 5

The ability of human Rad6b to assemble ubiquitin chains is inhibited by Rad18 interaction

Richard G. Hibbert[1*], Anding Huang[2*], Rolf Boelens[2] and Titia K. Sixma[1]

[1] Division of Biochemistry and center for Biomedical Genetics, Netherlands Cancer Institute, Plesmanlaan 121, 1066 CX Amsterdam, The Netherlands.

[2] Department of NMR Spectroscopy, Bijvoet Center for Biomolecular Research, Utrecht University, Padualaan 8, 3584 CH, Utrecht, The Netherlands.

*These authors contributed equally to this work

Manuscript in preparation

Abstract

In ubiquitin conjugation, different combinations of E2 and E3 enzymes catalyse either monoubiquitination or ubiquitin chain formation. Conjugation enzymes Rad6/Rad18 only monoubiquitinate PCNA to signal for 'error prone' DNA damage tolerance. Ubiquitin chain formation on PCNA is catalysed by a different set of conjugation enzymes: Ubc13/MMS2/Rad5. Here we show that E2 enzyme Rad6 is intrinsically capable of ubiquitin chain formation. The specificity of the reaction is provided by E3 enzyme Rad18, which prevents the chain-formation activity to direct the reaction towards monoubiquitination. The R6BD of Rad18 provides the inhibition by competing with ubiquitin for a non-covalent 'backside' binding site on Rad6. Our findings provide mechanistic insights into how E3 enzymes can regulate the ubiquitin conjugation process.

Introduction

Conjugation of ubiquitin to a target lysine occurs via an E1, E2, E3 enzyme cascade. The E2/E3 complex is the active ligase that transfers the ubiquitin moiety to the target. Within this complex one of about 32 E2 enzymes provides the enzyme activity while one of hundreds of E3 define the target specificity [213]. Ubiquitin conjugation can take several different forms. The most simple is monoubiquitination, which provides a signalling function. Since ubiquitin itself contains seven lysine residues, it can be ubiquitinated to form a multitude of different linkages of ubiquitin chains [214, 215].

The specificity for monoubiquitination or different ubiquitin chain linkages is either defined by the E2 enzyme, or by the E2/E3 complex. E2 enzymes can generate specific linkages of the ubiquitin chain: Ube2S, E2-25K and Ubc13/MMS2 are associated with K11, K48 and K63 chains, respectively [216, 217, 218]. In contrast, UbcH5c can form all possible linkages of ubiquitin chains [219]. Ubiquitin chains can be formed by combinations of two E2 enzymes acting in a sequential manner; such a mechanism has been shown for modifications of APC by Ubc4 and Ubc1 [220] and PCNA modification by Rad6 and then Ubc13/MMS2 [221, 222].

There is a strong correlation between the chain formation ability of an E2 enzyme and non-covalent binding of ubiquitin by the E2. Structural studies have identified the non-covalent binding site of ubiquitin on the 'backside' of the E2, on the opposite face from the active site cysteine. Mutagenesis at this site alters the chain formation propensity of the enzyme [219, 223, 225]. In most systems the specificity of chain formation is likely to be derived by a combination of E2 and E3 enzymes in vivo, since the diversity of E3 enzymes will be required for specificity of the conjugation process. The mechanism by which E3s activate and regulate E2s is an area of intense study

[213].

The functions of *Saccharomyces cerevisiae* E2 enzyme Rad6 and its human homologues, Rad6a/b, are of acute biological interest. Early studies in yeast identified important roles of the Rad6 gene in several functions, including DNA repair, and provided an initial role for ubiquitin conjugation [226]. Rad6 is predominantly considered to be a chain initiation enzyme that only monoubiquitinates its targets. This is best characterized for monoubiquitination of PCNA by the Rad6/Rad18 pair as a first step in DNA damage tolerance pathways at a stalled replication fork. The pathway has been extensively characterized as a two-step pathway. In a first step, Rad6/Rad18 monoubiquitinates PCNA on K164 to signal for recruitment of damage-tolerant polymerases. Next, Rad5/Ubc13/MMS2 can form K63-linked polyubiquitin chains on modified PCNA to initiate error free DNA repair [221, 222]. In this process Rad6 only monoubiquitinates PCNA, even *in vitro* [227, 228].

Two other major functions of Rad6 have been identified to date but the biochemical data for Rad6 mediated monoubiquitination or chain formation events in these systems are less compelling. Rad6a/b will monoubiquitinate histone H2B in human cells on K120 [229, 230] as an essential step prior to H3 methylation by COMPASS and Dot1. Rad6 is also essential for N-rule protein degradation in which K48 ubiquitin chains are formed on proteins bearing a N-degron, which marks the target for proteosomal degradation [231], but it is likely that other targets of Rad6 remain to be established [232]. Whereas the activity of many E2s for ubiquitin chain formation has been well studied, the ubiquitin chain assembly by Rad6b is not well understood.

In this article we show that Rad6b is capable of both non-covalent interaction with ubiquitin and formation of ubiquitin chains. We study the interaction of Rad6b with Rad18 and show that the major interaction surface of Rad18 overlaps with the non-covalent ubiquitin binding site on the 'backside' of Rad6. We demonstrate that Rad18 can compete with ubiquitin binding and modulate the ubiquitin chain formation of Rad6. Our results provide a mechanism by which different E3 enzymes can produce different molecular signals with the same E2 enzyme: Rad6 is able to form target-linked ubiquitin chains, catalysed by one or more E3 enzymes, but Rad18 can also utilize Rad6 for PCNA monoubiquitination.

Results

Rad6b both covalently and non-covalently interacts with ubiquitin

To understand the structure and activity of Rad6b, we first determined the structure of native Rad6b using X-ray crystallography at 1.4 Å resolution (Table 5.1, Supplementary Figure 5S.1). The structure shows the conserved fold of E2 ubiquitin conjugating enzymes and is highly similar to the published crystal structure of *Saccharomyces*

cerevisiae Rad6 (Root mean square deviation (RMSD)=0.97Å over 147 Cα atoms).

Table 5.1: Data collection and refinement statistics.

Data Collection Statistics	**Rad6b**	**Rad6b + Rad18 (339-366)**
Number of Crystals	1	1
Spacegroup	$P4_32_12$	$P6_522$
Unit Cell: a, b, c, (Å)	48.1 48.1 124.8	57.88 57.88 166.37
Alpha, beta, gamma	90.00 90.00 90.00	90.00 90.00 120.00
Resolution Limits (High)	44.839 – 1.399 (1.48-1.40)	24.924 – 2.001 (2.12 – 2.00)
Completeness	97.3 (95.7)	99.1 (95.0)
Number of unique reflections	53606 (8554)	11965 (1768)
Multiplicity	3.09 (3.00)	12.85 (11.60)
Low resolution Rmerge	0.048	0.019
Rmerge	0.156 (1.041)	0.079 (0.323)
<I/Sigma>	8.24 (1.63)	18.1 (4.83)
Wilson B factor ($Å^2$)	20.1	15.9
Model Refinement Statistics		
R factor[a]	0.166	0.191
R free[a]	0.207	0.246
Number of Protein Atoms	1234	1425
Number of Waters	135	79
Ramachandran Plot		
- favored[b]	95.95%	96.41%
- outliersb[b]	0.00%	0.00%
RMS bond, Z-bond (Å)[a]	0.0146, 0.623	0.0212, 0.881
RMS angle, Z-angle (deg)[a]	1.577, 0.753	1.667, 0.794

We studied the activity of Rad6b in real time using NMR spectroscopy. Like all catalytically active E2 enzymes, Rad6b is covalently loaded with ubiquitin on its active site cysteine during the E1, E2, E3 enzyme cascade. To study this process, ^{15}N-labeled Rad6b was incubated with ubiquitin and E1 activating enzyme and the reaction was started by addition of ATP/Mg^{2+}. The reaction was followed by a time-course of ^{1}H-^{15}N-HSQC experiments. Within one hour after addition of ATP, shifts were observed surrounding the active site cysteine of Rad6b consistent with Rad6b loading with ubiquitin (Figure 5.1A, Supplementary Figure 5S.1).

Even before addition of the ATP, however, small perturbations were observed on the back of Rad6b, consistent with a reported non-covalent interaction of Rad6b with ubiquitin [233]. A similar interaction is seem for many E2 enzymes, including UbcH5c and Ubc9 [219, 223, 224, 225]. We characterized the binding of ubiquitin with Rad6b using NMR titrations. The only significant chemical shifts mapped to β-strands β1-3 and helix α4 on Rad6b and close to the hydrophobic patch surrounding I44 of ubiquitin

(Figure 5.1B). These titrations revealed a fast exchange regime, and analysis of the observed chemical shift changes showed a weak (∼400μM) affinity, with no evidence for major structural changes of ubiquitin. Overall, the size of the chemical shifts and the size of the binding site on ubiquitin is smaller than that on Rad6b, consistent with local conformational changes in the β-strand region of the E2 upon binding to ubiquitin [219].

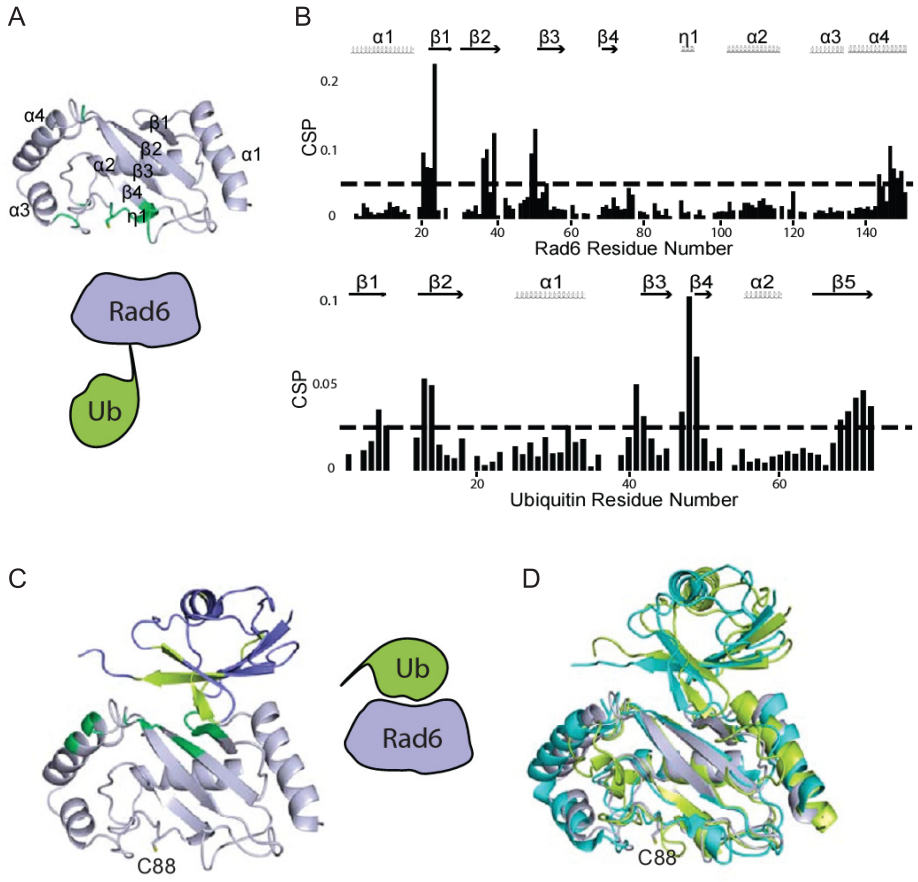

Figure 5.1: Covalent and non-covalent interactions of Rad6b with ubiquitin. **A.** Significant CSP were observed near the active site cysteine, C88, following thioester formation of Rad6b with ubiquitin. **B.** CSP data from the titrations of ubiquitin into Rad6b and Rad6b into ubiquitin. **C.** Lowest energy docking solution of Rad6b-ubiquitin complex and cartoon representation. Significant CSP of Rad6b (> 0.05) and ubiquitin (CSP > 0.025) are highlighted. **D.** Superposition of UbcH5c/ubiquitin (cyan) and MMS2/ubiquitin (green), and Rad6b (blue).

In the absence of a high-resolution structure of the Rad6-ubiquitin complex, we used a data driven docking approach to generate models of the complex [234]. As expected

the highest scoring models pack the hydrophobic core of ubiquitin, surrounding Ile44, against the small hydrophobic patch on Rad6b, around Val39 and Phe41 (Figure 5.1C). We compared our model and titration data with existing structures of E2s and E2 variants making non-covalent complexes with ubiquitin [219, 223, 224, 225]. The complexes are highly similar to each other and to our model and differ only by a small rotation in the orientation of the ubiquitin (Figure 5.1D). This confirms that the 'backside' of Rad6b interacts with ubiquitin via a canonical mode of interaction.

Rad6b can form ubiquitin chains

We studied the E1-catalyzed loading of ubiquitin to the active site of Rad6b at later time-points using NMR titrations. Remarkably, this revealed a molecular event distinct from covalent and non-covalent ubiquitin interactions. After the active site loading had reached saturation, an additional set of chemical shifts were seen on the back of Rad6b and an overall broadening of the NMR spectra was observed (Figure * 5.2A). Since the timing of broadening was later than the loading of the Rad6b, we interpret it to be the result of the enzymatic activity of the E2, but not a direct result of E2 loading. Several E2 enzymes are capable of forming free ubiquitin chains in solution and backside ubiquitin interaction is often a prerequisite for this ubiquitin chain formation [219, 223, 225]. We postulate that we were observing the formation of a heterogeneous mixture of free ubiquitin chains, catalysed by Rad6b. We interpret that the chains were bound by Rad6b via the non-covalent interaction, supported by the observation that many additional chemical shifts were observed in this region at later time points. The resulting increase in molecular weight of the complex causes the broadening of the NMR cross-peaks.

We directly studied if isolated Rad6b has the ability to form free ubiquitin chains in solution, using an *in vitro* reconstituted enzyme reaction. Rad6b showed a clear intrinsic ability to form ubiquitin chains (Figure * 5.2B). We studied the specificity of the ubiquitin chain linkages using mutants of ubiquitin that retained only a single lysine. The activity was reduced in all of the mutants compared with wild type ubiquitin. This is indicative of Rad6b forming mixed ubiquitin chains, although with a certain preference for K11- and K48-linked chain formation (Figure * 5.2C). Finally we studied if the chains were free in solution, linked to the active site cysteine, or linked to a lysine on Rad6b. Whereas there was no evidence for active site-linked ubiquitin chains, we could observe some modification of lysine residues in Rad6b. We deduced that most of the chains were free in solution, however (Supplementary Figure 5S.2).

Rad18 inhibits chain formation by Rad6

Since Rad6b is capable of forming ubiquitin chains in solution, but Rad6/Rad18 complexes only monoubiquitinate PCNA, we postulated that Rad18 inhibits the chain-

formation activity of Rad6b upon forming a binary Rad6/Rad18 complex. Therefore we tested the chain-forming activity of Rad6 in the presence of Rad18 (Figure 5.3A). In this assay the chain formation is abrogated when Rad18 is present in stoichiometric amounts.

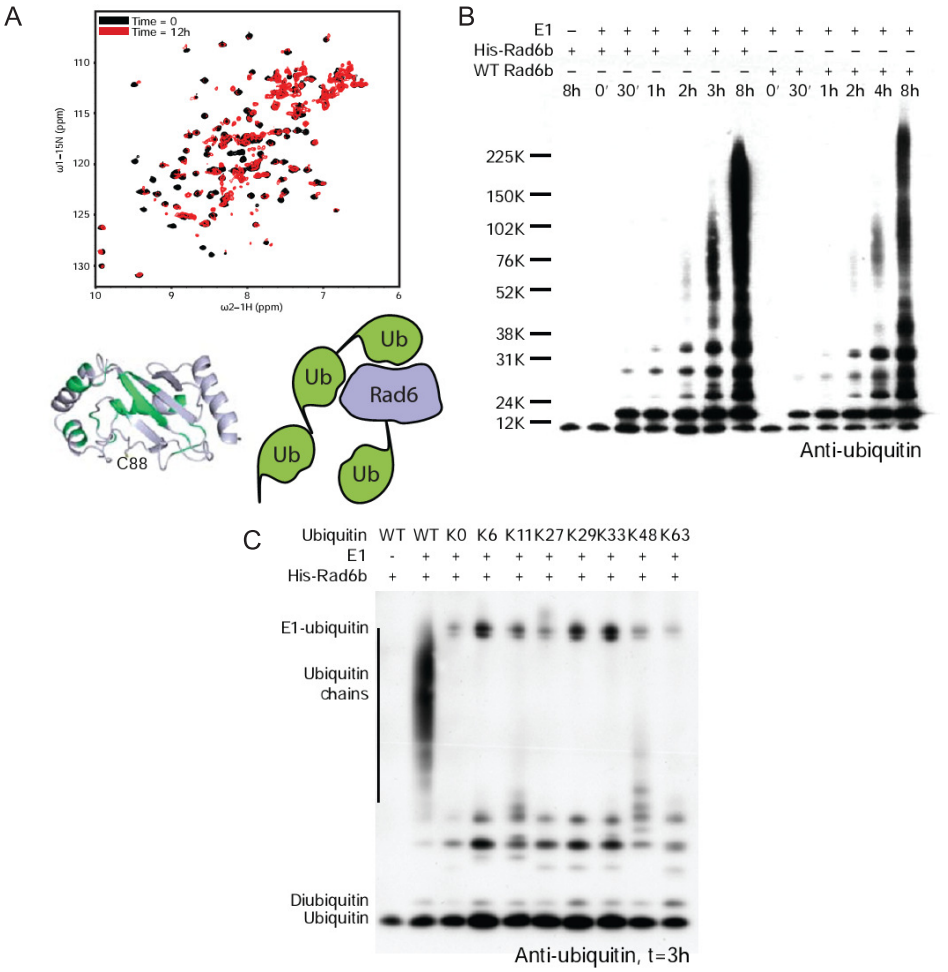

Figure * 5.2: Rad6b can form ubiquitin chains. **A.** At later time points of the thioester formation experiment, an overall broadening of the ^{1}H-^{15}N -HSQC spectra was observed and additional CSP mapped to the back of Rad6b. **B.** Rad6b can form free ubiquitin chains, using an *in vitro* system containing purified E1, Rad6b, ubiquitin and ATP/Mg^{2+}. The His-tagged Rad6b is marginally more efficient in chain formation. **C.** *In vitro* ubiquitination assays using single lysine mutants of ubiquitin suggest that the chains are mixed, with a preference for K11- and K48-linked ubiquitin chains.

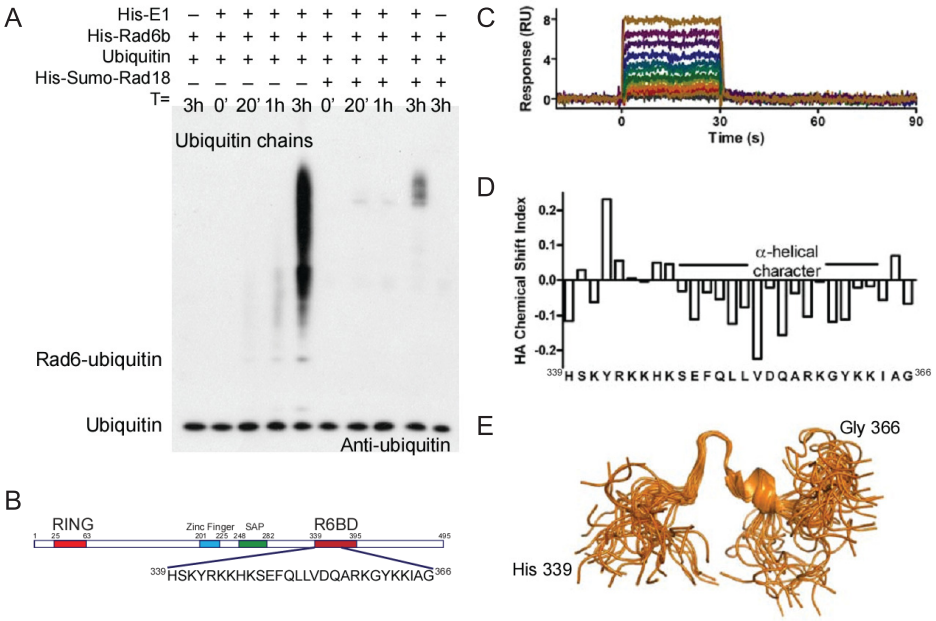

Figure 5.3: Characterizing the Rad18 R6BD. **A.** Full length Rad18 inhibits Rad6-mediated ubiquitin chain formation. **B.** The domain structure of Rad18, with the 28-mer R6BD peptide highlighted. **C.** Surface plasmon resonance studies of R6BD binding to Rad6b. Clear binding curves can be seen at all concentrations studied. **D.** Secondary HA chemical shift for the R6BD peptide. Residues 347-361 show α-helical characteristics. **E.** The R6BD is a loosely folded kinked helix in solution. The ensemble was superimposed using THESEAUS.

To understand the mechanism of this inhibition we studied the interactions between Rad6 and Rad18. Rad18 recognises Rad6 via an N-terminal RING domain and via a separate C-terminal Rad6 binding domain (R6BD) (Figure 5.3B) [235, 236]. Constructs containing this R6BD domain are able to form a stable complex with Rad6b that can be pulled down via a hexahistidine tag on Rad6b *in vitro* [228]. We studied the structure of the Rad18 (R6BD) and its interaction with Rad6b. The isolated 28 amino acid R6BD peptide recognised Rad6b with micromolar affinity (Figure 5.3C, Table 5.2).

We studied the structure of the free R6BD peptide in solution using NMR spectroscopy. Secondary structure analysis based on Hα chemical shift indices (CSI) predicted a helical conformation between residues Ser348-Tyr361 (Figure 5.3D). However the small CSI amplitude indicates that the peptide might be in rapid exchange between folded and unfolded states. In addition the natural abundance ^{1}H-^{15}N -HSQC spectrum of the synthesized peptide displayed relatively poor chemical shift dispersion, which also indicates a large fraction of random coil conformation for the R6BD peptide in solution (Supplementary Figure 5S.3A). The structure of free R6BD using NOE

Table 5.2: Summary of affinity constants of Rad6b from NMR and SPR measurements.

	SPR (μM)	NMR (μM)
R6BD	62.1 ± 8.9	32.1 ± 7.5
R6BD*	∼744	not measured

R6BD* contains four point mutants in the R6BD sequence, but retains approximately the same charge and total lumber of lysine residues. The affinity for R6BD* could not be accurately measured since non-specific binding of the peptide precluded concentrations above 256μM. The affinity was estimated from the magnitude of the responses compared with R6BD.

restraints shows that the peptide has only clear helical structure between residues Leu353-Gln356 but has further only helical propensity without a well-defined secondary structure (Figure 5.3E, Supplementary Table 5S.1). Clear NOEs were observed between residues Ser348 and Gln351, which induced a kink in all the peptide structures calculated (Figure 5.3E).

R6BD wraps around the backside of Rad6b

The location of the binding site of R6BD on Rad6b was identified using NMR chemical shift perturbation (CSP) experiments. The assignment of Rad6b has been published previously [237]. We expressed and purified uniformly ^{15}N-labeled Rad6b and validated the spectral characteristics of our protein preparation against the published assignment using standard triple-resonance NMR spectra [238].

The titrations of R6BD and Rad6b show fast-intermediate exchange behaviour, given that during the titration the H^N-N and H^C-C cross peaks of Rad6b were observed for most of the residues. The relatively fast off-rate is consistent with the 62 M affinity that we observed by SPR (Figure * 5.4A and Table 5.2). The observed chemical shift changes mapped the binding site of the R6BD at the backside of Rad6b, opposite to the active site cysteine, C88 (Figure * 5.4B). The major shifts were on β-strands β1, β2 and β3 and the C-terminal residues of Rad6b including conserved residues S25, N37, V39, T52 and K54.

To further characterize the interaction of Rad6b with R6BD, we co-crystallized Rad6b with the R6BD peptide and determined the crystal structure to 2Å resolution (Figure * 5.4C-F, Table 5.1). The structure shows Rad6b to have the same canonical E2 fold as the native structure, with no evidence for structural rearrangements (Supplementary Figure5S.1). The R6BD structure is that of a kinked helix with residues Ser348-Arg358 forming a long α-helix and residues Tyr342-Lys344 forming a second helix rotated by about 60° with respect to the first. Consistent with the NMR data, the peptide interacts with the backside of Rad6b opposite from the active site cysteine but is clearly more ordered in the crystal structure than free in solution. The peptide interacts with Rad6b via a series of hydrogen bonds, salt bridges and van der

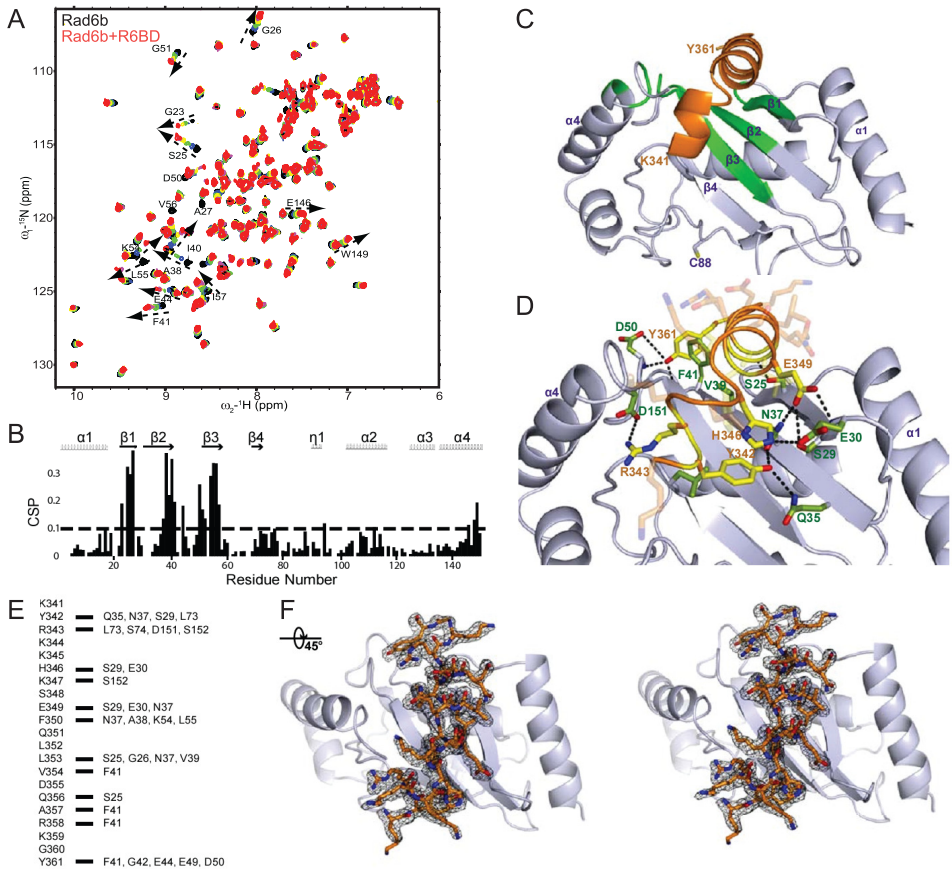

Figure * 5.4: The interaction of R6BD with Rad6b **A.** ^{1}H-^{15}N -HSQC of Rad6b alone (black) with increasing amounts of R6BD to a final Rad6b:R6BD ratio of 1:4 molar ratio of R6BD (red). **B** Magnitude of CSP plotted against residue number. Secondary structure elements of Rad6b are indicated. **C.** The crystal structure of the complex shows Rad6b to have a canonical E2 fold composed of a four-stranded antiparallel β-sheet (residues V24-S39, N32-F41, T52-E59 and T69-F72), four α-helices (residues P4-E19, V102-D114, S124-Q131, K134-Q137) and a short 310 helix (residues D90-L92). R6BD (orange) is a kinked helix that binds to the back of Rad6b. Significant (>0.1) CSPs of Rad6b are highlighted in green. The crystal structure is highly consistent with the NMR titration data. **D.** The interaction of the peptide with Rad6b is stabilized by potential hydrogen bonds to Tyr342, Arg343 and His346 at the kinked N-terminus of the peptide and Tyr361 at the C-terminus, although this residue may be somewhat mobile since it is less well resolved in the electron density. The interaction is also stabilized by a number of hydrophobic interactions including Val354 and Ala357, which are buried in a hydrophobic patch on Rad6b surrounding Val39 and Phe41. Residues at the interface on R6BD and Rad6b are coloured yellow and green, respectively. **E.** Summary of <3.8Å contacts between Rad6b and R6BD. F. Stereo representation of the R6BD-Rad6b complex. The refined electron density map (σA weighted 2Fo - Fc map, 2.0 Å, contoured at 1.0σ) for R6BD is shown.

Waals contacts (Figure * 5.4C).

R6BD competes with ubiquitin binding and chain formation

Ubiquitin conjugation is commonly regulated by weak protein-protein interactions. The major binding site of Rad18 (R6BD) on Rad6b overlays with the non-covalent ubiquitin interaction site (Figure 5.5A) and we wished to understand if this interaction has an effect on ubiquitin chain formation ability of Rad6. Firstly, we used our NMR assays to show that R6BD can compete with ubiquitin for backside binding (Figure 5.5B). Next, we studied if R6BD could compete with ubiquitin chain formation by Rad6b. We followed the free ubiquitin chains formed by Rad6b alone or in the presence of R6BD. We also used a control peptide, R6BD*, with four point mutants, that maintained the same overall charge as the native peptide and contained the same number of lysine residues, but bound with a lower affinity (Table 5.2). R6BD* still retains a small inhibition probably because it still has some affinity for Rad6b, or because of target effects in which the pool of free ubiquitin is depleted by conjugation to the peptide. However, ubiquitin chain formation by Rad6b was unequivocally inhibited by R6BD (Figure 5.5C).

Discussion

Our NMR and crystallographic structural studies provide a basis to understand the recognition of Rad6b by Rad18. The C-terminal interaction site of Rad18 with Rad6 was identified by yeast genetic studies [235] before the canonical interaction with the RING ligase domain was demonstrated [228, 236], consistent with the R6BD providing the majority of the binding energy of the interaction. Rad18 R6BD recognizes the backside of Rad6b via a network of hydrogen bonds, salt-bridges and van der Waals contacts. The isolated R6BD peptide binds with a modest affinity and is only partially structured in solution, while longer constructs can be pulled down by Rad6 as stoichiometric complexes [228], consistent with the R6BD domain binding with higher affinity in the full-length protein.

Non-RING interaction sites have been identified for several E3 enzymes. Indeed, even for highly active complexes, the RING-E2 interaction is usually very transient [213]. The presence of an additional site is often a prerequisite for a stable binary complex. These interfaces have been observed adjacent to the RING domain binding site for the c-Cbl-UbcH7 complex [239] or on the back of the E2 for Ube2g2 in complex with gp78 [240, 241]. Binding sites outside the canonical RING interface are also important for the other known ligands of Rad6b; Bre1 and Ubr1 [229, 242].

Using purified proteins, we demonstrate that isolated human Rad6b in capable of forming free ubiquitin chains in solution. *Saccharomyces cerevisiae* Rad6 has a propensity for ubiquitin chain formation that seems to depends on an acidic C-

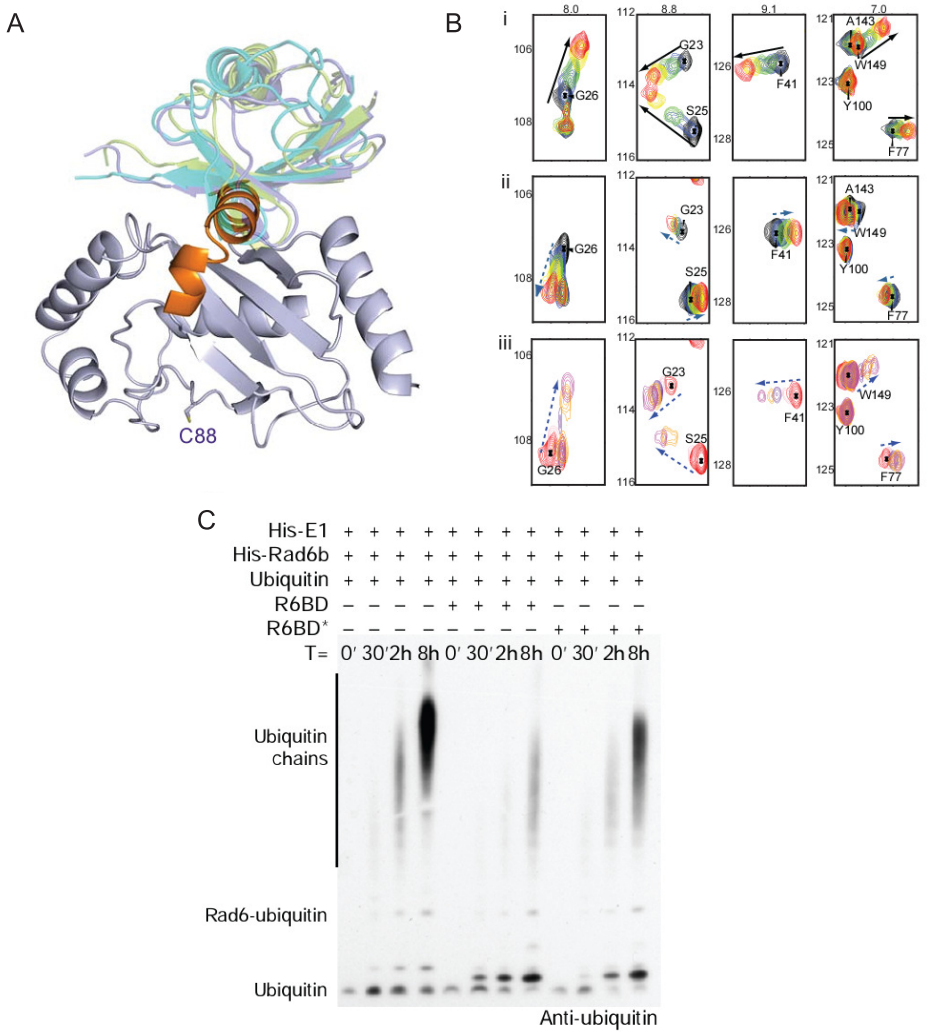

Figure 5.5: Ubiquitin chain formation by Rad6b is inhibited by competition with Rad18. **A.** Our structural data predicts that the binding sites of ubiquitin and R6BD on Rad6b overlap. **B.** R6BD can compete for backside ubiquitin binding. HSQC peaks were studied that had been perturbed in a different direction upon addition of ubiquitin (ii) and R6BD (i) during the separate titrations. A 15N-labeled sample of Rad6b was preincubated with ubiquitin as ii and R6BD (iii) was titrated into the sample.These peaks were observed to move to the same final positions (iii) as the single titration of R6BD into Rad6b (i), confirming that R6BD can compete with ubiquitin for binding to Rad6b. **C.** R6BD will inhibit Rad6-mediated ubiquitin chain formation, compared with a mutated R6BD* peptide.

terminus not conserved in higher eukaryotes [243] but chain formation by mammalian Rad6 homologues has not been extensively studied. Consistent with previous reports [233], Rad6 can non-covalently interact with ubiquitin. In several systems this non-covalent interaction will induce chain formation by one of several different mechanisms [219, 223, 224, 225, 244] that often involve dimerization or oligomerization of the E2. For CDC34 and UbcH5c, dimers or oligomers of the E2 are formed via the non-covalent interaction site upon ubiquitin loading [219, 244].

Oligomerization is required for ubiquitin chain formation by E2 enzyme Ube2g2, but surprisingly, the non-covalent interaction does not seem to be required for the chain formation in this case. The process of chain formation in Ube2g2 is unusual since it forms long ubiquitin chains on its active site cysteine. Our results show that Rad6b has the more common mechanism of forming free ubiquitin chains in solution. Ube2g2 utilizes a similar mode of interaction with its E3, gp78, to the complex between Rad6 and Rad18 [240, 241]: the gp78 peptide forms a continuous helix on the backside of Ube2g2. The binding location of this helix is similar to the R6BD, but it is oriented approximately perpendicular to that of Rad18 on Rad6. Binding of this gp78 peptide causes allosteric activation of Ube2g2 [240] that has not yet been shown in our system (Supplementary Figure 5S.1). Ube2g2 has evolved with changes surrounding its active site that activate it for a mechanism of chain formation distinct from Rad6b and other E2 [245]. The ubiquitin interaction is a prerequisite for chain formation by Rad6b, however, since the R6BD peptide that inhibited the interaction could also inhibit ubiquitin chain formation.

The correct E3 enzyme would be expected to activate Rad6b for ubiquitin chain formation. Rad6b may function in marking a target for proteosomal degradation, since it showed some specificity for K11 and K48 chains. A role of Rad6b-mediated ubiquitin chain formation in the Rad18 and Bre1 pathways is unlikely since Rad6 is currently believed to only monoubiquitinate the targets in these systems [222, 229]. K48-linked ubiquitin chain formation is a product of the N-rule degradation pathways, in which Rad6 is a key player, but it remains to be resolved if human homologues of Rad6 function alone or in tandem with other E2s. It is of particular interest that a recent reconstruction of the ubiquitin network in yeast identified Rad6 as a major hub. It also identified a Golgi-, vesicle-, or endosome-associated role for Rad6 while all the currently known functions are localised predominantly in the nucleus [232]. This suggests that more functions of Rad6 remain to be identified, on new targets or with different E3 ligases, which could utilize the intrinsic chain formation propensity of Rad6.

We find that the chain formation activity of Rad6 can be inhibited by E3 complex-formation with Rad18 and it is likely that interactions with other E3 enzymes would promote or inhibit chain formation in different biological contexts. This functional

diversity of a single E2 is not surprising given the low number of E2 enzymes compared with E3s and targets. Understanding how E3s modulate the activity of E2s towards chain formation on a particular target becomes an exciting area for future research.

Methods

Peptides, Plasmids and Antibodies

Rad18 R6BD (339-366) and R6BD* (H346A, L353A, V354A, A357R) were synthesized in house using standard Fmoc synthesis. Recombinant expression plasmids of His-TEV-Rad6b and ubiquitin have been described previously [228]. His-Rad6b residues 2-152 was cloned into pET28a with a fused N-terminal histidine tag of sequence MGSSHHHHHHSSGLYFQG. Human Uba1 with a C-terminal histidine tag was cloned into pET3a using NdeI/BamHI restriction sites. Full-length Rad18 was cloned into a pSUMO3 vector (SumoPro). Lysine mutants were from Boston Biochem. Mouse antibodies to ubiquitin (P4D1) and His-5 were obtained from Santa Cruz and Sigma, respectively. Goat anti-mouse secondary antibodies were from Biorad.

Protein expression and purification

Purification of ubiquitin, His-Rad6b and His-TEV-Rad6b was performed as described previously [228]. Uba1 and Rad18 were expressed in BL21(DE3) cells using 0.25mM IPTG induction overnight at 15°C. Purification of both proteins was performed by Talon beads (Clontech) in 20mM Tris (pH 8.0), 150mM NaCl, 0.5mM TCEP, with Uba1 eluted using 200-500 mM imidazole (pH 8.0). Further purification of Uba1 was achieved on a Resource Q column (GE Healthcare), using a gradient to 1M NaCl, followed by a Superdex 200 column (GE Healthcare). Rad18 was further purified on a Heparin column (GE Healthcare), and eluted at 500-650mM NaCl, followed by a Superdex 200 column (GE Healthcare).

NMR experiments

NMR experiments were performed in NMR buffer (50mM KH_2PO_4/K_2HPO_4 pH 8.0, 300mM NaCl, 1mM DTT and 5% D_2O and a small amount of complex protease inhibitor (Roche, 1:500 dilution) on a Bruker Avance2 750 MHz NMR spectrometer, at 310K, unless otherwise stated.

Thioester reaction The thioester reaction was performed at 450µl volume in the NMR tube at 303 K. 3µM E1 and 150-300µM ^{15}N-Rad6b and ubiquitin were first incubated in a reaction buffer (50mM Tris-HCl pH 7.5, 75mM NaCl, 5mM $MgCl_2$ and 0.5mM DTT) and the first ^{1}H-^{15}N HSQC spectrum was recorded. 10mM ATP was added and the reaction was followed by a series of ^{1}H-^{15}N HSQC spectra recorded every 45 minutes for 24 hours.

NMR titrations For the titrations of R6BD with Rad6b, the ^{1}H-^{15}N HSQC or ^{1}H-^{13}C HSQC spectra of 200μM isotopically labeled Rad6b were recorded alone and in complex with different ratios of R6BD. Combined CSPs were calculated using the equation, $\Delta\delta ppm = ((\Delta\delta HN)^2 + (\triangle\delta N/5)^2)^{1/2}$. The chemical shift changes were plotted against the molar ratio of Rad6b:R6BD and fitted to standard 1:1 binding curves using the software Origin 8.0 (OriginLab) to estimate the dissociation constants (K_D).

For the ubiquitin and Rad6b non-covalent binding experiments, unlabeled ubiquitin (Sigma; 5mM) was titrated into ^{15}N-labeled Rad6b (200μM) and followed by ^{1}H-^{15}N HSQC spectra. In the reciprocal experiments unlabeled Rad6b (1mM) was added to ^{15}N-labeled ubiquitin (100μM). The ^{1}H and ^{15}N backbone assignments of free ubiquitin were taken from the Biological Magnetic Resonance Data Bank entry 6457.

For the competition experiment, a ^{1}H-^{15}N HSQC spectra of 200μM Rad6b were recorded alone and with addition of ubiquitin at a 3:1 molar ubiquitin:Rad6b ratio. Subsequently, R6BD was titrated into the mixture to a final 3:3:1 R6BD:ubiquitin:Rad6b molar ratio and ^{1}H-^{15}N HSQC spectra were recorded to track the changes.

R6BD structure elucidation Rad18-R6BD was dissolved to a final concentration of 2mM. 2D TOCSY, NOESY, DQF-COSY and natural abundance ^{1}H-^{15}N HSQC spectra were recorded. The Wüthrich strategy was used to assign the 1H resonance frequencies [256]. Secondary Hα chemical shifts were calculated using BMRB random shift values. The CANDID module of the program CYANA was applied to automatically assign NOEs and to calculate the structure [247]. The final NOE restraints used are listed in Supplementary Table 5S.1.

Docking Structure docking of the non-covalent Rad6b/Ub complex was performed using the Haddock webserver [234, 248]. A combination of CSP data from both Rad6b and ubiquitin and the solvent accessibility were used as restraints with active residues defined as follows. Rad6b: 23, 25, 39, 41, 52, 146-147, 149; ubiquitin: 8, 42, 47-49, 68, 70-72. The final solution was an ensemble of 73 structures with root-mean-square deviation of 2.2 Å.

Crystallization, data collection and structure determination

Rad6b (550μM final concentration) was mixed in a 1:2 molar ratio with R6BD (339-366) in 10 mM Hepes (pH 7.5), 150mM NaCl, 0.5mM TCEP and incubated on ice for 10 minutes. Crystals were grown in a vapour diffusion experiment with mother liquor consisting of 2.1-2.3M ammonium sulphate, 100mM sodium cacodylate (pH 6.5) and 0-400mM NaCl. The complex crystallized as hexagonal crystals in space group $P6_522$ with a longest dimension of 100μM. Cryoprotection was achieved by increasing the concentration of glucose up to 150mg/mL in mother liquor (w/v). Data were collected on a single crystal that diffracted up to 2.0Å resolution at 100 K on European

Synchrotron Radiation Facility (ESRF) beam line ID23-2 (λ=0.873 Å). Rad6b also crystallized without R6BD in 200mM sodium tartrate, 100mM bis-tris pH 5.5 and 1.6M ammonium sulfate in space group $P4_32_12$. Cryoprotection was achieved with mineral oil. Crystals diffracted to 1.4Å resolution at 100 K on ESRF beam line ID14-1 (λ=0.934 Å). Data were processed with XDS [249].

Both structures were solved by molecular replacement using Phaser [250] using yeast Rad6 (PDB code 1AYZ) as a search model [251]. Automated model rebuilding by ARP/wARP [252] was followed by iterative model building and refinement sessions using Coot [253] and REFMAC [254]. Anisotropic B-factors were used for the high-resolution native structure and TLS refinement was used for the Rad6b-R6BD complex. For the structure of the complex, the R6BD peptide was clearly visible in the initial difference map and the side chains for residues Lys-341 – Tyr-361 were well resolved in the final map. Residues 339-340 and 362-366 were not resolved and are assumed to be flexible in the structure and were not included into the final model. The quality of model building was assessed using MolProbity [255]. Crystallographic parameters are summarized in Table 5.1. The contacts within the complex were analyzed using PISA [256]. All structure figures were generated using Pymol.

Surface plasmon resonance

Rad6 binding experiments to R6BD were performed at 25°C on a Biacore T-100 instrument (GE healthcare). Rad6b was biotinylated via lysine coupling to a soluble EZ-link reagent (Pierce) and coupled to an SA chip (GE healthcare) to an immobilization density of 120 RUs. During the binding experiment, R6BD was flowed over the chip in 10 mM Hepes, pH 7.5, 500mM NaCl, 0.5mM TCEP, 0.1mg/mL BSA and 0.05% [vol/vol] surfactant p20 at concentrations of 0, 0.75, 1.5, 3.0, 6.0, 12.0, 16.0, 24.0, 32.0, 48.0, 64.0, 96.0, 128.0 μM. Double referencing data subtraction methods were used and equilibrium responses from three independent experiments were fit with single site Langmuir isotherms using GraphPad.

***In vitro* ubiquitin chain formation assays**

Rad6b ubiquitin chain formation assays were performed at 32°C in buffer containing 50mM Tris (pH 8.0 or 8.5), 50mM NaCl, 50mM KCl, 10mM $MgCl_2$ and 0.1mM DTT. Reactions were performed with 80nM Uba1, 3μM Rad6b and 12μM ubiquitin or ubiquitin mutants alone or in the presence of 3μM Rad18 dimer. The peptide inhibition experiment was performed as above except using 20μM Rad6b and 20μM ubiquitin with or without 100mM R6BD or R6BD* peptides, as indicated. Reactions were started by addition of 3mM ATP and at the indicated time points samples were denatured in reducing loading buffer. Samples were run on NuPAGE gels using a MOPS buffer system (Invitrogen), immunoblotted and analyzed.

Acknowledgements

We are grateful to Dene Littler and Alex Faesen for crystallography data collection and Tassos Perrakis and Robbie Joosten for advice during data processing and refinement. Valerie Notenboom provided useful discussions and Tassos Perrakis, Judith Smit and Francesca Mattiroli provided comments on the manuscript. Funding was from EU-SPINE2COMPLEXES (T.K.S. and R.B.), NWO-TOP (R.B.) and EU-RUBICON (TKS).

Author contribution

All authors planned the experiments. R.G.H. and A.H. collected the data. All authors analysed the data. R.G.H. wrote the manuscript. All authors commented on the manuscript prior to submission.

Supplementary Material

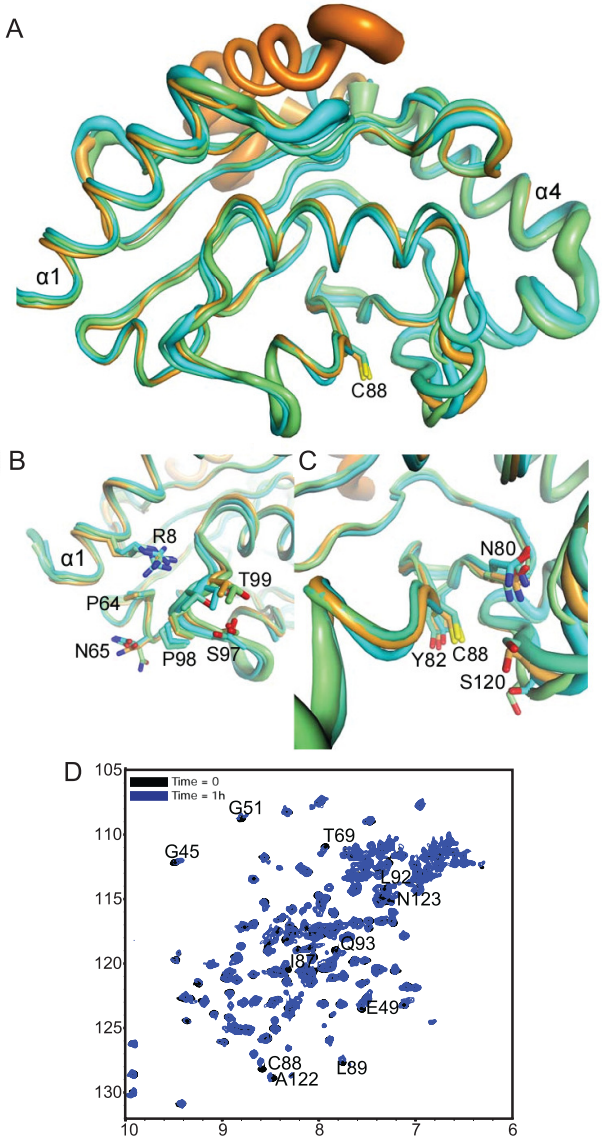

Figure 5S.1: There are no significant structural changes to Rad6b upon binding to R6BD. **A.** Rad6b in complex with R6BD is highly similar to yeast Rad6 (space group I222, PDB code 1AYZ) and native human Rad6b. **B.** No significant changes were observed at the RING interaction surface on Rad6. **C.** No systematic changes were observed around the active site cysteine upon binding to R6BD. The α3-α4 differed between the four structures, but S120 was in an intermediate position in the structure of the complex. The width of the "sausage" Cα trace is based on the B-factor from the PDB coordinate file. The residue numbering is from the human protein. **D.** Loading of Rad6b with ubiquitin, followed by ^{1}H-^{15}N -HSQC spectra.

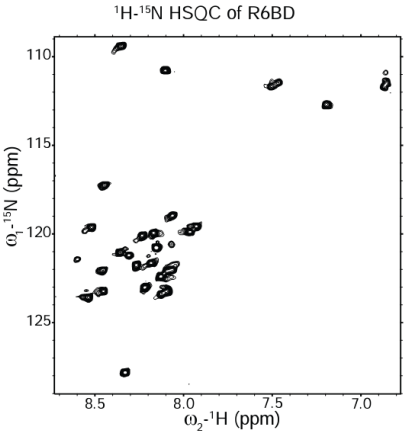

Figure 5S.3: Natural abundance ^{1}H-^{15}N-HSQC spectrum of synthesized peptide R6BD (339-366).

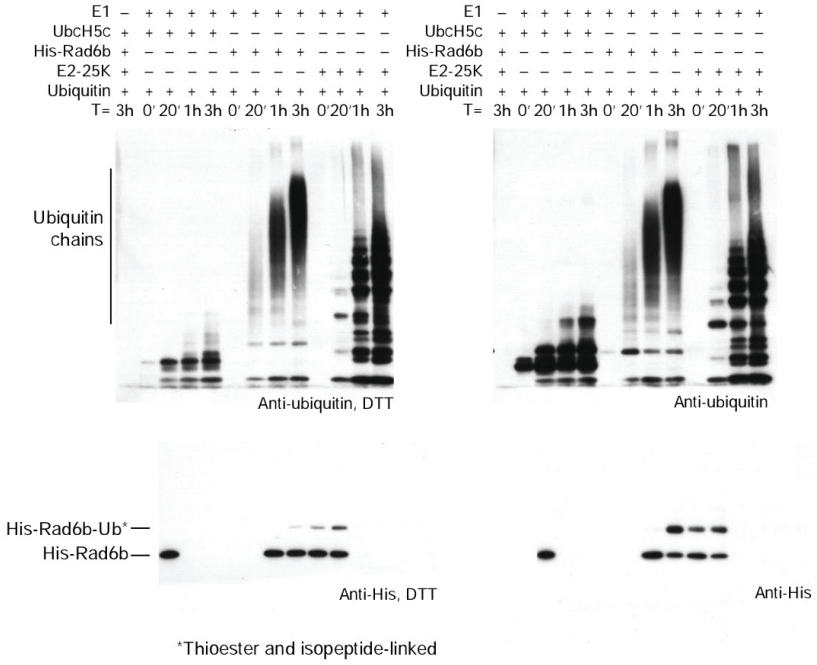

Figure 5S.2: Rad6b mainly forms free ubiquitin chains in solution. The ubiquitin chains formed by Rad6b are predominantly free in solution, with no evidence for ubiquitin chains on the active site cysteine or lysine residues of Rad6. UbcH5c was used as a positive control for thioester formation, whereas E2-25K forms predominantly K48-linked ubiquitin chains.

Table 5S.1: Structural statistics of the free peptide R6BD (339-366) in solution

Number of NMR restraints used in the structure calculation	
Short-range (|i-j| <=1)	234
Medium-range (1<|i-j|<5)	70
Long-range (|i-j|>=5)	5
Total NOE restraints	309
RMSD from mean (Å) for residue 345-360	
All backbone atoms	1.57
All heavy atoms	2.22

References

[1] A. Ciechanover, Tracing the history of the ubiquitin proteolytic system: the pioneering article. Biochem Biophys Res Commun 387 (2009) 1-10.

[2] J.D. Etlinger, A.L. Goldberg, A soluble ATP-dependent proteolytic system responsible for the degradation of abnormal proteins in reticulocytes. Proc Natl Acad Sci U S A 74 (1977) 54-58.

[3] A. Ciehanover, Y. Hod, A. Hershko, A heat-stable polypeptide component of an ATP-dependent proteolytic system from reticulocytes. Biochem Biophys Res Commun 81 (1978) 1100-1105.

[4] I.L. Goldknopf, H. Busch, Isopeptide linkage between nonhistone and histone 2A polypeptides of chromosomal conjugate-protein A24. Proc Natl Acad Sci U S A 74 (1977) 864-868.

[5] A. Ciechanover, S. Elias, H. Heller, S. Ferber, A. Hershko, Characterization of the heat-stable polypeptide of the ATP-dependent proteolytic system from reticulocytes. J Biol Chem 255 (1980) 7525-7528.

[6] K. Tanaka, L. Waxman, A.L. Goldberg, ATP serves two distinct roles in protein degradation in reticulocytes, one requiring and one independent of ubiquitin. J Cell Biol 96 (1983) 1580-1585.

[7] R. Hough, G. Pratt, M. Rechsteiner, Purification of two high molecular weight proteases from rabbit reticulocyte lysate. J Biol Chem 262 (1987) 8303-8313.

[8] B. Skaug, X. Jiang, Z.J. Chen, The role of ubiquitin in NF-kappaB regulatory pathways. Annu Rev Biochem 78 (2009) 769-796.

[9] A.L. Schwartz, A. Ciechanover, Targeting proteins for destruction by the ubiquitin system: implications for human pathobiology. Annu Rev Pharmacol Toxicol 49 (2009) 73-96.

[10] S. Bergink, S. Jentsch, Principles of ubiquitin and SUMO modifications in DNA repair. Nature 458 (2009) 461-467.

[11] V.G. Bhoj, Z.J. Chen, Ubiquitylation in innate and adaptive immunity. Nature 458 (2009) 430-437.

[12] D. Hoeller, I. Dikic, Targeting the ubiquitin system in cancer therapy. Nature 458 (2009) 438-444.

[13] C.M. Pickart, Mechanisms underlying ubiquitination. Annu Rev Biochem 70 (2001) 503-533.

[14] R.L. Welchman, C. Gordon, R.J. Mayer, Ubiquitin and ubiquitin-like proteins as multifunctional signals. Nat Rev Mol Cell Biol 6 (2005) 599-609.

[15] A. Hershko, A. Ciechanover, The ubiquitin system. Annu Rev Biochem 67 (1998) 425-479.

[16] D. Tu, W. Li, Y. Ye, A.T. Brunger, Inaugural Article: Structure and function of the yeast U-box-containing ubiquitin ligase Ufd2p. Proc Natl Acad Sci U S A 104 (2007) 15599-15606.

[17] E. Takahashi, D. Ayusawa, S. Kaneda, Y. Itoh, T. Seno, T. Hori, The human ubiquitin-activating enzyme E1 gene (UBE1) mapped to band Xp11.3—-p11.23 by fluorescence in situ hybridization. Cytogenet Cell Genet 59 (1992) 268-269.

[18] J. Jin, X. Li, S.P. Gygi, J.W. Harper, Dual E1 activation systems for ubiquitin differentially regulate E2 enzyme charging. Nature 447 (2007) 1135-1138.

[19] A.L. Haas, J.V. Warms, A. Hershko, I.A. Rose, Ubiquitin-activating enzyme. Mechanism and role in protein-ubiquitin conjugation. J Biol Chem 257 (1982) 2543-2548.

[20] B.A. Schulman, J.W. Harper, Ubiquitin-like protein activation by E1 enzymes: the apex for downstream signalling pathways. Nat Rev Mol Cell Biol 10 (2009) 319-331.

[21] T. Woelk, S. Sigismund, L. Penengo, S. Polo, The ubiquitination code: a signalling problem. Cell Div 2 (2007) 11.

[22] F.E. Reyes-Turcu, K.H. Ventii, K.D. Wilkinson, Regulation and cellular roles of ubiquitin-specific deubiquitinating enzymes. Annu Rev Biochem 78 (2009) 363-397.

[23] L. Hicke, H.L. Schubert, C.P. Hill, Ubiquitin-binding domains. Nat Rev Mol Cell Biol 6 (2005) 610-621.

[24] I. Dikic, S. Wakatsuki, K.J. Walters, Ubiquitin-binding domains - from structures to functions. Nat Rev Mol Cell Biol 10 (2009) 659-671.

[25] T.M. Venancio, S. Balaji, L.M. Iyer, L. Aravind, Reconstructing the ubiquitin network: cross-talk with other systems and identification of novel functions. Genome Biol 10 (2009) R33.

[26] Y. Ye, M. Rape, Building ubiquitin chains: E2 enzymes at work. Nat Rev Mol Cell Biol 10 (2009) 755-764.

[27] C. Michelle, P. Vourc'h, L. Mignon, C.R. Andres, What was the set of ubiquitin and ubiquitin-like conjugating enzymes in the eukaryote common ancestor? J Mol Evol 68 (2009) 616-628.

[28] M.K. Summers, B. Pan, K. Mukhyala, P.K. Jackson, The unique N terminus of the UbcH10 E2 enzyme controls the threshold for APC activation and enhances checkpoint regulation of the APC. Mol Cell 31 (2008) 544-556.

[29] M.T. Haldeman, G. Xia, E.M. Kasperek, C.M. Pickart, Structure and function of ubiquitin conjugating enzyme E2-25K: the tail is a core-dependent activity element. Biochemistry 36 (1997) 10526-10537.

[30] M.D. Petroski, R.J. Deshaies, Mechanism of lysine 48-linked ubiquitin-chain synthesis by the cullin-RING ubiquitin-ligase complex SCF-Cdc34. Cell 123 (2005) 1107-1120.

[31] P.Y. Wu, M. Hanlon, M. Eddins, C. Tsui, R.S. Rogers, J.P. Jensen, M.J. Matunis, A.M. Weissman, C. Wolberger, C.M. Pickart, A conserved catalytic residue in the ubiquitin-conjugating enzyme family. EMBO J 22 (2003) 5241-5250.

[32] A.A. Yunus, C.D. Lima, Lysine activation and functional analysis of E2-mediated conjugation in the SUMO pathway. Nat Struct Mol Biol 13 (2006) 491-499.

[33] A.M. Burroughs, M. Jaffee, L.M. Iyer, L. Aravind, Anatomy of the E2 ligase fold: implications for enzymology and evolution of ubiquitin/Ub-like protein conjugation. J Struct Biol 162 (2008) 205-218.

[34] L.M. Lois, C.D. Lima, Structures of the SUMO E1 provide mechanistic insights into SUMO activation and E2 recruitment to E1. EMBO J 24 (2005) 439-451.

[35] D.T. Huang, H.W. Hunt, M. Zhuang, M.D. Ohi, J.M. Holton, B.A. Schulman, Basis for a ubiquitin-like protein thioester switch toggling E1-E2 affinity. Nature 445 (2007) 394-398.

[36] I. Lee, H. Schindelin, Structural insights into E1-catalyzed ubiquitin activation and transfer to conjugating enzymes. Cell 134 (2008) 268-278.

[37] L.A. Durfee, M.L. Kelley, J.M. Huibregtse, The basis for selective E1-E2 interactions in the ISG15 conjugation system. J Biol Chem 283 (2008) 23895-23902.

[38] S.K. Olsen, A.D. Capili, X. Lu, D.S. Tan, C.D. Lima, Active site remodelling accompanies thioester bond formation in the SUMO E1. Nature 463 906-912.

[39] D.T. Huang, O. Ayrault, H.W. Hunt, A.M. Taherbhoy, D.M. Duda, D.C. Scott, L.A. Borg, G. Neale, P.J. Murray, M.F. Roussel, B.A. Schulman, E2-RING expansion of the NEDD8 cascade confers specificity to cullin modification. Mol Cell 33 (2009) 483-495.

[40] D.T. Huang, D.W. Miller, R. Mathew, R. Cassell, J.M. Holton, M.F. Roussel, B.A. Schulman, A unique E1-E2 interaction required for optimal conjugation of the ubiquitin-like protein NEDD8. Nat Struct Mol Biol 11 (2004) 927-935.

[41] H.C. Ardley, P.A. Robinson, E3 ubiquitin ligases. Essays Biochem 41 (2005) 15-30.

[42] S.J. van Wijk, S.J. de Vries, P. Kemmeren, A. Huang, R. Boelens, A.M. Bonvin, H.T. Timmers, A comprehensive framework of E2-RING E3 interactions of the human ubiquitin-proteasome system. Mol Syst Biol 5 (2009) 295.

[43] G. Markson, C. Kiel, R. Hyde, S. Brown, P. Charalabous, A. Bremm, J. Semple, J. Woodsmith, S. Duley, K. Salehi-Ashtiani, M. Vidal, D. Komander, L. Serrano, P. Lehner, C.M. Sanderson, Analysis of the human E2 ubiquitin conjugating enzyme protein interaction network. Genome Res 19 (2009) 1905-1911.

[44] L. Huang, E. Kinnucan, G. Wang, S. Beaudenon, P.M. Howley, J.M. Huibregtse, N.P. Pavletich, Structure of an E6AP-UbcH7 complex: insights into ubiquitination by the E2-E3 enzyme cascade. Science 286 (1999) 1321-1326.

[45] N. Zheng, P. Wang, P.D. Jeffrey, N.P. Pavletich, Structure of a c-Cbl-UbcH7 complex: RING domain function in ubiquitin-protein ligases. Cell 102 (2000) 533-539.

[46] P.S. Brzovic, J.R. Keeffe, H. Nishikawa, K. Miyamoto, D. Fox, 3rd, M. Fukuda, T. Ohta, R. Klevit, Binding and recognition in the assembly of an active BRCA1/BARD1 ubiquitin-ligase complex. Proc Natl Acad Sci U S A 100 (2003) 5646-5651.

[47] T.K. Albert, H. Hanzawa, Y.I. Legtenberg, M.J. de Ruwe, F.A. van den Heuvel, M.A. Collart, R. Boelens, H.T. Timmers, Identification of a ubiquitin-protein ligase subunit within the CCR4-NOT transcription repressor complex. EMBO J 21 (2002) 355-364.

[48] C. Dominguez, A.M. Bonvin, G.S. Winkler, F.M. van Schaik, H.T. Timmers, R. Boelens, Structural model of the UbcH5B/CNOT4 complex revealed by combining NMR, mutagenesis, and docking approaches. Structure 12 (2004) 633-644.

[49] M. Zhang, M. Windheim, S.M. Roe, M. Peggie, P. Cohen, C. Prodromou, L.H. Pearl, Chaperoned ubiquitylation–crystal structures of the CHIP U box E3 ubiquitin ligase and a CHIP-Ubc13-Uev1a complex. Mol Cell 20 (2005) 525-538.

[50] Z. Xu, E. Kohli, K.I. Devlin, M. Bold, J.C. Nix, S. Misra, Interactions between the quality control ubiquitin ligase CHIP and ubiquitin conjugating enzymes. BMC Struct Biol 8 (2008) 26.

[51] P.D. Mace, K. Linke, R. Feltham, F.R. Schumacher, C.A. Smith, D.L. Vaux, J. Silke, C.L. Day, Structures of the cIAP2 RING domain reveal conformational changes associated with ubiquitin-conjugating enzyme (E2) recruitment. J Biol Chem 283 (2008) 31633-31640.

[52] Q. Yin, S.C. Lin, B. Lamothe, M. Lu, Y.C. Lo, G. Hura, L. Zheng, R.L. Rich, A.D. Campos, D.G. Myszka, M.J. Lenardo, B.G. Darnay, H. Wu, E2 interaction and dimerization in the crystal structure of TRAF6. Nat Struct Mol Biol 16 (2009) 658-666.

[53] Z.M. Eletr, D.T. Huang, D.M. Duda, B.A. Schulman, B. Kuhlman, E2 conjugating enzymes must disengage from their E1 enzymes before E3-dependent ubiquitin and ubiquitin-like transfer. Nat Struct Mol Biol 12 (2005) 933-934.

[54] E. Ozkan, H. Yu, J. Deisenhofer, Mechanistic insight into the allosteric activation of a ubiquitin-conjugating enzyme by RING-type ubiquitin ligases. Proc Natl Acad Sci U S A 102 (2005) 18890-18895.

[55] A. Huang, R.N. de Jong, H. Wienk, G.S. Winkler, H.T. Timmers, R. Boelens, E2-c-Cbl recognition is necessary but not sufficient for ubiquitination activity. J Mol Biol 385 (2009) 507-519.

[56] D.E. Christensen, P.S. Brzovic, R.E. Klevit, E2-BRCA1 RING interactions dictate synthesis of mono- or specific polyubiquitin chain linkages. Nat Struct Mol Biol 14 (2007) 941-948.

[57] D.S. Kirkpatrick, N.A. Hathaway, J. Hanna, S. Elsasser, J. Rush, D. Finley, R.W. King, S.P. Gygi, Quantitative analysis of in vitro ubiquitinated cyclin B1 reveals complex chain topology. Nat Cell Biol 8 (2006) 700-710.

[58] H.T. Kim, K.P. Kim, F. Lledias, A.F. Kisselev, K.M. Scaglione, D. Skowyra, S.P. Gygi, A.L. Goldberg, Certain pairs of ubiquitin-conjugating enzymes (E2s) and ubiquitin-protein ligases (E3s) synthesize nondegradable forked ubiquitin chains containing all possible isopeptide linkages. J Biol Chem 282 (2007) 17375-17386.

[59] F. Wu-Baer, K. Lagrazon, W. Yuan, R. Baer, The BRCA1/BARD1 heterodimer assembles polyubiquitin chains through an unconventional linkage involving lysine residue K6 of ubiquitin. J Biol Chem 278 (2003) 34743-34746.

[60] W. Li, M.H. Bengtson, A. Ulbrich, A. Matsuda, V.A. Reddy, A. Orth, S.K. Chanda, S. Batalov, C.A. Joazeiro, Genome-wide and functional annotation of human E3 ubiquitin ligases identifies MULAN, a mitochondrial E3 that regulates the organelle's dynamics and signaling. PLoS One 3 (2008) e1487.

[61] K.S. Hamilton, M.J. Ellison, G.S. Shaw, Identification of the ubiquitin interfacial residues in a ubiquitin-E2 covalent complex. J Biomol NMR 18 (2000) 319-327.

[62] K.S. Hamilton, M.J. Ellison, K.R. Barber, R.S. Williams, J.T. Huzil, S. McKenna, C. Ptak, M. Glover, G.S. Shaw, Structure of a conjugating enzyme-ubiquitin thiolester intermediate reveals a novel role for the ubiquitin tail. Structure 9 (2001) 897-904.

[63] P.S. Brzovic, A. Lissounov, D.E. Christensen, D.W. Hoyt, R.E. Klevit, A UbcH5/ubiquitin noncovalent complex is required for processive BRCA1-directed ubiquitination. Mol Cell 21 (2006) 873-880.

[64] N. Merkley, K.R. Barber, G.S. Shaw, Ubiquitin manipulation by an E2 conjugating enzyme using a novel covalent intermediate. J Biol Chem 280 (2005) 31732-31738.

[65] M.J. Eddins, C.M. Carlile, K.M. Gomez, C.M. Pickart, C. Wolberger, Mms2-Ubc13 covalently bound to ubiquitin reveals the structural basis of linkage-specific polyubiquitin chain formation. Nat Struct Mol Biol 13 (2006) 915-920.

[66] T. Miura, W. Klaus, B. Gsell, C. Miyamoto, H. Senn, Characterization of the binding interface between ubiquitin and class I human ubiquitin-conjugating enzyme 2b by multidimensional heteronuclear NMR spectroscopy in solution. J Mol Biol 290 (1999) 213-228.

[67] A. Saha, R.J. Deshaies, Multimodal activation of the ubiquitin ligase SCF by Nedd8 conjugation. Mol Cell 32 (2008) 21-31.

[68] M. Windheim, M. Peggie, P. Cohen, Two different classes of E2 ubiquitin-conjugating enzymes are required for the mono-ubiquitination of proteins and elongation by polyubiquitin chains with a specific topology. Biochem J 409 (2008) 723-729.

[69] K.S. Ryu, Y.S. Choi, J. Ko, S.O. Kim, H.J. Kim, H.K. Cheong, Y.H. Jeon, B.S. Choi, C. Cheong, Direct characterization of E2-dependent target specificity and processivity using an artificial p27-linker-E2 ubiquitination system. BMB Rep 41 (2008) 852-857.

[70] M.C. Rodrigo-Brenni, D.O. Morgan, Sequential E2s drive polyubiquitin chain assembly on APC targets. Cell 130 (2007) 127-139.

[71] C. Hoege, B. Pfander, G.L. Moldovan, G. Pyrowolakis, S. Jentsch, RAD6-dependent DNA repair is linked to modification of PCNA by ubiquitin and SUMO. Nature 419 (2002) 135-141.

[72] P. Knipscheer, W.J. van Dijk, J.V. Olsen, M. Mann, T.K. Sixma, Noncovalent interaction between Ubc9 and SUMO promotes SUMO chain formation. EMBO J 26 (2007) 2797-2807.

[73] A.D. Capili, C.D. Lima, Structure and analysis of a complex between SUMO and Ubc9 illustrates features of a conserved E2-Ubl interaction. J Mol Biol 369 (2007) 608-618.

[74] V. Bailly, S. Lauder, S. Prakash, L. Prakash, Yeast DNA repair proteins Rad6 and Rad18 form a heterodimer that has ubiquitin conjugating, DNA binding, and ATP hydrolytic activities. J Biol Chem 272 (1997) 23360-23365.

[75] V. Notenboom, R.G. Hibbert, S.E. van Rossum-Fikkert, J.V. Olsen, M. Mann, T.K. Sixma, Functional characterization of Rad18 domains for Rad6, ubiquitin, DNA binding and PCNA modification. Nucleic Acids Res 35 (2007) 5819-5830.

[76] J.W. Back, V. Notenboom, L.J. de Koning, A.O. Muijsers, T.K. Sixma, C.G. de Koster, L. de Jong, Identification of cross-linked peptides for protein interaction studies using mass spectrometry and 18O labeling. Anal Chem 74 (2002) 4417-4422.

[77] Y. Xie, A. Varshavsky, The E2-E3 interaction in the N-end rule pathway: the RING-H2 finger of E3 is required for the synthesis of multiubiquitin chain. EMBO J 18 (1999) 6832-6844.

[78] W. Li, D. Tu, L. Li, T. Wollert, R. Ghirlando, A.T. Brunger, Y. Ye, Mechanistic insights into active site-associated polyubiquitination by the ubiquitin-conjugating enzyme Ube2g2. Proc Natl Acad Sci U S A 106 (2009) 3722-3727.

[79] J. Kim, M. Guermah, R.K. McGinty, J.S. Lee, Z. Tang, T.A. Milne, A. Shilatifard, T.W. Muir, R.G. Roeder, RAD6-Mediated transcription-coupled H2B ubiquitylation directly stimulates H3K4 methylation in human cells. Cell 137 (2009) 459-471.

[80] W. Li, D. Tu, A.T. Brunger, Y. Ye, A ubiquitin ligase transfers preformed polyubiquitin chains from a conjugating enzyme to a substrate. Nature 446 (2007) 333-337.

[81] R. Das, J. Mariano, Y.C. Tsai, R.C. Kalathur, Z. Kostova, J. Li, S.G. Tarasov, R.L. McFeeters, A.S. Altieri, X. Ji, R.A. Byrd, A.M. Weissman, Allosteric activation of E2-RING finger-mediated ubiquitylation by a structurally defined specific E2-binding region of gp78. Mol Cell 34 (2009) 674-685.

[82] X. Varelas, C. Ptak, M.J. Ellison, Cdc34 self-association is facilitated by ubiquitin thiolester formation and is required for its catalytic activity. Mol Cell Biol 23 (2003) 5388-5400.

[83] R.G. Hibbert, F. Mattiroli, T.K. Sixma, Structural aspects of multi-domain RING/Ubox E3 ligases in DNA repair. DNA Repair (Amst) 8 (2009) 525-535.

[84] G.L. Moldovan, B. Pfander, S. Jentsch, PCNA, the maestro of the replication fork. Cell 129 (2007) 665-679.

[85] K. Watanabe, S. Tateishi, M. Kawasuji, T. Tsurimoto, H. Inoue, M. Yamaizumi, Rad18 guides poleta to replication stalling sites through physical interaction and PCNA monoubiquitination. EMBO J 23 (2004) 3886-3896.

[86] P.L. Kannouche, J. Wing, A.R. Lehmann, Interaction of human DNA polymerase eta with monoubiquitinated PCNA: a possible mechanism for the polymerase switch in response to DNA damage. Mol Cell 14 (2004) 491-500.

[87] H.D. Ulrich, S. Jentsch, Two RING finger proteins mediate cooperation between ubiquitin-conjugating enzymes in DNA repair. EMBO J 19 (2000) 3388-3397.

[88] H. Zhang, C.W. Lawrence, The error-free component of the RAD6/RAD18 DNA damage tolerance pathway of budding yeast employs sister-strand recombination. Proc Natl Acad Sci U S A 102 (2005) 15954-15959.

[89] K.M. Sakamoto, Ubiquitin-dependent proteolysis: its role in human diseases and the design of therapeutic strategies. Mol Genet Metab 77 (2002) 44-56.

[90] A. Ciechanover, A.L. Schwartz, The ubiquitin system: pathogenesis of human diseases and drug targeting. Biochim Biophys Acta 1695 (2004) 3-17.

[91] M.D. Petroski, The ubiquitin system, disease, and drug discovery. BMC Biochem 9 Suppl 1 (2008) S7.

[92] G.L. Bond, W. Hu, A.J. Levine, MDM2 is a central node in the p53 pathway: 12 years and counting. Curr Cancer Drug Targets 5 (2005) 3-8.

[93] N.P. Pavletich, K.A. Chambers, C.O. Pabo, The DNA-binding domain of p53 contains the four conserved regions and the major mutation hot spots. Genes Dev 7 (1993) 2556-2564.

[94] S. Shangary, S. Wang, Small-molecule inhibitors of the MDM2-p53 protein-protein interaction to reactivate p53 function: a novel approach for cancer therapy. Annu Rev Pharmacol Toxicol 49 (2009) 223-241.

[95] T.A. Soucy, P.G. Smith, M.A. Milhollen, A.J. Berger, J.M. Gavin, S. Adhikari, J.E. Brownell, K.E. Burke, D.P. Cardin, S. Critchley, C.A. Cullis, A. Doucette, J.J. Garnsey, J.L. Gaulin, R.E. Gershman, A.R. Lublinsky, A. McDonald, H. Mizutani, U. Narayanan, E.J. Olhava, S. Peluso, M. Rezaei, M.D. Sintchak, T. Talreja, M.P. Thomas, T. Traore, S. Vyskocil, G.S. Weatherhead, J. Yu, J. Zhang, L.R. Dick, C.F. Claiborne, M. Rolfe, J.B. Bolen, S.P. Langston, An inhibitor of NEDD8-activating enzyme as a new approach to treat cancer. Nature 458 (2009) 732-736.

[96] R. Lovering, I.M. Hanson, K.L. Borden, S. Martin, N.J. O'Reilly, G.I. Evan, D. Rahman, D.J. Pappin, J. Trowsdale, P.S. Freemont, Identification and preliminary characterization of a protein motif related to the zinc finger. Proc Natl Acad Sci U S A 90 (1993) 2112-2116.

[97] C.M. Pickart, Mechanisms underlying ubiquitination. Annu Rev Biochem 70 (2001) 503-533.

[98] R.J. Deshaies, C.A. Joazeiro, RING domain E3 ubiquitin ligases. Annu Rev Biochem 78 (2009) 399-434.

[99] K.L. Borden, P.S. Freemont, The RING finger domain: a recent example of a sequence-structure family. Curr Opin Struct Biol 6 (1996) 395-401.

[100] P.S. Freemont, The RING finger. A novel protein sequence motif related to the zinc finger. Ann N Y Acad Sci 684 (1993) 174-192.

[101] H. Hanzawa, M.J. de Ruwe, T.K. Albert, P.C. van Der Vliet, H.T. Timmers, R. Boelens, The structure of the C4C4 ring finger of human NOT4 reveals features distinct from those of C3HC4 RING fingers. J Biol Chem 276 (2001) 10185-10190.

[102] L. Aravind, E.V. Koonin, The U box is a modified RING finger - a common domain in ubiquitination. Curr Biol 10 (2000) R132-134.

[103] M.D. Ohi, C.W. Vander Kooi, J.A. Rosenberg, W.J. Chazin, K.L. Gould, Structural insights into the U-box, a domain associated with multi-ubiquitination. Nat Struct Biol 10 (2003) 250-255.

[104] G. Markson, C. Kiel, A.R. Hyde, S. Brown, P. Charalabous, A. Bremm, J. Semple, J. Woodsmith, S. Duley, K. Salehi-Ashtiani, M. Vidal, D. Komander, L. Serrano, P. Lehner, C. Sanderson, Analysis of the human E2 ubiquitin conjugating enzyme protein interaction network. Genome Res (2009).

[105] S.J. van Wijk, S.J. de Vries, P. Kemmeren, A. Huang, R. Boelens, A.M. Bonvin, H.T. Timmers, A comprehensive framework of E2-RING E3 interactions of the human ubiquitin-proteasome system. Mol Syst Biol 5 (2009) 295.

[106] D.E. Christensen, P.S. Brzovic, R.E. Klevit, E2-BRCA1 RING interactions dictate synthesis of mono- or specific polyubiquitin chain linkages. Nat Struct Mol Biol 14 (2007) 941-948.

[107] P.S. Brzovic, R.E. Klevit, Ubiquitin transfer from the E2 perspective: why is UbcH5 so promiscuous? Cell Cycle 5 (2006) 2867-2873.

[108] C. Hoege, B. Pfander, G.L. Moldovan, G. Pyrowolakis, S. Jentsch, RAD6-dependent DNA repair is linked to modification of PCNA by ubiquitin and SUMO. Nature 419 (2002) 135-141.

[109] D. Esposito, D.K. Chatterjee, Enhancement of soluble protein expression through the use of fusion tags. Curr Opin Biotechnol 17 (2006) 353-358.

[110] G.E. Folkers, B.N. van Buuren, R. Kaptein, Expression screening, protein purification and NMR analysis of human protein domains for structural genomics. J Struct Funct Genomics 5 (2004) 119-131.

[111] R.N. de Jong, M.A. Daniels, R. Kaptein, G.E. Folkers, Enzyme free cloning for high throughput gene cloning and expression. J Struct Funct Genomics 7 (2006) 109-118.

[112] M. Jansson, Y.C. Li, L. Jendeberg, S. Anderson, B.T. Montelione, B. Nilsson, High-level production of uniformly 15N- and 13C-enriched fusion proteins in Escherichia coli. J Biomol NMR 7 (1996) 131-141.

[113] J.R. Huth, C.A. Bewley, B.M. Jackson, A.G. Hinnebusch, G.M. Clore, A.M. Gronenborn, Design of an expression system for detecting folded protein domains and mapping macromolecular interactions by NMR. Protein Sci 6 (1997) 2359-2364..

[114] E.R. LaVallie, E.A. DiBlasio, S. Kovacic, K.L. Grant, P.F. Schendel, J.M. McCoy, A thioredoxin gene fusion expression system that circumvents inclusion body formation in the E. coli cytoplasm. Biotechnology (N Y) 11 (1993) 187-193.

[115] D.B. Smith, K.S. Johnson, Single-step purification of polypeptides expressed in Escherichia coli as fusions with glutathione S-transferase. Gene 67 (1988) 31-40.

[116] E.A. Woestenenk, M. Hammarstrom, S. van den Berg, T. Hard, H. Berglund, His tag effect on solubility of human proteins produced in Escherichia coli: a comparison between four expression vectors. J Struct Funct Genomics 5 (2004) 217-229.

[117] M. Hammarstrom, E.A. Woestenenk, N. Hellgren, T. Hard, H. Berglund, Effect of N-terminal solubility enhancing fusion proteins on yield of purified target protein. J Struct Funct Genomics 7 (2006) 1-14.

[118] M. Hammarstrom, N. Hellgren, S. van Den Berg, H. Berglund, T. Hard, Rapid screening for improved solubility of small human proteins produced as fusion proteins in Escherichia coli. Protein Sci 11 (2002) 313-321.

[119] S. Katoh, C. Hong, Y. Tsunoda, K. Murata, R. Takai, E. Minami, T. Yamazaki, E. Katoh, High precision NMR structure and function of the RING-H2 finger domain of EL5, a rice protein whose expression is increased upon exposure to pathogen-derived oligosaccharides. J Biol Chem 278 (2003) 15341-15348.

[120] N.G. Kandias, C.T. Chasapis, D. Bentrop, V. Episkopou, G.A. Spyroulias, High yield expression and NMR characterization of Arkadia E3 ubiquitin ligase RING-H2 finger domain. Biochem Biophys Res Commun 378 (2009) 498-502.

[121] K.L. Lorick, J.P. Jensen, A.M. Weissman, Expression, purification, and properties of the Ubc4/5 family of E2 enzymes. Methods Enzymol 398 (2005) 54-68.

[122] G.F. John T. Edsall, DeWitt S. Goodman, Frank R. N. Gurd, The Association of Imidazole with the Ions of Zinc and Cupric Copper, J. Am. Chem. Soc.„ 1954, pp. 3054–3061.

[123] L. Nieba, S.E. Nieba-Axmann, A. Persson, M. Hamalainen, F. Edebratt, A. Hansson, J. Lidholm, K. Magnusson, A.F. Karlsson, A. Pluckthun, BIACORE analysis of histidine-tagged proteins using a chelating NTA sensor chip. Anal Biochem 252 (1997) 217-228.

[124] R.J.S.a.R.B. MARTIN, Interactions of Histidine and Other Imidazole Derivatives with Transition Metal Ions in Chemical and Biological Systems. Chemical Reviews Vol. 74, No. 4 (1974).

[125] G.S. Makowski, F.W. Sunderman, Jr., The interactions of zinc, nickel, and cadmium with Xenopus transcription factor IIIA, assessed by equilibrium dialysis. J Inorg Biochem 48 (1992) 107-119.

[126] A. Huang, R.N. de Jong, H. Wienk, G.S. Winkler, H.T. Timmers, R. Boelens, E2-c-Cbl recognition is necessary but not sufficient for ubiquitination activity. J Mol Biol 385 (2009) 507-519.

[127] Pickart, C. M. (2001). Mechanisms underlying ubiquitination. Annu Rev Biochem 70, 503-33.

[128] Kerscher, O., Felberbaum, R. & Hochstrasser, M. (2006). Modification of proteins by ubiquitin and ubiquitin-like proteins. Annu Rev Cell Dev Biol 22, 159-80.

[129] Andersen, P. L., Zhou, H., Pastushok, L., Moraes, T., McKenna, S., Ziola, B., Ellison, M. J., Dixit, V. M. & Xiao, W. (2005). Distinct regulation of Ubc13 functions by the two ubiquitin-conjugating enzyme variants Mms2 and Uev1A. J Cell Biol 170, 745-55.

[130] Brzovic, P. S., Lissounov, A., Christensen, D. E., Hoyt, D. W. & Klevit, R. E. (2006). A UbcH5/ubiquitin noncovalent complex is required for processive BRCA1-directed ubiquitination. Mol Cell 21, 873-80.

[131] Zheng, N., Wang, P., Jeffrey, P. D. & Pavletich, N. P. (2000). Structure of a c-Cbl-UbcH7 complex: RING domain function in ubiquitin-protein ligases. Cell 102, 533-9.

[132] Huang, L., Kinnucan, E., Wang, G., Beaudenon, S., Howley, P. M., Huibregtse, J. M. & Pavletich, N. P. (1999). Structure of an E6AP-UbcH7 complex: insights into ubiquitination by the E2-E3 enzyme cascade. Science 286, 1321-6.

[133] Dominguez, C., Bonvin, A. M., Winkler, G. S., van Schaik, F. M., Timmers, H. T. & Boelens, R. (2004). Structural model of the UbcH5B/CNOT4 complex revealed by combining NMR, mutagenesis, and docking approaches. Structure 12, 633-44.

[134] Zhang, M., Windheim, M., Roe, S. M., Peggie, M., Cohen, P., Prodromou, C. & Pearl, L. H. (2005). Chaperoned ubiquitylation–crystal structures of the CHIP U box E3 ubiquitin ligase and a CHIP-Ubc13-Uev1a complex. Mol Cell 20, 525-38.

[135] Hamilton, K. S., Ellison, M. J., Barber, K. R., Williams, R. S., Huzil, J. T., McKenna, S., Ptak, C., Glover, M. & Shaw, G. S. (2001). Structure of a conjugating enzyme-ubiquitin thiolester intermediate reveals a novel role for the ubiquitin tail. Structure 9, 897-904.

[136] Jin, J., Li, X., Gygi, S. P. & Harper, J. W. (2007). Dual E1 activation systems for ubiquitin differentially regulate E2 enzyme charging. Nature 447, 1135-8.

[137] Glickman, M. H. & Ciechanover, A. (2002). The ubiquitin-proteasome proteolytic pathway: destruction for the sake of construction. Physiol Rev 82, 373-428.

[138] Kus, B. M., Caldon, C. E., Andorn-Broza, R. & Edwards, A. M. (2004). Functional interaction of 13 yeast SCF complexes with a set of yeast E2 enzymes in vitro. Proteins 54, 455-67.

[139] Petroski, M. D. & Deshaies, R. J. (2005). Mechanism of lysine 48-linked ubiquitin-chain synthesis by the cullin-RING ubiquitin-ligase complex SCF-Cdc34. Cell 123, 1107-20.

[140] Jin, L., Williamson, A., Banerjee, S., Philipp, I. & Rape, M. (2008). Mechanism of ubiquitin-chain formation by the human anaphase-promoting complex. Cell 133, 653-65.

[141] Kirkpatrick, D. S., Hathaway, N. A., Hanna, J., Elsasser, S., Rush, J., Finley, D., King, R. W. & Gygi, S. P. (2006). Quantitative analysis of in vitro ubiquitinated cyclin B1 reveals complex chain topology. Nat Cell Biol 8, 700-10.

[142] Brzovic, P. S., Keeffe, J. R., Nishikawa, H., Miyamoto, K., Fox, D., 3rd, Fukuda, M., Ohta, T. & Klevit, R. (2003). Binding and recognition in the assembly of an active BRCA1/BARD1 ubiquitin-ligase complex. Proc Natl Acad Sci U S A 100, 5646-51.

[143] Buchwald, G., van der Stoop, P., Weichenrieder, O., Perrakis, A., van Lohuizen, M. & Sixma, T. K. (2006). Structure and E3-ligase activity of the Ring-Ring complex of polycomb proteins Bmi1 and Ring1b. EMBO J 25, 2465-74.

[144] Peschard, P., Kozlov, G., Lin, T., Mirza, I. A., Berghuis, A. M., Lipkowitz, S., Park, M. & Gehring, K. (2007). Structural basis for ubiquitin-mediated dimerization and activation of the ubiquitin protein ligase Cbl-b. Mol Cell 27, 474-85.

[145] Joazeiro, C. A., Wing, S. S., Huang, H., Leverson, J. D., Hunter, T. & Liu, Y. C. (1999). The tyrosine kinase negative regulator c-Cbl as a RING-type, E2-dependent ubiquitin-protein ligase. Science 286, 309-12.

[146] Ogunjimi, A. A., Briant, D. J., Pece-Barbara, N., Le Roy, C., Di Guglielmo, G. M., Kavsak, P., Rasmussen, R. K., Seet, B. T., Sicheri, F. & Wrana, J. L. (2005). Regulation of Smurf2 ubiquitin ligase activity by anchoring the E2 to the HECT domain. Mol Cell 19, 297-308.

[147] Gallagher, E., Gao, M., Liu, Y. C. & Karin, M. (2006). Activation of the E3 ubiquitin ligase Itch through a phosphorylation-induced conformational change. Proc Natl Acad Sci U S A 103, 1717-22.

[148] Yokouchi, M., Kondo, T., Houghton, A., Bartkiewicz, M., Horne, W. C., Zhang, H., Yoshimura, A. & Baron, R. (1999). Ligand-induced ubiquitination of the epidermal growth factor receptor involves the interaction of the c-Cbl RING finger and UbcH7. J Biol Chem 274, 31707-12.

[149] Yokouchi, M., Kondo, T., Sanjay, A., Houghton, A., Yoshimura, A., Komiya, S., Zhang, H. & Baron, R. (2001). Src-catalyzed phosphorylation of c-Cbl leads to the interdependent ubiquitination of both proteins. J Biol Chem 276, 35185-93.

[150] Levkowitz, G., Waterman, H., Ettenberg, S. A., Katz, M., Tsygankov, A. Y., Alroy, I., Lavi, S., Iwai, K., Reiss, Y., Ciechanover, A., Lipkowitz, S. & Yarden, Y. (1999). Ubiquitin ligase activity and tyrosine phosphorylation underlie suppression of growth factor signaling by c-Cbl/Sli-1. Mol Cell 4, 1029-40.

[151] Kim, M., Tezuka, T., Tanaka, K. & Yamamoto, T. (2004). Cbl-c suppresses v-Src-induced transformation through ubiquitin-dependent protein degradation. Oncogene 23, 1645-55.

[152] Lorick, K. L., Jensen, J. P., Fang, S., Ong, A. M., Hatakeyama, S. & Weissman, A. M. (1999). RING fingers mediate ubiquitin-conjugating enzyme (E2)-dependent ubiquitination. Proc Natl Acad Sci U S A 96, 11364-9.

[153] Thien, C. B. & Langdon, W. Y. (2005). c-Cbl and Cbl-b ubiquitin ligases: substrate diversity and the negative regulation of signalling responses. Biochem J 391, 153-66.

[154] Ozkan, E., Yu, H. & Deisenhofer, J. (2005). Mechanistic insight into the allosteric activation of a ubiquitin-conjugating enzyme by RING-type ubiquitin ligases. Proc Natl Acad Sci U S A 102, 18890-5.

[155] Winn, P. J., Zahran, M., Battey, J. N., Zhou, Y., Wade, R. C. & Banerjee, A. (2007). Structural and electrostatic properties of ubiquitination and related pathways. Front Biosci 12, 3419-30.

[156] Christensen, D. E., Brzovic, P. S. & Klevit, R. E. (2007). E2-BRCA1 RING interactions dictate synthesis of mono- or specific polyubiquitin chain linkages. Nat Struct Mol Biol 14, 941-8.

[157] Geetha, T., Jiang, J. & Wooten, M. W. (2005). Lysine 63 polyubiquitination of the nerve growth factor receptor TrkA directs internalization and signaling. Mol Cell 20, 301-12.

[158] Albert, T. K., Hanzawa, H., Legtenberg, Y. I., de Ruwe, M. J., van den Heuvel, F. A., Collart, M. A., Boelens, R. & Timmers, H. T. (2002). Identification of a ubiquitin-protein ligase subunit within the CCR4-NOT transcription repressor complex. EMBO J 21, 355-64.

[159] Winkler, G. S., Albert, T. K., Dominguez, C., Legtenberg, Y. I., Boelens, R. & Timmers, H. T. (2004). An altered-specificity ubiquitin-conjugating enzyme/ubiquitin-protein ligase pair. J Mol Biol 337, 157-65.

[160] Eletr, Z. M. & Kuhlman, B. (2007). Sequence determinants of E2-E6AP binding affinity and specificity. J Mol Biol 369, 419-28.

[161] de Jong, R. N., Daniels, M. A., Kaptein, R. & Folkers, G. E. (2006). Enzyme free cloning for high throughput gene cloning and expression. J Struct Funct Genomics 7, 109-18.

[162] Folkers, G. E., van Buuren, B. N. & Kaptein, R. (2004). Expression screening, protein purification and NMR analysis of human protein domains for structural genomics. J Struct Funct Genomics 5, 119-31.

[163] Sattler, M., Schleucher, J. & Griesinger, C. (1999). Heteronuclear multidimensional NMR experiments for the structure determination of proteins in solution employing pulsed field gradients. Progress in Nuclear Magnetic Resonance Spectroscopy 34, 93-158.

[164] Goddard, T. D. & Kneller, D. G. (2004). SPARKY 3 (University of California, San Francisco).

[165] Herrmann, T., Guntert, P. & Wuthrich, K. (2002). Protein NMR structure determination with automated NOE assignment using the new software CANDID and the torsion angle dynamics algorithm DYANA. J Mol Biol 319, 209-27.

[166] Vriend, G. (1990). WHAT IF: a molecular modeling and drug design program. J Mol Graph 8, 52-6, 29.

[167] Morris, A. L., MacArthur, M. W., Hutchinson, E. G. & Thornton, J. M. (1992). Stereochemical quality of protein structure coordinates. Proteins 12, 345-64.

[168] DeLano, W. (2002). The PyMOL Molecular Graphics System. San Carlos, CA, USA DeLano Scientific.

[169] Houben, K., Dominguez, C., van Schaik, F. M., Timmers, H. T., Bonvin, A. M. & Boelens, R. (2004). Solution structure of the ubiquitin-conjugating enzyme UbcH5B. J Mol Biol 344, 513-26.

[170] Serniwka, S. A. & Shaw, G. S. (2007). 1H, 13C,and 15N resonance assignments for the human E2 conjugating enzyme, UbcH7. Biomolecular NMR Assignments.

[171] M. Zhang, M. Windheim, S.M. Roe, M. Peggie, P. Cohen, C. Prodromou, L.H. Pearl, Chaperoned ubiquitylation–crystal structures of the CHIP U box E3 ubiquitin ligase and a CHIP-Ubc13-Uev1a complex. Mol Cell 20 (2005) 525-538.

[172] O. Kerscher, R. Felberbaum, M. Hochstrasser, Modification of proteins by ubiquitin and ubiquitin-like proteins. Annu Rev Cell Dev Biol 22 (2006) 159-180.

[173] R.G. Hibbert, F. Mattiroli, T.K. Sixma, Structural aspects of multi-domain RING/Ubox E3 ligases in DNA repair. DNA Repair (Amst) 8 (2009) 525-535.

[174] S. Bergink, S. Jentsch, Principles of ubiquitin and SUMO modifications in DNA repair. Nature 458 (2009) 461-467.

[175] G.L. Moldovan, B. Pfander, S. Jentsch, PCNA, the maestro of the replication fork. Cell 129 (2007) 665-679.

[176] A.R. Lehmann, A. Niimi, T. Ogi, S. Brown, S. Sabbioneda, J.F. Wing, P.L. Kannouche, C.M. Green, Translesion synthesis: Y-family polymerases and the polymerase switch. DNA Repair (Amst) 6 (2007) 891-899.

[177] M. Budzowska, R. Kanaar, Mechanisms of dealing with DNA damage-induced replication problems. Cell Biochem Biophys 53 (2009) 17-31.

[178] J.C. Harrison, J.E. Haber, Surviving the breakup: the DNA damage checkpoint. Annu Rev Genet 40 (2006) 209-235.

[179] V. Bailly, S. Lauder, S. Prakash, L. Prakash, Yeast DNA repair proteins Rad6 and Rad18 form a heterodimer that has ubiquitin conjugating, DNA binding, and ATP hydrolytic activities. J Biol Chem 272 (1997) 23360-23365.

[180] H.P. Roest, W.M. Baarends, J. de Wit, J.W. van Klaveren, E. Wassenaar, J.W. Hoogerbrugge, W.A. van Cappellen, J.H. Hoeijmakers, J.A. Grootegoed, The ubiquitin-conjugating DNA repair enzyme HR6A is a maternal factor essential for early embryonic development in mice. Mol Cell Biol 24 (2004) 5485-5495.

[181] S. Tateishi, Y. Sakuraba, S. Masuyama, H. Inoue, M. Yamaizumi, Dysfunction of human Rad18 results in defective postreplication repair and hypersensitivity to multiple mutagens. Proc Natl Acad Sci U S A 97 (2000) 7927-7932.

[182] S. Tateishi, H. Niwa, J. Miyazaki, S. Fujimoto, H. Inoue, M. Yamaizumi, Enhanced genomic instability and defective postreplication repair in RAD18 knockout mouse embryonic stem cells. Mol Cell Biol 23 (2003) 474-481.

[183] C. Lawrence, The RAD6 DNA repair pathway in Saccharomyces cerevisiae: what does it do, and how does it do it? Bioessays 16 (1994) 253-258.

[184] H.D. Ulrich, S. Jentsch, Two RING finger proteins mediate cooperation between ubiquitin-conjugating enzymes in DNA repair. EMBO J 19 (2000) 3388-3397.

[185] C. Hoege, B. Pfander, G.L. Moldovan, G. Pyrowolakis, S. Jentsch, RAD6-dependent DNA repair is linked to modification of PCNA by ubiquitin and SUMO. Nature 419 (2002) 135-141.

[186] A.A. Davies, D. Huttner, Y. Daigaku, S. Chen, H.D. Ulrich, Activation of ubiquitin-dependent DNA damage bypass is mediated by replication protein a. Mol Cell 29 (2008) 625-636.

[187] K. Watanabe, S. Tateishi, M. Kawasuji, T. Tsurimoto, H. Inoue, M. Yamaizumi, Rad18 guides poleta to replication stalling sites through physical interaction and PCNA monoubiquitination. EMBO J 23 (2004) 3886-3896.

[188] P.L. Kannouche, J. Wing, A.R. Lehmann, Interaction of human DNA polymerase eta with monoubiquitinated PCNA: a possible mechanism for the polymerase switch in response to DNA damage. Mol Cell 14 (2004) 491-500.

[189] H. Zhang, C.W. Lawrence, The error-free component of the RAD6/RAD18 DNA damage tolerance pathway of budding yeast employs sister-strand recombination. Proc Natl Acad Sci U S A 102 (2005) 15954-15959.

[190] S. Miyase, S. Tateishi, K. Watanabe, K. Tomita, K. Suzuki, H. Inoue, M. Yamaizumi, Differential regulation of Rad18 through Rad6-dependent mono- and polyubiquitination. J Biol Chem 280 (2005) 515-524.

[191] V. Notenboom, R.G. Hibbert, S.E. van Rossum-Fikkert, J.V. Olsen, M. Mann, T.K. Sixma, Functional characterization of Rad18 domains for Rad6, ubiquitin, DNA binding and PCNA modification. Nucleic Acids Res 35 (2007) 5819-5830.

[192] V. Bailly, J. Lamb, P. Sung, S. Prakash, L. Prakash, Specific complex formation between yeast RAD6 and RAD18 proteins: a potential mechanism for targeting RAD6 ubiquitin-conjugating activity to DNA damage sites. Genes Dev 8 (1994) 811-820.

[193] V. Bailly, S. Prakash, L. Prakash, Domains required for dimerization of yeast Rad6 ubiquitin-conjugating enzyme and Rad18 DNA binding protein. Mol Cell Biol 17 (1997) 4536-4543.

[194] H.C. Ardley, P.A. Robinson, E3 ubiquitin ligases. Essays Biochem 41 (2005) 15-30.

[195] B.T. Dye, B.A. Schulman, Structural mechanisms underlying posttranslational modification by ubiquitin-like proteins. Annu Rev Biophys Biomol Struct 36 (2007) 131-150.

[196] R.J. Deshaies, C.A. Joazeiro, RING domain E3 ubiquitin ligases. Annu Rev Biochem 78 (2009) 399-434.

[197] M.D. Ohi, C.W. Vander Kooi, J.A. Rosenberg, W.J. Chazin, K.L. Gould, Structural insights into the U-box, a domain associated with multi-ubiquitination. Nat Struct Biol 10 (2003) 250-255.

[198] P.S. Brzovic, P. Rajagopal, D.W. Hoyt, M.C. King, R.E. Klevit, Structure of a BRCA1-BARD1 heterodimeric RING-RING complex. Nat Struct Biol 8 (2001) 833-837.

[199] G. Buchwald, P. van der Stoop, O. Weichenrieder, A. Perrakis, M. van Lohuizen, T.K. Sixma, Structure and E3-ligase activity of the Ring-Ring complex of polycomb proteins Bmi1 and Ring1b. EMBO J 25 (2006) 2465-2474.

[200] K. Linke, P.D. Mace, C.A. Smith, D.L. Vaux, J. Silke, C.L. Day, Structure of the MDM2/MDMX RING domain heterodimer reveals dimerization is required for their ubiquitylation in trans. Cell Death Differ 15 (2008) 841-848.

[201] S.F. Bellon, K.K. Rodgers, D.G. Schatz, J.E. Coleman, T.A. Steitz, Crystal structure of the RAG1 dimerization domain reveals multiple zinc-binding motifs including a novel zinc binuclear cluster. Nat Struct Biol 4 (1997) 586-591.

[202] P.D. Mace, K. Linke, R. Feltham, F.R. Schumacher, C.A. Smith, D.L. Vaux, J. Silke, C.L. Day, Structures of the cIAP2 RING domain reveal conformational changes associated with ubiquitin-conjugating enzyme (E2) recruitment. J Biol Chem 283 (2008) 31633-31640.

[203] Q. Yin, S.C. Lin, B. Lamothe, M. Lu, Y.C. Lo, G. Hura, L. Zheng, R.L. Rich, A.D. Campos, D.G. Myszka, M.J. Lenardo, B.G. Darnay, H. Wu, E2 interaction and dimerization in the crystal structure of TRAF6. Nat Struct Mol Biol 16 (2009) 658-666.

[204] M.D. Ohi, C.W. Vander Kooi, J.A. Rosenberg, L. Ren, J.P. Hirsch, W.J. Chazin, T. Walz, K.L. Gould, Structural and functional analysis of essential pre-mRNA splicing factor Prp19p. Mol Cell Biol 25 (2005) 451-460.

[205] C.W. Vander Kooi, M.D. Ohi, J.A. Rosenberg, M.L. Oldham, M.E. Newcomer, K.L. Gould, W.J. Chazin, The Prp19 U-box crystal structure suggests a common dimeric architecture for a class of oligomeric E3 ubiquitin ligases. Biochemistry 45 (2006) 121-130.

[206] P.S. Brzovic, J.R. Keeffe, H. Nishikawa, K. Miyamoto, D. Fox, 3rd, M. Fukuda, T. Ohta, R. Klevit, Binding and recognition in the assembly of an active BRCA1/BARD1 ubiquitin-ligase complex. Proc Natl Acad Sci U S A 100 (2003) 5646-5651.

[207] Z. Xu, E. Kohli, K.I. Devlin, M. Bold, J.C. Nix, S. Misra, Interactions between the quality control ubiquitin ligase CHIP and ubiquitin conjugating enzymes. BMC Struct Biol 8 (2008) 26.

[208] T. Miura, W. Klaus, A. Ross, P. Guntert, H. Senn, The NMR structure of the class I human ubiquitin-conjugating enzyme 2b. J Biomol NMR 22 (2002) 89-92.

[209] P. Garg, P.M. Burgers, Ubiquitinated proliferating cell nuclear antigen activates translesion DNA polymerases eta and REV1. Proc Natl Acad Sci U S A 102 (2005) 18361-18366.

[210] L. Haracska, I. Unk, L. Prakash, S. Prakash, Ubiquitylation of yeast proliferating cell nuclear antigen and its implications for translesion DNA synthesis. Proc Natl Acad Sci U S A 103 (2006) 6477-6482.

[211] L. Holm, S. Kaariainen, P. Rosenstrom, A. Schenkel, Searching protein structure databases with DaliLite v.3. Bioinformatics 24 (2008) 2780-2781.

[212] E. Krissinel, K. Henrick, Protein structure comparison service SSM at European Bioinformatics Institute (http://www.ebi.ac.uk/msd-srv/ssm).

[213] Deshaies,R.J. & Joazeiro,C.A. RING domain E3 ubiquitin ligases. Annu. Rev. Biochem. 78, 399-434 (2009).

[214] Ikeda,F. & Dikic,I. Atypical ubiquitin chains: new molecular signals. 'Protein Modifications: Beyond the Usual Suspects' review series. EMBO Rep. 9, 536-542 (2008).

[215] Ye,Y. & Rape,M. Building ubiquitin chains: E2 enzymes at work. Nat. Rev. Mol. Cell Biol. 10, 755-764 (2009).

[216] Williamson,A. et al. Identification of a physiological E2 module for the human anaphase-promoting complex. Proc. Natl. Acad. Sci. U S A 106, 18213-18218 (2009).

[217] VanDemark,A.P., Hofmann,R.M., Tsui,C., Pickart,C.M., & Wolberger,C. Molecular insights into polyubiquitin chain assembly: crystal structure of the Mms2/Ubc13 heterodimer. Cell 105, 711-720 (2001).

[218] Haldeman,M.T., Xia,G., Kasperek,E.M., & Pickart,C.M. Structure and function of ubiquitin conjugating enzyme E2-25K: the tail is a core-dependent activity element. Biochemistry 36, 10526-10537 (1997).

[219] Brzovic,P.S., Lissounov,A., Christensen,D.E., Hoyt,D.W., & Klevit,R.E. A UbcH5/ubiquitin noncovalent complex is required for processive BRCA1-directed ubiquitination. Mol. Cell 21, 873-880 (2006).

[220] Rodrigo-Brenni,M.C. & Morgan,D.O. Sequential E2s drive polyubiquitin chain assembly on APC targets. Cell 130, 127-139 (2007).

[221] Hoege,C., Pfander,B., Moldovan,G.L., Pyrowolakis,G., & Jentsch,S. RAD6-dependent DNA repair is linked to modification of PCNA by ubiquitin and SUMO. Nature 419, 135-141 (2002).

[222] Parker,J.L. & Ulrich,H.D. Mechanistic analysis of PCNA poly-ubiquitylation by the ubiquitin protein ligases Rad18 and Rad5. EMBO J.(2009).

[223] Capili,A.D. & Lima,C.D. Structure and analysis of a complex between SUMO and Ubc9 illustrates features of a conserved E2-Ubl interaction. J. Mol. Biol. 369, 608-618 (2007).

[224] Eddins,M.J., Carlile,C.M., Gomez,K.M., Pickart,C.M., & Wolberger,C. Mms2-Ubc13 covalently bound to ubiquitin reveals the structural basis of linkage-specific polyubiquitin chain formation. Nat. Struct. Mol. Biol. 13, 915-920 (2006).

[225] Knipscheer,P., van Dijk,W.J., Olsen,J.V., Mann,M., & Sixma,T.K. Noncovalent interaction between Ubc9 and SUMO promotes SUMO chain formation. EMBO J 26, 2797-2807 (2007).

[226] Jentsch,S., McGrath,J.P., & Varshavsky,A. The yeast DNA repair gene RAD6 encodes a ubiquitin-conjugating enzyme. Nature 329, 131-134 (1987).

[227] Garg,P. & Burgers,P.M. Ubiquitinated proliferating cell nuclear antigen activates translesion DNA polymerases eta and REV1. Proc Natl Acad Sci U S A 102, 18361-18366 (2005).

[228] Notenboom,V. et al. Functional characterization of Rad18 domains for Rad6, ubiquitin, DNA binding and PCNA modification. Nucleic Acids Res 35, 5819-5830 (2007).

[229] Kim,J. et al. RAD6-Mediated transcription-coupled H2B ubiquitylation directly stimulates H3K4 methylation in human cells. Cell 137, 459-471 (2009).

[230] Wood,A. et al. Bre1, an E3 ubiquitin ligase required for recruitment and substrate selection of Rad6 at a promoter. Mol. Cell 11, 267-274 (2003).

[231] Varshavsky,A. The N-end rule: functions, mysteries, uses. Proc. Natl. Acad. Sci. U S A 93, 12142-12149 (1996).

[232] Venancio,T.M., Balaji,S., Iyer,L.M., & Aravind,L. Reconstructing the ubiquitin network: cross-talk with other systems and identification of novel functions. Genome Biol. 10, R33 (2009).

[233] Miura,T., Klaus,W., Gsell,B., Miyamoto,C., & Senn,H. Characterization of the binding interface between ubiquitin and class I human ubiquitin-conjugating enzyme 2b by multidimensional heteronuclear NMR spectroscopy in solution. J. Mol. Biol. 290, 213-228 (1999).

[234] Dominguez,C., Boelens,R., & Bonvin,A.M. HADDOCK: a protein-protein docking approach based on biochemical or biophysical information. J. Am. Chem. Soc. 125, 1731-1737 (2003).

[235] Bailly,V., Prakash,S., & Prakash,L. Domains required for dimerization of yeast Rad6 ubiquitin-conjugating enzyme and Rad18 DNA binding protein. Mol Cell Biol 17, 4536-4543 (1997).

[236] Miyase,S. et al. Differential regulation of Rad18 through Rad6-dependent mono- and polyubiquitination. J Biol Chem 280, 515-524 (2005).

[237] Miura,T., Klaus,W., Ross,A., Guntert,P., & Senn,H. The NMR structure of the class I human ubiquitin-conjugating enzyme 2b. J. Biomol. NMR 22, 89-92 (2002).

[238] Sattler,M., Schleucher,J., & Griesinger,C. Heteronuclear multidimensional NMR experiments for the structure determination of proteins in solution employing pulsed field gradients. Progress in Nuclear Magnetic Resonance Spectroscopy 34, 93-158. 1999. Ref Type: Generic

[239] Zheng,N., Wang,P., Jeffrey,P.D., & Pavletich,N.P. Structure of a c-Cbl-UbcH7 complex: RING domain function in ubiquitin-protein ligases. Cell 102, 533-539 (2000).

[240] Das,R. et al. Allosteric activation of E2-RING finger-mediated ubiquitylation by a structurally defined specific E2-binding region of gp78. Mol. Cell 34, 674-685 (2009).

[241] Li,W. et al. Mechanistic insights into active site-associated polyubiquitination by the ubiquitin-conjugating enzyme Ube2g2. Proc. Natl. Acad. Sci. U S A 106, 3722-3727 (2009).

[242] Xie,Y. & Varshavsky,A. The E2-E3 interaction in the N-end rule pathway: the RING-H2 finger of E3 is required for the synthesis of multiubiquitin chain. EMBO J. 18, 6832-6844 (1999).

[243] Sung,P., Prakash,S., & Prakash,L. The RAD6 protein of Saccharomyces cerevisiae polyubiquitinates histones, and its acidic domain mediates this activity. Genes Dev. 2, 1476-1485 (1988).

[244] Varelas,X., Ptak,C., & Ellison,M.J. Cdc34 self-association is facilitated by ubiquitin thiolester formation and is required for its catalytic activity. Mol. Cell Biol. 23, 5388-5400 (2003).

[245] Li,W., Tu,D., Brunger,A.T., & Ye,Y. A ubiquitin ligase transfers preformed polyubiquitin chains from a conjugating enzyme to a substrate. Nature 446, 333-337 (2007).

[256] Wuthrich K. NMR of Proteins and Nucleic Acids. 1986. Ref Type: Generic

[247] Herrmann,T., Guntert,P., & Wuthrich,K. Protein NMR structure determination with automated NOE assignment using the new software CANDID and the torsion angle dynamics algorithm DYANA. J. Mol. Biol. 319, 209-227 (2002).

[248] de Vries,S.J. et al. HADDOCK versus HADDOCK: new features and performance of HADDOCK2.0 on the CAPRI targets. Proteins 69, 726-733 (2007).

[249] Kabsch,W. Automatic processing of rotation diffraction data from crystals of initially unknown symmetry and cell constants. J Appl Cryst 26, 795-800. 1993. Ref Type: Generic

[250] McCoy,A.J. et al. Phaser crystallographic software. J Appl Cryst 40, 658-674. 2007. Ref Type: Generic

[251] Worthylake,D.K., Prakash,S., Prakash,L., & Hill,C.P. Crystal structure of the Saccharomyces cerevisiae ubiquitin-conjugating enzyme Rad6 at 2.6 A resolution. J Biol Chem 273, 6271-6276 (1998).

[252] Cohen,S.X. et al. ARP/wARP and molecular replacement: the next generation. Acta Crystallogr. D Biol. Crystallogr. 64, 49-60 (2008).

[253] Emsley,P. & Cowtan,K. Coot: model-building tools for molecular graphics. Acta Crystallogr. D Biol. Crystallogr. 60, 2126-2132 (2004).

[254] Murshudov,G.N., Vagin,A.A., & Dodson,E.J. Refinement of macromolecular structures by the maximum-likelihood method. Acta Crystallogr. D Biol. Crystallogr. 53, 240-255 (1997).

[255] Davis,I.W. et al. MolProbity: all-atom contacts and structure validation for proteins and nucleic acids. Nucleic acids research 35, W375-W383. 2007. Ref Type: Generic

[256] Krissinel,E. & Henrick,K. Inference of macromolecular assemblies from crystalline state. J. Mol. Biol. 372, 774-797 (2007).

Summary

Protein modification by ubiquitin conjugation (ubiquitination) is responsible for degradation of most cellular proteins, including short-lived, regulatory, misfolded and denatured proteins, and therefore is crucial to most aspects of eukaryotic cells. Recently, various non-proteolytic functions have been shown for this pathway, such as histone regulation and viral budding. Numerous diseases, including hypoxia, inflammatory diseases, muscle wasting disorders and cancer, were discovered to be affected by aberrations in the ubiquitin system. Ubiquitination is a highly regulated system carried out by complex processes through the hierarchical E1-E2-E3 enzyme cascade, which involves thousands of enzymes and substrates in human cells. The growing knowledge of the molecular components and mechanisms of the ubiquitin system improved our understanding about both regulatory steps and strategies for therapeutic intervention. However, the detailed molecular mechanisms underlying these complex processes, the specificity of E1-E2, E2-E3, and E3-substrate recognition are poorly understood. **Chapter 1** reviews the current knowledge of ubiquitin system, including the ubiquitin enzyme cascade, molecular mechanisms underlying ubiquitination and ubiquitin system related diseases and drug discovery. Since the current thesis focuses on the structural and functional studies of E2 and E3 enzymes, there is a comprehensive discussion about human E2 conjugating enzymes, their interactions to different components in the pathway, such as E1, E3 and ubiquitin, and their regulatory roles of these processes based on their structural and functional analysis.

The structural and functional studies of proteins start with protein expression, which can prove a major hurdle in many cases. This also holds true for the production of E3 RING domain proteins for NMR structural study, caused by the two zinc ions and more than eight cysteine/histidine residues present in RING domains. **Chapter 2** describes our strategy for producing correctly folded RING domain E3 proteins for structure studies. Fusion tags such as GB1, Trx or GST significantly improved the expression and solubility of RING proteins as compared to His6 tag alone. More importantly, high imidazole concentrations used in metal affinity chromatography during purification of His-tagged RING proteins can cause protein unfolding due to competition with the zinc coordinating Cys/His residues, making His tags unsuitable

for purification of RING E3 proteins. In contrast, the GST fusion tag was shown to significantly improve the expression and solubility of RING domains and was a reliable purification tag for production with good yields too, thus a better method for RING expression.

RING/U-box E3 ligases underlie ubiquitin ligase activity by preferentially binding certain E2 enzymes through the RING/U-box domains and facilitate transfer of ubiquitin from E2s to substrates. One complicating observation is that there appeared to be poor correlation between E3 ligase activity and its binding affinity to a particular E2. Aiming to understand the difference between E2-E3 binding and functionally productive interaction, we studied the binding and functional specificity of the two E2 ubiquitin conjugating enzymes UbcH7 and UbcH5B to the RING domain of E3 ligase c-Cbl in **Chapter 3**. Although UbcH7 and UbcH5B were found to bind to c-Cbl RING in a similar manner using our NMR titration experiments, only UbcH5B can support ubiquitination of c-Cbl and substrate (Src) in a reconstituted system. NMR chemical shift changes that occurred in titrations of the RING domain of c-Cbl with UbcH5B and UbcH7 revealed the involvement of the helix H1, Loop L1 and L2 regions in binding. By performing quantitative binding and enzymatic assays using mutants containing these UbcH7 regions in an UbcH5B scaffold, we concluded that none of the interface regions is essential for specificity in ubiquitination. Instead, the E2 activity studies of transferring the E2∼ubiquitin thioester to different ubiquitin acceptors indicated that UbcH5B might be a relatively pliable E2 enzyme and UbcH7 a more specific E2 enzyme. Accessory factors might be needed to help the release of ubiquitin from UbcH7∼Ub thioester to its substrates or E3, and we suggested that the interaction specificity between c-Cbl and E2 is required, but not sufficient for transfer of ubiquitin to potential targets.

Ubiquitination participates in almost all DNA repair pathways by mono- or polyubiquitination of proteins, and one of the best studied examples is the ubiquitination of PCNA, a homotrimeric protein which encircles DNA and acts as processivity factor for DNA polymerases. The E2/E3 pair Rad6/Rad18 regulates monoubiquitination of PCNA on the Lys164 residue, while a second E2/E3 pair Ubc13-MMS2/Rad5 extends the chain on the same residue of PCNA. Although the principle of PCNA ubiquitination in the post-replication repair pathway to avoid DNA damage in the replication fork is relatively well understood, detailed molecular mechanism underlying this ubiquitin conjugation and structural information on these components at atomic level are still lacking. In **Chapter 4 and 5**, we present our progress in the structure study of Rad6/Rad18 complex and their regulatory role in the ubiquitination of PCNA.

Chapter 4 describes the structure of E3 Rad18 RING-RING symmetric dimer determined by X-ray, and proposes the RING domain is the dimerization interface of full-length Rad18 based on previous studies and our results. The four-helical bundle

of N- and C-terminal extensions of the Rad18 RING core domain forms the major dimerization interface while the β-strands of the RING core domain contribute secondarily. This kind of dimerization manner resembles other RING/U-box dimers, such as the heterodimers BRCA1/BARD1 and RING1b/BMI1. NMR titration experiments provided the residues of E2 enzyme Rad6b involved in Rad18 RING binding, which suggested that similar elements as other E2-E3 RING/U-box structures are found on the interface. Based on these results, we built a structure model of the Rad6b with Rad18 RING dimer, demonstrating that the Rad18 RING homodimer can bind to two Rad6b molecules. Interestingly, the stoichiometry study of full-length Rad18 homodimer with Rad6b showed that only a single Rad6b interacted with the homodimer. This result is extremely exciting, since the full-length CHIP (U-box E3) homodimer was demonstrated to bind to one E2 proteins as well, while the only U-box domain dimer of CHIP can recruit two E2 proteins. Thus, we proposed that Rad18 homodimer is asymmetric in solution. The Rad18 and CHIP asymmetric dimers suggest that more E3 dimers might be asymmetric in structure which provides space just for one single E2 binding.

In **chapter 5**, we solved the crystal structure of E2 enzyme Rad6b in complex with the E3 Rad18 R6BD domain, the second and major interaction site of Rad18 to Rad6b. R6BD bound to Rad6b though the "backside" of the E2, which is on the opposite face of the active site cysteine. We also mapped the interaction surfaces of Rad6b with ubiquitin non-covalent and covalent binding using NMR spectroscopy, and found that the "backside" binding face of Rad6b to R6BD is overlapped with the ubiquitin non-covalent binding interface on Rad6b. NMR spectra showed that R6BD can compete with ubiquitin for Rad6 binding. More importantly, R6BD can inhibit the Rad6b-mediated ubiquitin chain formation in solution by the in vitro ubiquitination assay. Combining with the emerging idea that there is a strong correlation between the chain formation ability of an E2 enzyme and its non-covalent binding ability to ubiquitin, we propose that the Rad6 mediated monoubiquitination of PCNA might be regulated by Rad18 through inhibiting its ubiquitin non-covalent binding.

Samenvatting

Eiwitmodificatie door ubiquitine-conjugatie is verantwoordelijk voor de afbraak van de meeste cellulaire eiwitten, inclusief kortlevende, regulerende, misgevouwen en gedenatureerde eiwitten, en is daarom essentieel voor de meeste aspecten van eukaryotische cellen. Recent onderzoek aan deze pathway heeft ook verschillende non-proteolytische functies blootgelegd, waaronder histon-regulatie en virale ontkieming. Talloze ziekten, waaronder hypoxia, ontstekingen, spierziekten en kanker blijken beïnvloed te worden door afwijkingen in het ubiquitinesysteem. Ubiquitinering is een sterk gereguleerd systeem dat uitgevoerd wordt door complexe processen door middel van de hiërarchische E1-E2-E3 enzymcascade, waarbij in de menselijke cel duizenden enzymen en substraten betrokken zijn. De groeiende kennis van de moleculaire componenten en mechanismen van het ubiquitinesysteem heeft ons inzicht verschaft in zowel de regulatie als in strategieën voor therapeutisch ingrijpen. Echter, de precieze moleculaire mechanismen die aan deze complexe processen ten grondslag liggen worden nog niet goed begrepen. **Hoofdstuk 1** geeft een overzicht van de huidige kennis van het ubiquitinesysteem, waaronder de ubiquitine enzymcascade, moleculaire mechanismen van ubiquitinering en ziekten gerelateerd aan het ubiquitinesysteem, en medicijnonderzoek. Aangezien dit proefschrift zich richt op structureel en functioneel onderzoek aan E2 en E3 enzymen, is er een uitgebreide discussie over menselijke E2 en E3 enzymen, een uitgebreide discussie over menselijk E2 conjugerende enzymen, hun interacties met verschillende componenten in de pathway, zoals E1, E3 en ubiquitine, en hun regulerende rol in deze processen gebaseerd op structurele en functionele analyse.

Structureel en functionele onderzoek van eiwit begint met eiwitexpressie, wat in vele gevallen een aanzienlijk struikelblok blijkt te zijn. Dit geldt ook voor de productie van E3 RING domein eiwitten voor NMR structuuronderzoek, vanwege de twee zinkionen en meer dan acht cysteïne/histidineresiduen die aanwezig zijn in RING domeinen. **Hoofdstuk 2** beschrijft onze strategie voor het produceren van correct gevouwen RING domein E3 eiwitten voor structuuronderzoek. Fusion tags zoals GB1, Trx en GST verbeterden aanzienlijk de expressie en oplosbaarheid van RING eiwitten in vergelijking met de His6 tag alleen. Belangrijker nog, de hoge imidazolconcentraties die gebruikt worden in metal affinity chromatografie tijdens opzuivering van RING eiwitten die een

His-tag hebben, kan eiwitontvouwing veroorzaken vanwege de competitie met de zink-coordinerende Cys/His residuen, wat His-tags ongeschikt maakt voor opzuivering van RING E3 eiwitten. De GST fusion tag daarentegen bleek de expressie en oplosbaarheid van RING domeinen aanzienlijk te verbeteren, en was een betrouwbare tag voor opzuivering en tevens voor productie met hoge opbrengst, en daarom een betere methode voor RING expressie.

RING/U-box E3 ligases liggen ten grondslag aan ubiquitine ligase activiteit door specifiek bepaalde E2 enzymen te binden via RING/U-box domeinen en door ubiquitine-overdracht van E2s naar substraten mogelijk te maken. Een complicerende observatie is dat er een slechte correlatie lijkt te zijn tussen de ligase activiteit van een E3 en zijn binding aan een bepaalde E2. Om het verschil te begrijpen tussen E2-E3 binding en een functioneel productieve interactie bestudeerden we de binding en functionele specificiteit van de twee E2 ubiquitine-conjugerende enzymen UbcH7 en UbcH5B aan het RING domein van E3 ligase c-Cbl in **hoofdstuk 3**. Hoewel UbcH7 en UbcH5B bij onze NMR titratie-experimenten op een vergelijkbare manier aan c-Cbl RING bleken te binden, kan alleen UbcH5B de ubiquitinering van c-Cbl en substrate (Src) in een gereconstitueerd systeem ondersteunen. Veranderingen in NMR chemical shift die voorkwamen in titraties van het RING domein van c-Cbl met UbcH5B en UbcH7 toonden de rol aan van de helix H1, loop L1 en L2 regio's in binding. Door het uitvoeren van kwantitatieve bindings- en enzymatische assays met UbcH5B mutanten die deze UbcH7 regio's bevatten, concludeerden we dat geen van deze interface regio's essentieel is voor de specificiteit van ubiquitinering. In plaats daarvan toonde het onderzoek naar E2 activiteit via overdracht van E2-ubiquitine thio-ester naar verschillende ubiquitine-acceptoren aan dat UbcH5B wel eens een relatief plooibaar E2 enzym zou kunnen zijn en UbcH7 een meer specifiek E2 enzym. Toegangsfactoren zouden wel eens nodig kunnen zijn om het loslaten van ubiquitine van UbcH7-Ub thio-ester naar zijn substraten of E3 te bevorderen, en wij stelden voor dat de interactiespecificiteit tussen c-Cbl en E2 vereist is, maar niet voldoende is, voor de overdracht van ubiquitine naar mogelijke targets.

Ubiquitinering neemt deel aan vrijwel alle DNA reparatiepathways door middel van mono- of polyubiquitinering van eiwitten, en één van de best onderzochte voorbeelden is de ubiquitinering van PCNA, een homotrimerisch eiwit dat DNA omringt en functioneert als procesvoortgangsfactor voor DNA polymerases. Het E2/E3 paar Rad6/Rad18 reguleert monoubiquitinering van PCNA op het Lys164-residu, terwijl een tweede E2/E3 paar Ubc13-MMS2/Rad5 de keten verlengt op hetzelfde residu van PCNA. Hoewel het principe van PCNA-ubiquitinering in de post-replicatie reparatiepathway om DNA-schade te vermijden relatief goed begrepen is, ontbreken nog steeds precieze moleculaire mechanismen die ten grondslag liggen aan deze ubiquitine-conjugatie en structuurinformatie over deze componenten op atomair niveau. In **hoofstuk 4 en**

5 presenteren we onze voortgang in het structuuronderzoek aan het Rad6/Rad18 complex en hun regulerende functie in de ubiquitinering van PCNA.

Hoofdstuk 4 beschrijft de structuur van de E3 Rad18 RING-RING symmetrische dimeer, bepaald via röntgen-kristallografie, en stelt dat het RING domein de dimerisatieinterface van het volledige Rad18 is, gebaseerd op eerder onderzoek en op onze resultaten. De vier-helixbundel van de N- en C-terminale extensies van het Rad18 RING kerndomein vormt de voornaamste dimerisatieinterface, terwijl de β-strands van het RING kerndomein een secondaire bijdrage leveren. Deze manier van dimerisatie lijkt op andere RING/U-box dimeren, zoals de heterodimeren BRCA1/BARD1 en RING1b/BMI1. NMR titratie experimenten verschaften de residuen van E2 enzym Rad6b die betrokken zijn bij Rad18 RING binding, wat suggereerde dat elementen vergelijkbaar met andere E2-E3 RING/U-boc structuren aanwezig zijn in de interface. Aan de hand van deze resultaten bouwden we een structuurmodel van de Rad6b met Rad18 RING dimeer, waarbij we aantoonden dat de Rad18 RING homodimeer aan twee Rad6b moleculen kan binden. Interessant was dat het stoichiometrie-onderzoek van de volledige Rad18 homodimeer met Rad6b liet zien dat slechts één Rad6b een interactie aanging met de homodimeer. Dit resultaat is zeer interessant, aangezien de volledige CHIP (U-box E3) homodimeer ook één E2 eiwit bleek te binden, terwijl alleen de U-box domein dimeer van CHIP twee E2 eiwitten kan recruteren. Om die reden stelden wij dat de Rad18 homodimeer asymmetrisch is in oplossing. De Rad18 en CHIP asymmetrische dimeren suggereren dat meer E3 dimeren wel eens een asymmetrische structuur zouden kunnen hebben, die ruimte biedt voor slechts één enkele E2 binding.

In **hoofdstuk 5** losten we de kristalstructuur op van E2 enzym Rad6b in complex met het E3 Rad18 R6BD domein, de tweede en voornaamste interactiesite van Rad18 met Rad16. R6BD bond aan Rad6b via de ”achterkant” van de E2, die aan de tegengestelde kant is van de active-site cysteïne. We brachten ook de interactieoppervlakken van Rad6b met non-covalente en covalente ubiquitinebindingen in kaart met NMR spectroscopie, en we vonden dat het ”achterkant”-bindingsoppervlak van Rad6b aan R6BD overlapt met de non-covalente ubiquitinebindingsinterface op Rad6b. NMR spectra lieten zien dat R6BD competitie kan aangaan met ubiquitine voor Rad6 binding. Belangrijker nog, R6BD kan de Rad6b-gemedieerde ubiquitineketenformatie in oplossing remmen, gemeten door het in vitroubiquitineringsassay. Gecombineerd met het opkomende idee dat er een sterke correlatie is tussen de mogelijkheid van ketenformatie van een E2 enzym en zijn vermogen om non-covalent aan ubiquitine te binden, stellen we voor dat de Rad6-gemedieerde mono-ubiquitinering van PCNA gereguleerd zou kunnen zijn door Rad18 door middel van het remmen van zijn non-covalente binding aan ubiquitine.

Curriculum Vitae

Anding Huang was born in Chongqing, China, on 18 April, 1980. In 1998, she attended University of Science and Technology of China (USTC), where she obtained her Bachelor Degrees in Biological Sciences (major) and Electronic Engineering (minor). Her final year project was under the supervision of Prof. Shi Yunyu. From 2004 to 2010, she worked for her doctoral thesis in the NMR department of the Bijvoet Center for Biomolecular Research, at Utrecht University, under the supervision of Prof. dr. Rolf Boelens and Dr. Rob N. de Jong.

Publications

- Zhou H., Xu Y., Yang Y., **Huang A.**, Wu J., Shi Y. J. (2005) "Solution structure of AF-6 PDZ domain and its interaction with the C-terminal peptides from Neurexin and Bcr", *J. Biol. Chem. 280, 13841-13847*

- **Huang A.**, de Jong R.N., Wienk H., Winkler G.S., Timmers H.T.M., Boelens R. (2009) "E2-c-Cbl recognition is necessary but not sufficient for ubiquitination activity", *J. Mol. Biol. 385, 507-519*

- van Wijk S.J.L., de Vries S.J, Kemmeren P., **Huang A.**, Boelens R., Bonvin A.M., Timmers H.T.M. (2009) "A comprehensive framework of E2-RING E3 interactions of the human ubiquitin proteasome system", *Mol. Syst. Biol. 5, 295*

- **Huang A.**, de Jong R.N., Folkers G.E., Boelens R. (2010) "Strategy for production of correctly folded E3 RING domains", *J. Struct. Biol. (Submitted for publication)*

- Hibbert R.G.*, **Huang A.***, Boelens R. and Sixma T.K. (2010) "The E3 ligase Rad18 selects for monoubiquitination rather than ubiquitin chain formation by E2 enzyme Rad6", *Nat. Struct. Mol. Biol. (Submitted for publication)*

- **Huang A.***, Hibbert R.G.*, de Jong R.N., Das D., Sixma T.K., Boelens R. (2010) "Symmetry and asymmetry of the RING-RING dimer of Rad18", *Manuscript In preparation*

* These authors contributed equally to this work

Acknowledgement

Aside from the hard work for research, these years of my PhD life will be remembered for many more. I am grateful to all the people who I have met, shared time with and helped me, who had made these years of my life so special.

First of all, I would like to express my gratitude to my promotor Prof. dr. Rolf Boelens and Prof. dr. Robert Kaptein for providing me the opportunity to join the research group. Rolf, I am grateful to you for supervising my whole PhD studies. Thank for your enormous encouragement and patience on me, and I'm glad that I made it. I'm deeply indebted to Dr. Rob N. de Jong, my daily supervisor who instructed me going through the toughest years. I'm so amazed at that your ingenious ideas which always came out in such a short time. Dr. Gert Folkers, thank you for your brilliant ideas and advice in our discussion and aids in the wet lab, especially grateful for your polishing the manuscript of RING production and performing experiments. I'm very grateful to our collaborators from the NKI Amsterdam. With our great collective efforts, the challenging and exciting work about Rad6-Rad18 is at last to be finalized and I'm looking forward to the outcome of this great work. Prof. dr. Titia Sixma, thanks for your assistance and supervision of the Rad6-Rad18 project. Rick, it was a pleasure to work with you, your knowledge and precise in research really impressed me.

My dear colleagues, who are or were in this laboratory, I want thank you guys deeply for helping and companying me in the past few years. Julija, Devashish, Sjoerd, Marc, Mickael and Kostas, thanks for sharing these tough PhD time with me and many talks we had during these years are precious to me, wish you guys good luck in the future career and life. Monique, Adrien and Egzi, my dear office mates, it is pleasure to share office with you. Alex, thanks for your help in docking. Hans and Eiso thank for helping me out the structure calculation. Barbara, I enjoyed the women's talk with you! Johan, I admire your patient with my computer problems! Klaartje, Ludovic, Danny, Cyril, Aurelien, Jenny, Suat, Hogo, Karine, Aurelien, Jeff, Tammo, Gloria, Eiso, Manuel, Nathalie, Eugene, Roberto. Thanks!

I also would like to thank people from my former lab in China. Prof. Shi, you are the real model of us, thanks for your supervision and recommendation. Zhou Heyue,

Zhang Xuecheng, Cai Zheng, Li Xuan, Xu Chao, Sun Jianping, Pu Chunlei and many others, your guys are not only my colleagues but also good friends, and I won't forget our happy time in laboratory 317 in 2003.

Last but also the first, my lovingly thanks go to my hubby Xiaodong for always being here with me. This book is dedicated to you and our coming baby with my deepest love.

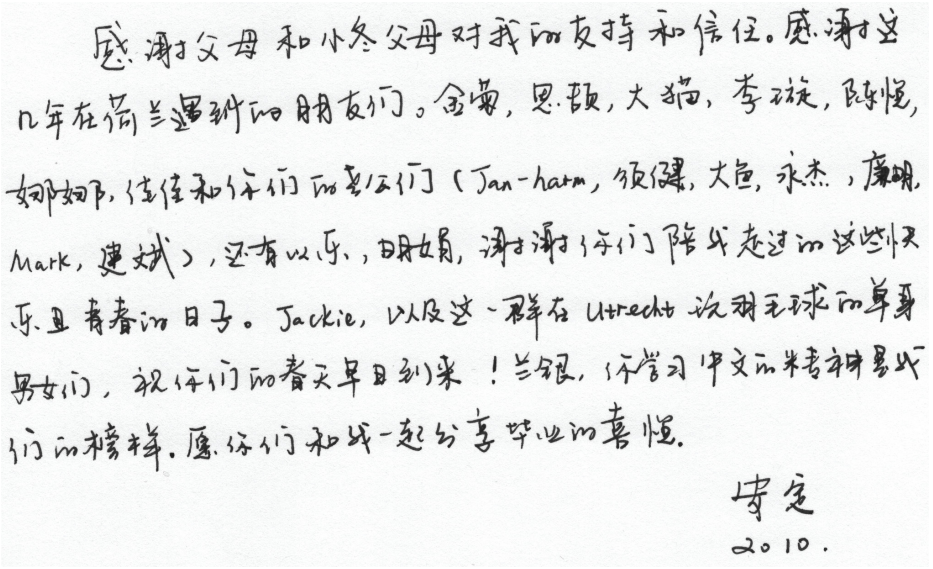

Full Colour Figures

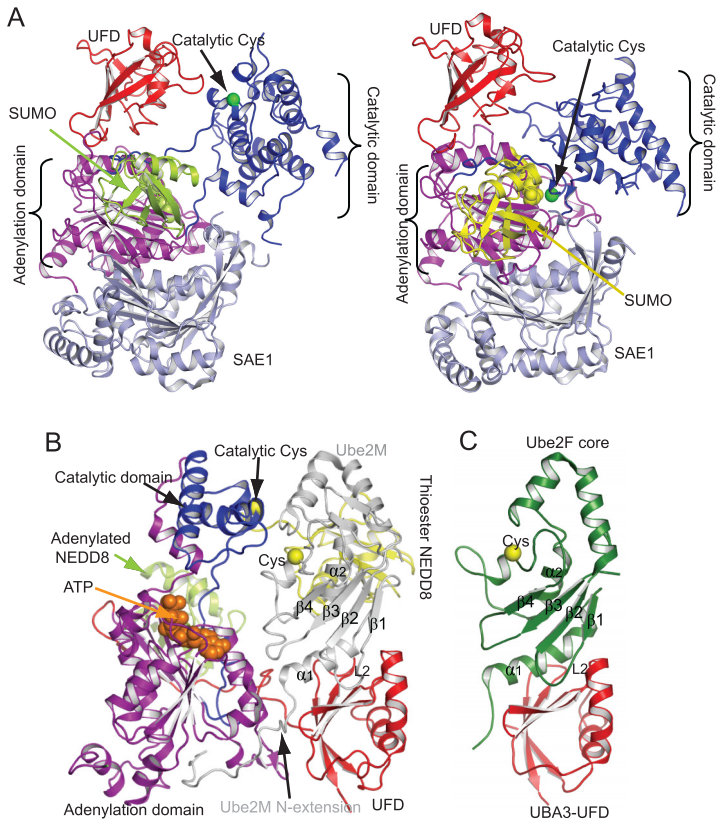

Figure * 1.3: Structure of the ubiquitin-activating enzyme E1 and of the complex with E2. **A.** Crystal structures of human SUMO E1/SUMO1-AMSN adenylate analogue (3KYC, left) and human SUMO E1∼SUMO1-AVSN intermediate analogue (3KYD, right). The UFD domain of UBA2 is colored in red, the catalytic domain of UBA2 in blue, the adenylation domain in purple, and the SAE1 in lightblue. The catalytic cysteine is represented as a green ball. SUMO is colored in limo (left) and yellow (right). **B.** Crystal structure of Human NEDD8 E1 UBA3 loaded with both NEDD8 and the E2 Ube2M (C111A)(2NVU). Ube2M (grey) is bound to the UFD domain of UBA3 (red); The thioester-linked NEDD8 (yellow) is attached to catalytic cysteine (yellow ball) of the catalytic domain of UBA3 (blue); the adenylated NEDD8 (lime) is non-covalently bound to the adenylation domain of UBA3 (purple). ATP is colored in orange. The red arrow indicates the distance between the two catalytic cysteines in E1 and E2. **C.** Crystal structure of the core domain of the complex of Ube2F (forest) with the UFD domain (red) of human NEDD8 E1 UBA3 (3FN1).

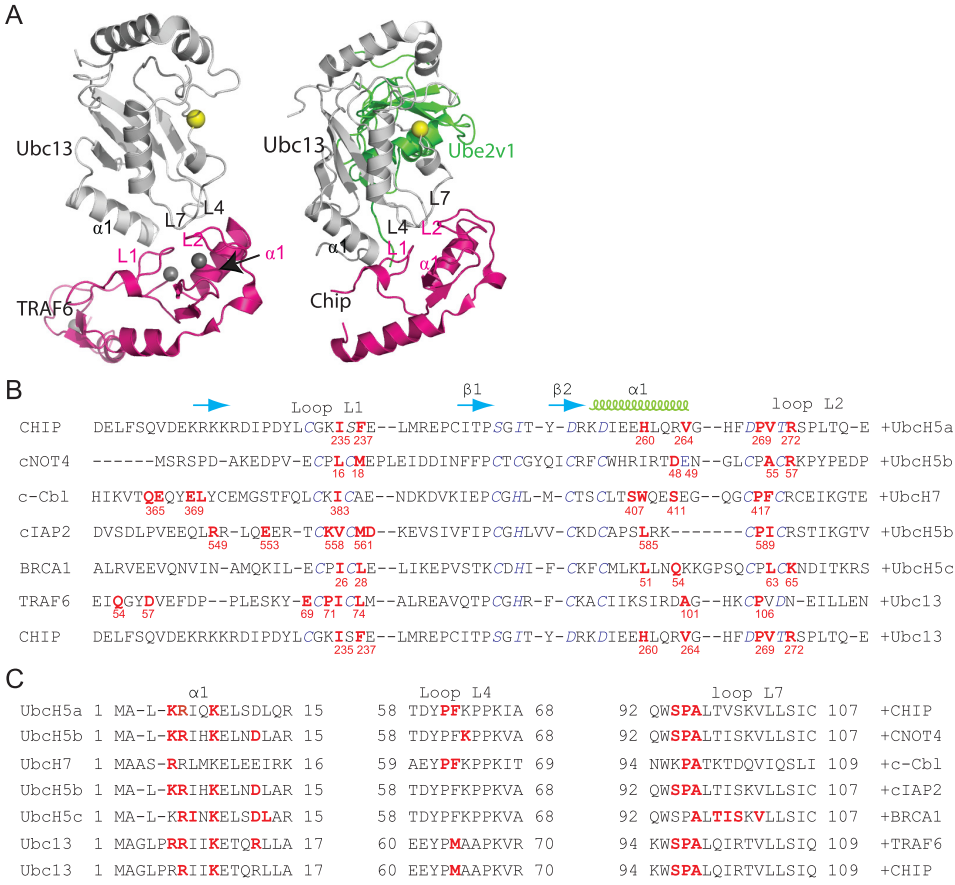

Figure * 1.4: Interactions of E2 enzymes with the E3 RING/Ubox domains. **A.** Crystal structures of TRAF6-Ubc13 (3HCT) and CHIP-Ubc13-Ube2v1 (2C2V). The E2 is colored grey and the E3 colored in deeppink. **B.** Contacts between the E2 core domain and the E3 RING/U-box domains. The important residues on the E3 RING/U-box, which are involved in binding to E2, are highlighted in bold red and the zinc-coordinating residues in the RING domain or the equivalent residues in the U-box are highlighted in italic blue. **C.** Residues of E2 enzymes involved in E3 RING/U-box binding. The major interacting residues are highlighted in bold red.

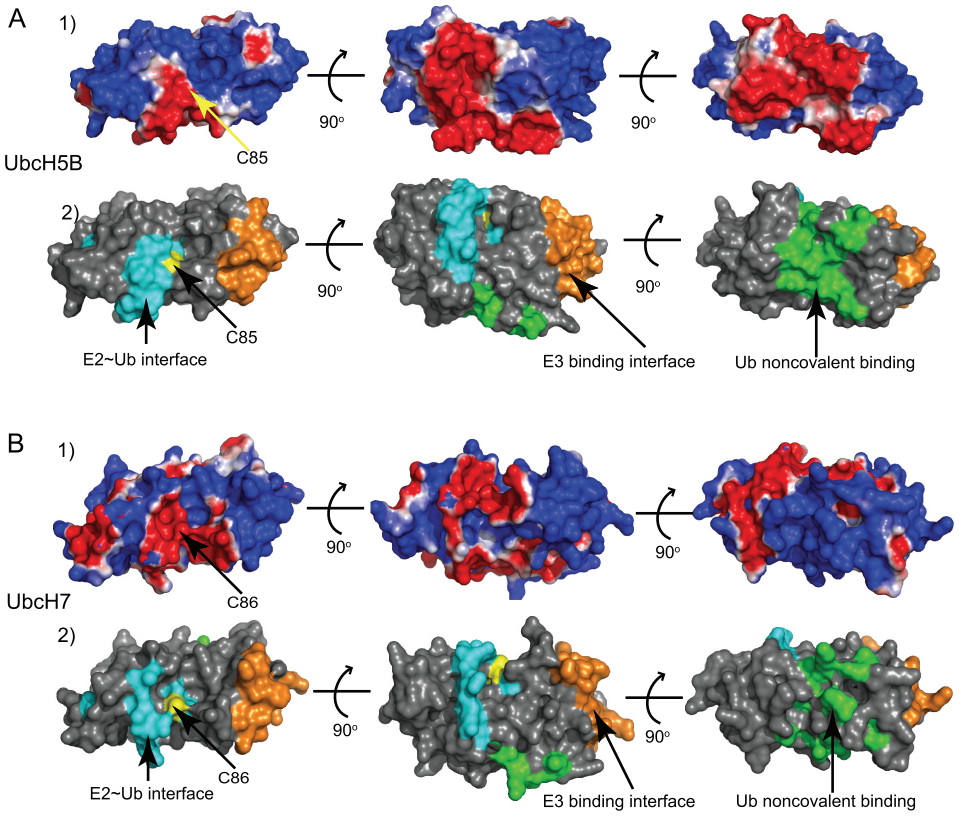

Figure * 3.7: Comparison of surface properties of UbcH5B and UbcH7. **A**. Top: electrostatic surface potential of UbcH5B was calculated using the APBS plugin to PyMol and indicated as a charge scale from negative (red) to positive (blue). Bottom: surface representation of interaction sites on UbcH5B. The catalytic site (yellow), E2∼Ub binding interface (cyan), E3 binding interface (orange), and the non-covalent Ub-binding interface on UbcH5B (green) are indicated. **B**. UbcH7 electrostatic surface potential (top) and interaction sites (bottom), colored as indicated under (A).

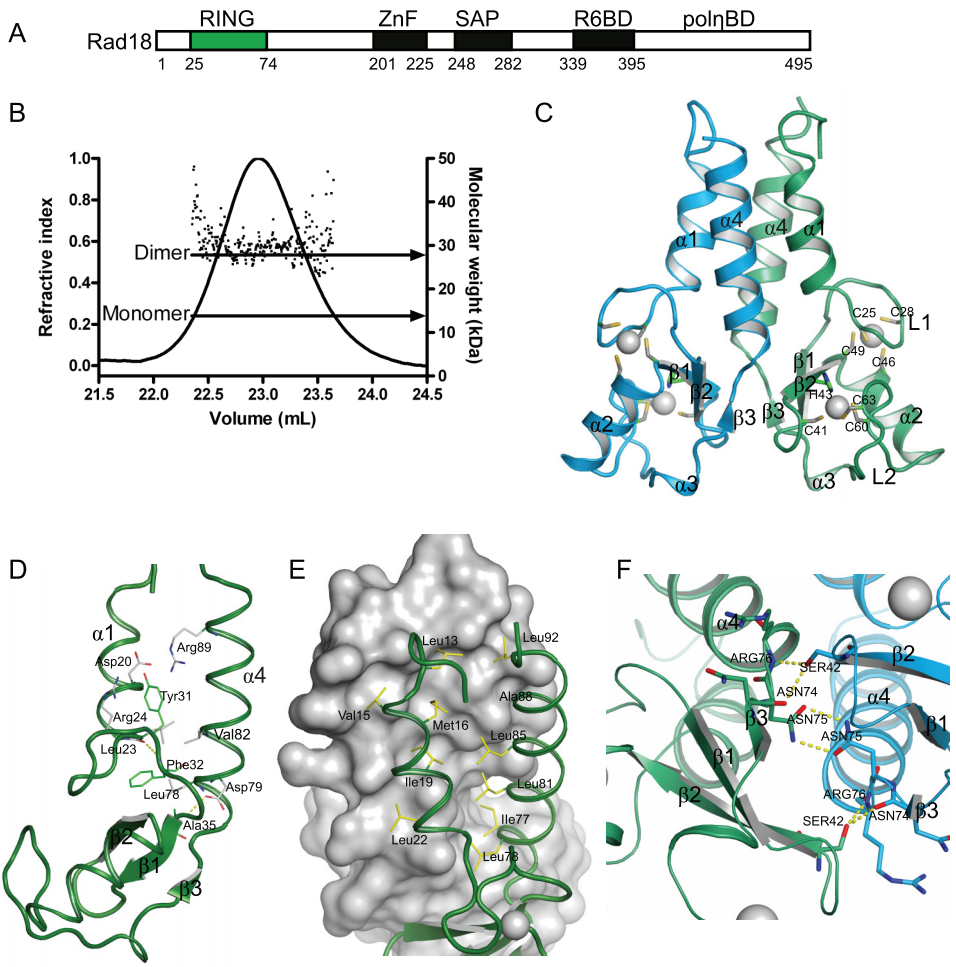

Figure * 4.1: Structure of the Rad18. **A.** Domain organization of Rad18. **B.** Oligomeric state of Rad18 (1-121) RING. MALLS profile showing refractive indices for monomeric and dimeric Rad18 RING domains. **C.** Secondary structure cartoon of the Rad18 RING (1-99) homodimer. The secondary structure elements are labeled. **D.** Detailed view on the interaction between helices α1, α4 and the RING core motif. The yellow dashes indicate stabilizing hydrogen bonds. **E.** Detailed view on the interaction at the dimerization interface of the four-helix bundle consisting of α1, α4, α1' and α4' at the C- and N-terminus of Rad18 RING (1-99). **F.** Hydrogen bonding network of the dimerization interface of the central core RING motif.

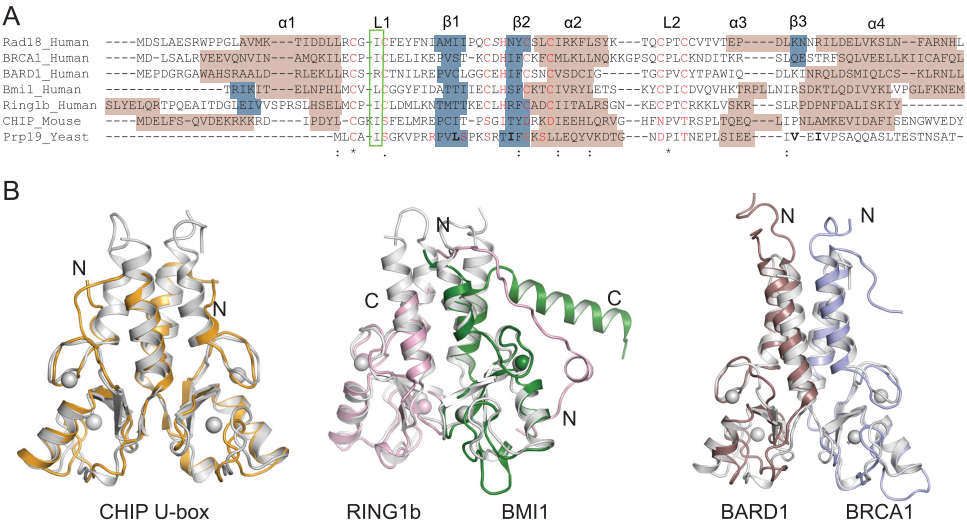

Figure * 4.2: Comparison of the Rad18 RING with other RING/U-box domains. **A.** Sequence alignment of Rad18 RING with other RING/U-box domains. Secondary structures are labeled and shaded (helix-light pink, s-blue). Zinc coordinating residues are highlighted in red. The green box indicates I27 of Rad18 in loop L1. **B.** Superposition of the structures of Rad18 RING dimer (grey) with CHIP U-box domain (2C2V, orange, left panel), of Rad18 RING dimer (grey) with RING1b/BMI1 (2CKL, middle panel), and of Rad18 RING dimer with BRCA1/BARD1 (1JM7, right panel).

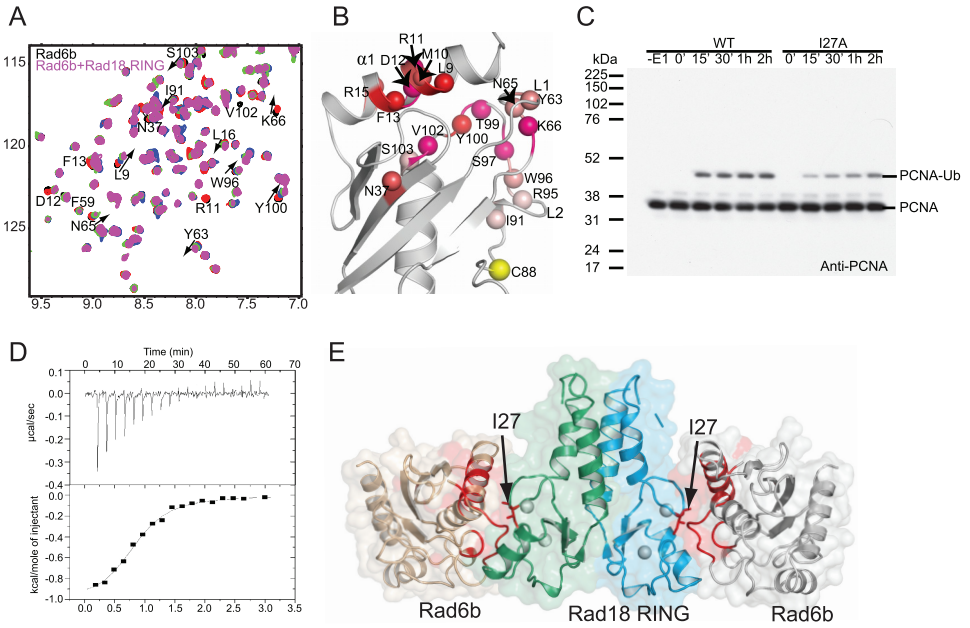

Figure * 4.3: Rad18-Rad6b complex formation. **A.** NMR titration of Rad6b and Rad18 RING dimer. The figure shows an overlay of representative regions of ^{1}H-^{15}N HSQC spectra of Rad6b in the absence (black) and presence of increasing concentrations of unlabeled Rad18 RING domain (ratios of Rad6b:Rad18 RING=1:0.3 [red];1:0.6 [blue]; 1:1 [green]; 1:1.5 [magenta]). **B.** Chemical shift mapping of the Rad18 RING domain binding site on Rad6b. Residues experiencing significant NMR chemical shift changes (>0.034 ppm) are colored with a linear gradient from white (<0.034ppm) to red (=0.1ppm). Spheres represent the nitrogen atoms of the affected residues. **C.** Ubiquitination of PCNA by Rad18 (I27A) and Rad6b. **D.** ITC binding study of Rad18 RING dimer with Rad6b. Analysis of the ITC data shows a Kd (Rad18 RING dimer: Rad6b) of 35 µM. **E.** Structural model of Rad6-Rad18 RING complex. The model is obtained by aligning the structure of Rad18 dimer and Rad6b with CHIP dimer and UbcH5, respectively, with the complex CHIP-UbcH5 structure (2OXQ). The Rad6b residues located in the Rad18 binding interface by NMR titration experiment are colored red. The sidechain of the mutated residue I27 of Rad18 is indicated in red.

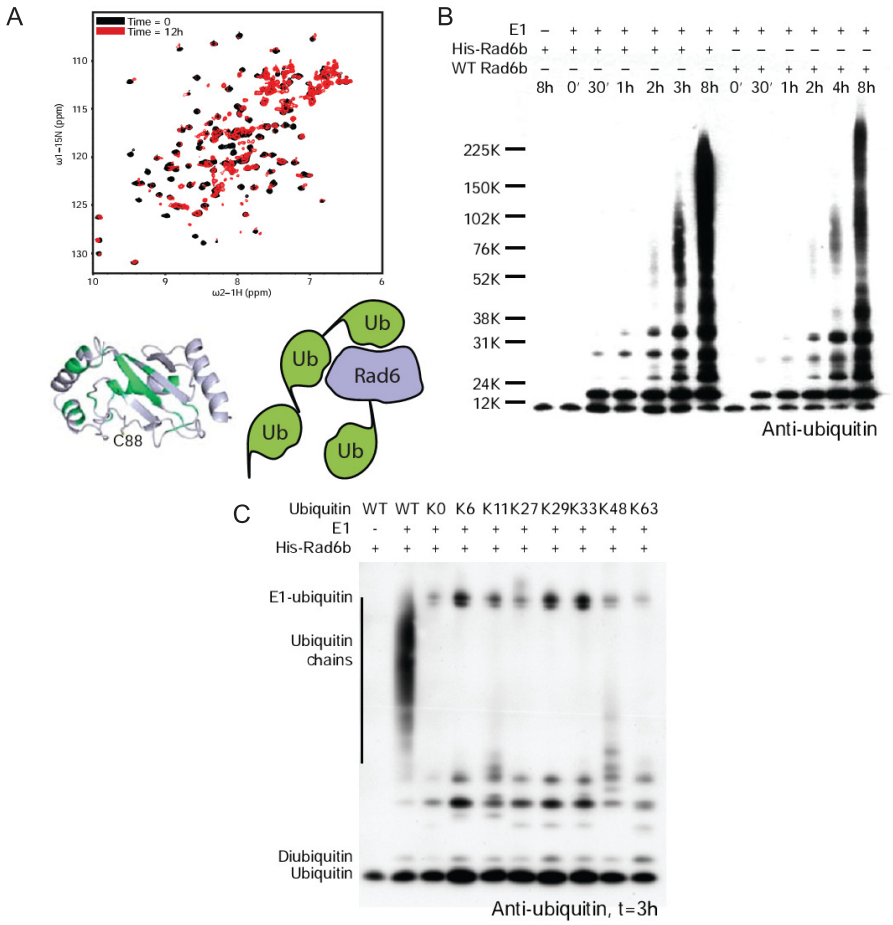

Figure * 5.2: Rad6b can form ubiquitin chains. **A.** At later time points of the thioester formation experiment, an overall broadening of the ^{1}H-^{15}N -HSQC spectra was observed and additional CSP mapped to the back of Rad6b. **B.** Rad6b can form free ubiquitin chains, using an *in vitro* system containing purified E1, Rad6b, ubiquitin and ATP/Mg^{2+}. The His-tagged Rad6b is marginally more efficient in chain formation. **C.** *In vitro* ubiquitination assays using single lysine mutants of ubiquitin suggest that the chains are mixed, with a preference for K11- and K48-linked ubiquitin chains.

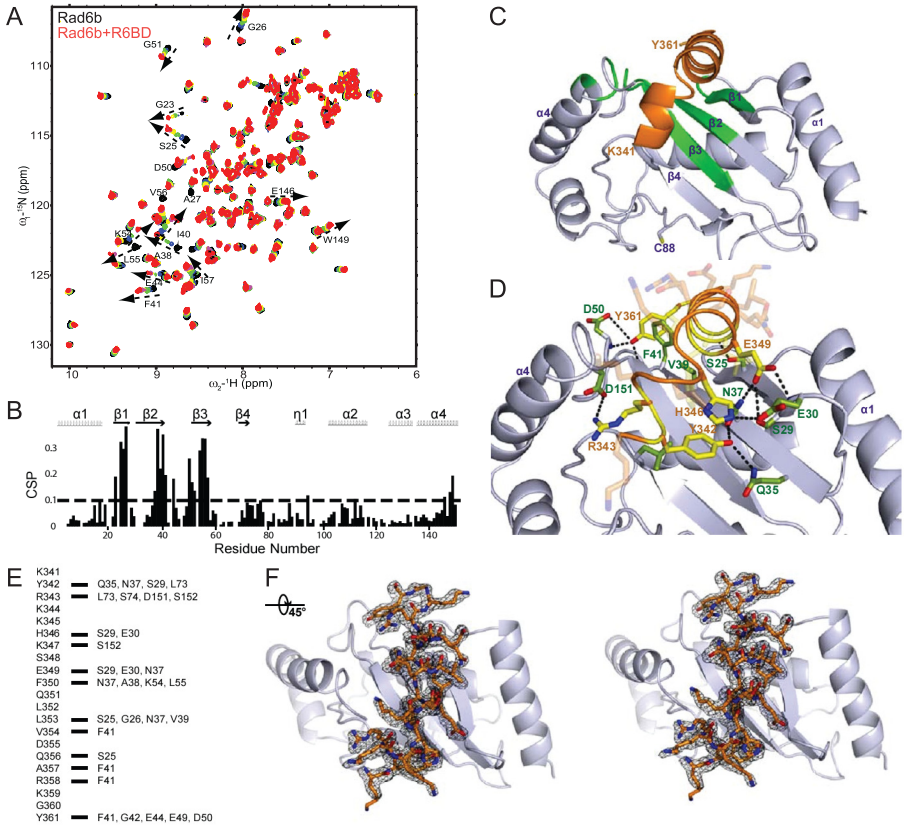

Figure * 5.4: The interaction of R6BD with Rad6b **A.** ^{1}H-^{15}N -HSQC of Rad6b alone (black) with increasing amounts of R6BD to a final Rad6b:R6BD ratio of 1:4 molar ratio of R6BD (red). **B** Magnitude of CSP plotted against residue number. Secondary structure elements of Rad6b are indicated. **C.** The crystal structure of the complex shows Rad6b to have a canonical E2 fold composed of a four-stranded antiparallel β-sheet (residues V24-S39, N32-F41, T52-E59 and T69-F72), four α-helices (residues P4-E19, V102-D114, S124-Q131, K134-Q137) and a short 310 helix (residues D90-L92). R6BD (orange) is a kinked helix that binds to the back of Rad6b. Significant (>0.1) CSPs of Rad6b are highlighted in green. The crystal structure is highly consistent with the NMR titration data. **D.** The interaction of the peptide with Rad6b is stabilized by potential hydrogen bonds to Tyr342, Arg343 and His346 at the kinked N-terminus of the peptide and Tyr361 at the C-terminus, although this residue may be somewhat mobile since it is less well resolved in the electron density. The interaction is also stabilized by a number of hydrophobic interactions including Val354 and Ala357, which are buried in a hydrophobic patch on Rad6b surrounding Val39 and Phe41. Residues at the interface on R6BD and Rad6b are coloured yellow and green, respectively. **E.** Summary of <3.8Å contacts between Rad6b and R6BD. F. Stereo representation of the R6BD-Rad6b complex. The refined electron density map (σA weighted 2Fo - Fc map, 2.0 Å, contoured at 1.0σ) for R6BD is shown.